Prague Medical REPORT

(Sborník lékařský)

Multidisciplinary Biomedical Journal
of the First Faculty of Medicine,
Charles University

Vol. 126 (2025) No. 4

Prague Medical Report (Prague Med Rep) is indexed and abstracted by Index-medicus, MEDLINE, PubMed, EuroPub, CNKI, DOAJ, EBSCO, and Scopus.

Abstracts and full-texts of published papers can be retrieved from the World Wide Web (https://pmr.lf1.cuni.cz).

Melnick-Needles Syndrome: Synthesizing Current Knowledge on Etiology, Clinical Presentation, Diagnostic Methods, and Potential Therapeutic Options

Vinod Kumar Mugada[1], Praveena Guntupalli[1], Vijaya Gudaparthi[1], Saritha Medapati[2], Srinivasa Rao Yarguntla[2]

[1] Department of Pharmacy Practice, Vignan Institute of Pharmaceutical Technology, Duvvada, Visakhapatnam, AP, India;
[2] Department of Pharmaceutics, Vignan Institute of Pharmaceutical Technology, Duvvada, Visakhapatnam, AP, India

Received January 2, 2025; Accepted November 21, 2025.

Key words: Melnick-Needles syndrome – Filamin-A – X-linked – Otopalatodigital syndrome

Abstract: Melnick-Needles syndrome (MNS) is a rare *X-linked* dominant skeletal dysplasia caused by pathogenic *FLNA* variants, primarily affecting females due to male lethality. Characterised by severe craniofacial and skeletal abnormalities, MNS exhibits marked phenotypic variability influenced by skewed X-inactivation, somatic mosaicism, and variant-specific functional consequences. Recent advances in next-generation sequencing and ACMG-based variant classification have refined diagnosis, particularly for pathogenic variants in exon 22, yet genotype-phenotype correlations remain incompletely defined. Differential diagnosis within the otopalatodigital spectrum, including OPD1, OPD2, and Frank-Ter Haar syndrome, remains challenging due to overlapping features, necessitating comprehensive radiological and molecular evaluation. Clinical manifestations span craniofacial dysmorphism, thoracic hypoplasia, respiratory compromise, and multisystem involvement. Management requires interdisciplinary coordination encompassing respiratory support, orthognathic surgery, dental reconstruction, and monitoring for complications such as glaucoma and psychiatric comorbidities. Evidence for the use of recombinant human bone morphogenetic protein-2 (rhBMP-2) and mandibular distraction techniques highlights surgical adaptability, though altered bone metabolism in MNS necessitates modified approaches. Rare associations with periventricular nodular heterotopia and bipolar disorder suggest a broader neurodevelopmental impact of *FLNA* dysfunction. Despite expanding clinical insight, the rarity of MNS limits population-level studies, constraining understanding of natural history and long-term outcomes. Future research must prioritise elucidating modifier genes, therapeutic targets such as antisense oligonucleotides, and prenatal detection strategies. A synthesis of genetic, clinical, and surgical domains is essential to optimise care pathways, improve prognosis, and inform genetic counselling for families affected by this phenotypically diverse and medically complex disorder.

Mailing Address: Assoc. Prof. Vinod Kumar Mugada, Department of Pharmacy Practice, Vignan Institute of Pharmaceutical Technology, Kapujaggaraju peta, Near VSEZ, Duvvada, Visakhapatnam, AP, 530049, India; Phone: +91 939 097 89 70; e-mail: mugadavinodkumar18@gmail.com

https://doi.org/10.14712/23362936.2025.30

Prague Medical Report / Vol. 126 (2025) No. 4, p. 183–192

Introduction

In addition to defining skeletal and craniofacial features, Melnick-Needles syndrome (MNS) exemplifies the interplay between genotype and phenotype in rare disorders. MNS arises from pathogenic variants in the *X-linked FLNA* gene, which encodes Filamin A – a protein essential for cytoskeletal stability – and affects fewer than 1 in 100,000 individuals (Robertson, 2007). The lethality of *FLNA* hemizygosity typically restricts survival to females, who manifest overlapping otopalatodigital spectrum dysplasia features (Robertson et al., 2003), yet rare male survivors reveal the syndrome's remarkable phenotypic heterogeneity.

An autosomal recessive form, Ter Haar syndrome, shares key craniofacial and skeletal anomalies but adds congenital glaucoma and cardiovascular defects, underscoring the need for tailored genetic counselling (Ter Haar et al., 1982; Donnenfeld et al., 1987; Krajewska-Walasek et al., 1987). Clinical severity further depends on variant context: *de novo FLNA* variants in males often yield milder, female-like phenotypes, whereas inherited truncating alleles cause severe dysmorphisms or embryonic lethality unless hypomorphic pathogenic variants preserve residual function (Donnenfeld et al., 1987; van der Lely et al., 1991; Robertson et al., 1997; Cannaerts et al., 2018; Luo et al., 2023).

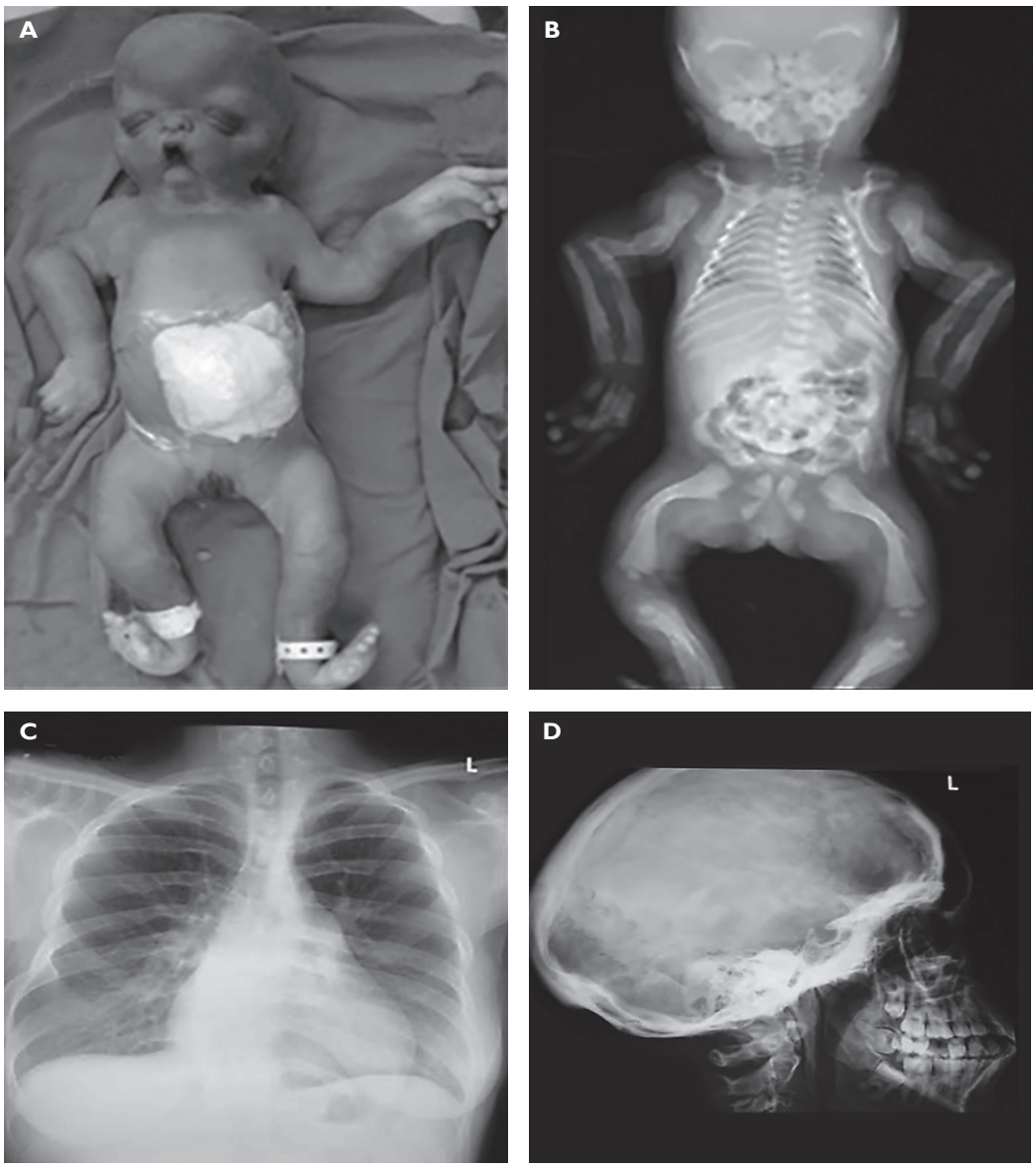

Figure 1: Phenotype of the proband and his mother. A) The proband presents with distinct clinical features, including down-slanting palpebral fissures, hypertelorism, micrognathia, low-set ears, bowed limbs, an omphalocele, a hypoplastic scrotum, and abnormalities in the hands and feet. B) X-ray imaging of the infant shows underdeveloped calvarial ossification with sclerotic supraorbital ridges, thin and curved ribs, scoliosis, and shortened, bowed long bones. C and D) X-ray imaging of the mother reveals ribs with irregular cortical margins, scoliosis, and a sclerotic skull base (Spencer et al., 2018).

Advances in molecular diagnostics – including next-generation sequencing and ACMG-guided variant interpretation – have refined the detection of pathogenic *FLNA* variants, particularly rod domain glycine substitutions that disrupt actin binding and compromise cytoskeletal networks vital for skeletal and craniofacial development (Kunishima et al., 2010; Richards et al., 2015; Cannaerts et al., 2018). Although mouse models bearing analogous variants replicate midline dysplasia, they fail to capture human-specific features such as omphalocele, suggesting species-specific genetic modifiers (Katz et al., 2004; Lian et al., 2017; Hauptman et al., 2018). Differential diagnosis within the otopalatodigital (OPD) spectrum remains challenging due to overlap with OPD1, OPD2, and frontometaphyseal dysplasia, but distinctive phalangeal abnormalities and periventricular nodular heterotopia aid in distinguishing MNS (Melnick and Needles, 1966; Poznanski, 1984; Silverman, 1985; Kristiansen et al., 2002; de Wit et al., 2009; Lord et al., 2014). Management relies on multidisciplinary care – including craniofacial surgery, orthopaedic interventions, and glaucoma surveillance – and, while antisense oligonucleotides offer theoretical promise for correcting *FLNA* splicing defects, their application in MNS remains under preclinical investigation (Robertson, 2007; Foley et al., 2010; Zanga et al., 2023).

Despite these advances, significant research gaps persist. The rarity of MNS limits large-scale studies, hindering a comprehensive understanding of its molecular mechanisms and phenotypic variability (Danks and Mayne, 1974). Furthermore, the roles of X inactivation mosaicism in females and somatic mosaicism or hypomorphic alleles in males – potentially explaining milder phenotypes – require deeper exploration (Edey et al., 2023; Protic et al., 2024). Elucidating these factors is critical for advancing targeted therapies and improving outcomes for affected individuals.

This paper aims to comprehensively synthesise current knowledge on MNS, a rare X-linked skeletal dysplasia caused by *FLNA* mutations. It explores the genetic basis, clinical variability, diagnostic advancements, and multidisciplinary management approaches, including surgical and respiratory interventions.

Clinical features

The craniofacial phenotype of MNS is typically evident at birth, featuring proptosis, micrognathia, hypertelorism, a high forehead, and full cheeks (Figure 1) (Melnick and Needles, 1966). Additional dental anomalies, including malocclusion, coronoid process hypoplasia, and widely spaced teeth, are frequently observed (Gorlin and Knier, 1982). Skeletal abnormalities encompass radial and tibial bowing, coxa valga, genu valgum, and cranial hyperostosis (Donnenfeld et al., 1987). Radiological studies further reveal metaphyseal elongation, rib irregularities, and scoliosis (Figure 1) (Melnick and Needles, 1966; Krajewska-Walasek et al., 1987).

Respiratory compromise is a hallmark of MNS, with affected individuals experiencing respiratory distress at birth, recurrent infections, and pulmonary artery hypertension (Masurel-Paulet et al., 2011; Lord et al., 2014). Systemic involvement extends to hydrocephalus, cerebellar hypoplasia, omphalocele, and urological anomalies such as hydronephrosis and hydroureter (Gorlin and Cohen, 1969; Klint et al., 1977). These manifestations underscore the syndrome's multisystem impact.

Craniofacial anomalies in MNS contribute to upper airway obstruction, with approximately 6% of patients developing obstructive sleep apnoea syndrome (OSAS) (Rojewski et al., 1984). While adenotonsillar hypertrophy is the primary cause of paediatric OSAS, untreated craniofacial malformations in MNS may progress to respiratory failure or pulmonary hypertension, necessitating interventions such as tracheostomy (Lowe et al., 1986). In addition to its core features, MNS is occasionally associated with rare complications. For instance, isolated reports describe premature stroke and multiple sclerosis, though mechanistic links to *FLNA* gain-of-function pathogenic variants – implicated in neurovascular integrity – remain speculative (Fox et al., 1998; Feng et al., 2006).

Neurological manifestations such as periventricular nodular heterotopia and epilepsy have been documented alongside sensorineural hearing loss attributed to cochlear anomalies (Shah et al., 2001; Zenker et al., 2004). Craniosynostosis has been anecdotally reported, though further validation is required (Stratton and Bluestone, 1991). MNS exhibits marked sexual dimorphism due to its X-linked dominant inheritance. Females commonly present with short stature, delayed motor development, and urethral stenosis, whereas males display severe manifestations – including exophthalmia, renal hypoplasia, and multiple organ malformations – often resulting in perinatal lethality (Donnenfeld et al., 1987; Robertson, 2007).

Skewed X-inactivation (uneven silencing of one X chromosome in females) and somatic mosaicism (presence of genetically distinct cell populations) in females mitigate symptom severity, while hemizygosity in males exacerbates pathogenic effects (Robertson et al., 2006; Naudion et al., 2016). MNS overlaps

Prague Medical Report / Vol. 126 (2025) No. 4, p. 183–192

Table 1: Comparison of key clinical features in MNS, OPD1, and OPD2

Clinical feature	Specific symptom	MNS (female phenotype)	OPD1 (male phenotype)	OPD2 (male phenotype)	Notes
Craniofacial	prominent supraorbital ridges	yes (common)	yes (characteristic)	yes (characteristic, often pronounced)	common across spectrum (Robertson, 2007)
	hypertelorism	yes (reported)	yes (characteristic)	yes (characteristic)	common across spectrum (MedlinePlus, 2019)
	down slanted palpebral fissures	not typically emphasized	yes (characteristic)	yes (characteristic)	more typical of OPD1/OPD2 (MedlinePlus, 2019)
	nasal bridge	normal/variable	broad, flat/ depressed (characteristic)	broad, flat/ depressed, stubby (characteristic)	broad/flat bridge typical of OPD1/OPD2 (MedlinePlus, 2019)
	micrognathia	yes (marked, 100%)	mild/absent	yes (often severe, pierre robin common)	severity differs: marked in MNS, severe in OPD2, mild/absent in OPD1 (MedlinePlus, 2019)
	cleft palate	yes (reported)	yes (75%)	yes (80%)	common in OPD1/OPD2, less emphasized in MNS females (MedlinePlus, 2019)
	exophthalmos/ proptosis	yes (common)	no	no	characteristic of MNS (Robertson, 2007)
	full cheeks	yes (common)	no	no	characteristic of MNS (Robertson, 2007)
Skeletal – axial	short stature	yes (100%)	yes (mild/variable)	yes (common)	common across spectrum, most consistent in MNS females (MedlinePlus, 2019)
	thoracic hypoplasia	yes (100%)	mild/variable (reported)	yes (100%, severe, causes respiratory failure)	defining feature of severe OPD2/MNS males; present but less severe in MNS females (National Library of Medicine, 2025)
	rib abnormalities	ribbon-like, wavy, irregular (characteristic)	normal/mild changes	thin, short, underdeveloped (common)	ribbon ribs specific to MNS (Robertson, 2007); thin/short ribs common in OPD2 (National Library of Medicine, 2025)
	scoliosis/ kyphoscoliosis	yes (common)	yes (reported)	yes (occasional)	can occur in all, prominent in MNS (Robertson, 2007)
Skeletal – appendicular	limb bowing	yes (marked, often S-curve, 100%)	yes (mild, frequency unknown in Table)	yes (severe, common)	severity gradient: mild (OPD1) < marked (MNS) ≈ severe (OPD2) (MedlinePlus, 2019)
	joint subluxation	yes (common)	no	no	characteristic of MNS (National Library of Medicine, 2022)
	limited joint mobility	yes (elbow reported)	yes (elbow/wrist, almost all)	yes (elbow/knee contractures common)	common across spectrum, pattern may differ; most characteristic in OPD1 (Robertson, 2019)
	characteristic digital pattern	long digits, mild distal hypoplasia	spatulate tips, short/proximal thumb, short great toe, long 2nd toe, sandal gap (100%)	hypoplastic/ absent 1st digits, camptodactyly, syndactyly (common)	distinct patterns aid diagnosis (MedlinePlus, 2019)
	fibular agenesis/ hypoplasia	no	no	yes (common)	characteristic of OPD2 (National Library of Medicine, 2025)
Auditory	hearing loss (conductive/ sensorineural)	yes (common)	yes (100%)	yes (common)	frequent across spectrum (Robertson, 2007)

Clinical feature	Specific symptom	MNS (female phenotype)	OPD1 (male phenotype)	OPD2 (male phenotype)	Notes
Systemic	hydronephrosis/ureteric obstruction	yes (common)	no	yes (common)	common in MNS and OPD2 (National Library of Medicine, 2025)
	cardiac defects	yes (valve prolapse common)	rare/absent	yes (septal/valvular defects common)	common in MNS and OPD2 (National Library of Medicine, 2025)
	omphalocele	yes (lethal males)	no	yes (common)	associated with severe male MNS/OPD2 (National Library of Medicine, 2022)
	CNS anomalies	rare (PVNH reported with MNS)	no	yes (hydrocephalus, cerebellar hypoplasia common)	primarily associated with OPD2 (National Library of Medicine, 2025)
	developmental delay/intellectual disability	no (intelligence typically normal)	no (intelligence typically normal; mild ID disputed)	yes (common in survivors)	primarily associated with OPD2 survivors (National Library of Medicine, 2025); MNS/OPD1 typically normal intelligence (MedlinePlus, 2019)

MNS – Melnick-Needles syndrome; OPD – otopalatodigital syndrome; CNS – central nervous system; PVNH – periventricular nodular heterotopia; ID – intellectual disability

with *FLNA*-related disorders such as otopalatodigital syndrome (OPD) and frontometaphyseal dysplasia (FMD). OPD lacks craniosynostosis, whereas OPD2 resembles severe MNS but presents milder maternal phenotypes (Verloes et al., 2000). Frank-Ter Haar syndrome, distinguished by congenital glaucoma and cardiac defects, serves as another differential diagnosis (Maas et al., 2004). The rarity of MNS has hindered a comprehensive understanding of vascular complications and genotype-phenotype correlations. Further studies are needed to clarify the role of *FLNA* in craniosynostosis, refine therapeutic strategies for OSAS, and improve outcomes in severely affected males (Feng and Walsh, 2004; Santos et al., 2010). The clinical features were summarized in Table 1.

Diagnosis

The definitive diagnosis of MNS relies on identifying pathogenic variants in the *FLNA* gene, with pathogenic variants in exon 22 (e.g., *p.Ala1188Thr*) frequently associated with severe, postnatally lethal phenotypes (Robertson et al., 2003; Naudion et al., 2016). Genetic testing distinguishes MNS from other skeletal dysplasias, such as osteodysplastic syndromes, and resolves ambiguities in inheritance patterns (Gorlin and Langer, 1978). In atypical presentations, such as co-occurring perinatal haemorrhagic nephropathy (PNH), *FLNA* sequencing provides clarity (Parrini et al., 2006). Genetic counselling is pivotal for female heterozygotes (carriers of one mutated *X chromosome*), who have a 50% chance of transmitting the pathogenic variant to offspring. However, due to *X-linked* dominance and male hemizygosity, the risk of severe manifestations in male offspring is 25% (Melnick and Needles, 1966; Santos et al., 2010).

Radiological imaging is indispensable for confirming MNS and differentiating it from other skeletal dysplasias. Key findings include skull abnormalities such as increased skull opacity, a dense skull base, and a thickened cranial vault (Melnick and Needles, 1966). Axial skeletal deformities encompass vertebral body height irregularities and scoliosis, while long bone anomalies feature bowing of the radii and tibiae, metaphyseal elongation, and femoral neck deformities (Donnenfeld et al., 1987). Pulmonary findings, often identified via lung biopsies, include alveolar simplification, which correlates with respiratory complications (Lord et al., 2014). In paediatric patients with hearing loss, temporal bone imaging is critical, as it frequently reveals cochlear hypoplasia requiring early intervention (Sellars and Beighton, 1978). Beyond skeletal and craniofacial features, MNS manifests with rare complications linked to *FLNA*'s role in cytoskeletal and vascular integrity. These include severe gastroesophageal reflux and dysphagia lusoria (compression of the oesophagus by an aberrant right subclavian artery), which may reflect impaired vascular remodelling (Harper et al., 2006). Such findings underscore the syndrome's systemic nature and necessitate comprehensive clinical evaluation.

The phenotypic variability of MNS complicates differentiation from autosomal dominant or recessive disorders, particularly in sporadic cases. While advances in genetic testing have improved diagnostic

Prague Medical Report / Vol. 126 (2025) No. 4, p. 183–192

accuracy, gaps persist in understanding genotype-phenotype correlations. For example, limited data exist on how specific *FLNA* variants (e.g., *p.Ala1188Thr*) influence renal or vascular phenotypes. Longitudinal studies are needed to elucidate the functional consequences of these pathogenic variants and refine prognostic accuracy.

The *FLNA* pathogenic variants rarely reduce protein expression but instead alter its function, leading to dysregulated actin networks. Notably, specific substitutions – such as *A1188T* and *S1199L* located in exon 22 – exert gain-of-function effects, driving exaggerated skeletal dysplasia, skull hyperostosis, tubular bone anomalies, and cleft palate (Robertson et al., 2003; Santos et al., 2010). *FLNA* pathogenic variants also underlie other laminopathies within the OPDSD spectrum, including OPD1/2, frontometaphyseal dysplasia (FMD), and periventricular nodular heterotopia (PNH). However, MNS remains phenotypically distinct for its severity and skeletal patterning (Robertson, 2007).

In females, a single pathogenic allele is sufficient to cause the disorder. Phenotypic variability is frequently observed due to skewed X-inactivation, with presentations ranging from severe skeletal dysplasia to asymptomatic carrier states. Conversely, affected males typically experience embryonic or perinatal lethality due to the absence of a compensatory X chromosome (Robertson et al., 2003). While most cases result from *de novo* pathogenic variants, female carriers have a 50% chance of transmitting the variant to offspring. Genetic counselling and clinical evaluation of at-risk relatives are essential for detecting subclinical manifestations and guiding reproductive decision-making. A rare autosomal recessive form involving loci beyond *FLNA* has been reported and is associated with poor prognosis due to additional cardiovascular anomalies (Krajewska-Walasek et al., 1987).

Next-generation sequencing (NGS) represents the primary diagnostic approach for detecting *FLNA* pathogenic variants. Fulgent Genetics offers an *NGS*-based *FLNA* single gene test with >99% sensitivity for both sequence variants and copy number variations, reporting variants classified as uncertain significance (VUS), likely pathogenic, or pathogenic (Fulgent Genetics, 2025). This targeted approach is appropriate for individuals with clinical features or family history suggestive of MNS.

Trio-whole exome sequencing (trio-WES) has proven effective in identifying novel *FLNA* variants. A 2023 study employed trio-WES to identify a hemizygous *c.3562G>A* (*p.A1188T*) missense variant in a fetus with MNS, subsequently confirming maternal inheritance through Sanger sequencing (Zou et al., 2023). This comprehensive approach allows the detection of variants across multiple genes while capturing family segregation data crucial for variant classification.

For known familial variants, targeted Sanger sequencing remains standard practice. Diagnostic laboratories, including Oxford Genetics Laboratories (UK) and the University of Otago Clinical Genetics Group (New Zealand), utilize specific primers for *FLNA* analysis (Fennell et al., 2015). IVAMI laboratory performs complete PCR amplification of *FLNA* exons followed by sequencing, requiring either EDTA blood for leukocyte separation or dried blood samples on cards (IVAMI, 2025).

FLNA variants are classified according to American College of Medical Genetics and Genomics (ACMG) guidelines. A 2023 study demonstrated the classification of the *c.3562G>A* variant as likely pathogenic based on multiple lines of evidence (PS4+PM2_Supporting+PP3+PP4) (Zou et al., 2023). Proper interpretation requires consideration of particular pathogenic variant patterns in OPDSD – a 2016 report identified pathogenic variants primarily clustered in specific *FLNA* domains with genotype-phenotype correlations now emerging (Moutton et al., 2016).

Prenatal diagnosis via chorionic villus sampling or amniocentesis can confirm MNS in at-risk pregnancies with known maternal *FLNA* pathogenic variants. While prenatal ultrasound may detect suggestive skeletal abnormalities, definitive diagnosis requires molecular confirmation. Given the X-linked dominant inheritance pattern with male lethality in MNS, genetic counselling with cascade testing is essential for female relatives of affected individuals (Tran and Cook, 2022).

Beyond diagnostic settings, more comprehensive approaches, including exome sequencing, are employed in research contexts. A 2018 study confirmed the recurrent (*p.Ala1188Thr*) variant in a male with lethal MNS (Spencer et al., 2018), while a 2023 case report emphasized molecular confirmation for unusual presentations (Zanga et al., 2023). These approaches continue to reveal the *FLNA* variants responsible for the phenotypic spectrum.

Management and treatment

MNS necessitates a multidisciplinary management approach due to its multisystem involvement, encompassing craniofacial, skeletal, respiratory, and psychological challenges. Care strategies integrate non-invasive and surgical interventions tailored to symptom severity, prioritising early diagnosis, interdisciplinary collaboration, and long-term monitoring to optimise outcomes.

Respiratory management

MNS is characterized by skeletal abnormalities – including a narrow thoracic cage with irregular ribbon-like ribs, narrow shoulders, and severe mandibular hypoplasia – that result in restrictive pulmonary mechanics and upper airway obstruction. These structural anomalies predispose patients to pulmonary hypertension (PH), obstructive sleep apnoea syndrome, recurrent pneumonia, and respiratory failure (Robertson, 2015; Tran and Cook, 2022).

Non-invasive ventilation (NIV) effectively alleviates PH and improves ventricular function, exercise tolerance, and quality of life (Nickol et al., 2005), with notable benefits for sleep-disordered breathing and coexisting conditions like obesity hypoventilation syndrome (Corral et al., 2018). Continuous positive airway pressure (CPAP) or bilevel positive airway pressure (BiPAP) is recommended for OSAS management, though alternative approaches may be required in cases of recurrent pneumonia (Unal et al., 2004). A tracheostomy may be necessary for severe respiratory failure to secure airway patency (Tran and Cook, 2022).

Prophylactic measures, such as pneumococcal and annual influenza vaccinations, are critical to mitigate infection risks, and early aggressive treatment of upper respiratory infections prevents lower tract involvement (Oh et al., 2020). Regular polysomnography is advised for patients with severe micrognathia to detect OSAS, while upper airway assessments and pulmonary function testing help monitor for obstructions and respiratory decline, particularly in progressive thoracic deformities or scoliosis (Tran and Cook, 2022).

Dental management

The dental and maxillofacial manifestations in MNS patients present significant functional and aesthetic challenges. Patients typically present with abnormal bite patterns, mandibular hypoplasia, misaligned teeth, and partial absence of teeth (oligodontia). Orthodontic evaluation should begin early to address malocclusion. Treatment plans must account for the abnormal bone structure and potential healing complications in MNS patients. Bilateral sagittal split osteotomy (BSSO) has been successfully employed to correct skeletal malocclusion in MNS patients. This surgical approach improves masticatory function, speech, and facial aesthetics. However, procedures must be adapted for the fragile trabecular bone structure and increased bleeding tendency characteristic of MNS (Pocket Dentistry, 2018).

Monocortical plate fixation has shown efficacy in MNS patients undergoing orthognathic surgery. The altered collagen structure and bone architecture necessitate modified approaches to surgical fixation (Pocket Dentistry, 2018). Recent research on filamin-A, the protein affected in MNS, demonstrates its role in dental epithelial cell migration and root formation. This molecular understanding may inform future therapeutic approaches for dental abnormalities in MNS patients (Hino et al., 2020).

Bone healing and stimulation

The role of bone-stimulating agents, such as recombinant human bone morphogenetic protein type 2 (rhBMP-2), remains debated. While rhBMP-2 shows potential for augmenting bone formation, successful outcomes in mandibular distraction and fibula lengthening have been achieved without adjunctive therapies (Unal et al., 2004; Molina et al., 2008). Conservative management suffices for non-lethal deformities, with surgical correction (e.g., spinal fusion) reserved for severe spinal anomalies (Lykissas et al., 2013).

Literature on the specific application of rhBMP-2 in MNS patients remains limited. A documented case reported the successful use of rhBMP-2 with internal mandibular distraction for a young adult MNS patient experiencing chronic temporomandibular joint dislocation. This patient, who had severe bite dysfunction related to mandibular hypoplasia, underwent bilateral mandibular distraction using rhBMP-2 and a prolonged distraction protocol, achieving complete symptom resolution lasting over 24 months post-treatment (Kelley et al., 2010).

Surgical interventions for craniofacial and skeletal abnormalities

Craniofacial deformities frequently require surgical correction to address functional and structural impairments. Mandibular distraction osteogenesis (a jaw lengthening procedure) is a cornerstone technique for managing obstructive sleep apnoea and craniofacial anomalies, enhancing upper airway dimensions and reducing reliance on tracheostomy. However, altered bone metabolism in MNS may prolong consolidation phases due to delayed bone formation (Unal et al., 2004; Kelley et al., 2010). Imaging studies corroborate the procedure's success in improving mandibular volume and respiratory function (Gorlin and Langer, 1978; Chen et al., 2011).

Orthognathic surgery, including sagittal split osteotomy, offers therapeutic benefits but poses

Prague Medical Report / Vol. 126 (2025) No. 4, p. 183–192

challenges due to inherent bone fragility and potential collagen synthesis defects in MNS. Midface or maxillary advancement osteotomy may benefit paediatric patients with severe craniofacial abnormalities and OSAS, though long-term stability of these interventions remains uncertain (Lauritzen et al., 1986; Colmenero et al., 1991).

Psychiatric and psychosocial considerations

Recent evidence indicates that patients with MNS may develop psychiatric disorders, particularly when periventricular nodular heterotopia (PNH) co-occurs. The first documented cases of bipolar disorder in MNS patients were reported in 2021 (Riccio et al., 2021). Recommended psychotherapeutic approaches include individual psychotherapy targeting emotional regulation. Neuroimaging is recommended for all MNS patients to detect PNH, which may predispose them to psychiatric disorders (Riccio et al., 2021). Emerging evidence links MNS to psychiatric comorbidities, including bipolar disorder. The pathophysiological basis for these associations may reflect *FLNA*'s role in neurovascular signalling, though further research is required (Robertson, 2007; Goldstein et al., 2017).

Conclusion

MNS represents a complex multisystem disorder rooted in pathogenic *FLNA* variants, which disrupt cytoskeletal integrity and cellular signalling, leading to hallmark craniofacial, skeletal, and visceral anomalies. Its X-linked dominant inheritance, marked by significant sexual dimorphism and phenotypic variability, underscores the interplay between genetic context and clinical severity. While males often face perinatal lethality, females exhibit a spectrum of manifestations influenced by skewed X-inactivation and somatic mosaicism. Advances in molecular diagnostics, including next-generation sequencing, have refined identifying *FLNA* variants. However, challenges persist in elucidating genotype-phenotype correlations and managing rare autosomal recessive variants with distinct prognoses.

Multidisciplinary care remains pivotal, integrating respiratory support, surgical correction of craniofacial and skeletal defects, and psychological interventions to address comorbidities. Early diagnosis and tailored strategies – such as non-invasive ventilation or mandibular distraction osteogenesis – improve quality of life, though long-term outcomes depend on complication severity. Despite progress, the syndrome's rarity hinders large-scale studies, leaving critical gaps in understanding molecular mechanisms, vascular complications, and therapeutic potential. Future research must prioritise longitudinal studies to unravel the role of genetic modifiers, X-inactivation dynamics, and novel therapies like antisense oligonucleotides. Collaborative efforts across genetics, paediatrics, and allied disciplines are essential to optimise management and empower affected families through informed genetic counselling. Bridging these knowledge gaps will enhance prognostic accuracy and therapeutic innovation for this profoundly heterogeneous disorder.

References

Cannaerts, E., Shukla, A., Hasanhodzic, M., Alaerts, M., Schepers, D., Van Laer, L., Girisha, K. M., Hojsak, I., Loeys, B., Verstraeten, A. (2018) *FLNA* mutations in surviving males presenting with connective tissue findings: Two new case reports and review of the literature. *BMC Med. Genet.* **19(1)**, 140.

Chen, J., Fan, G. K., Mao, B., Zhang, Z. (2011) Mandibular distraction osteogenesis reconstructed the upper airway in a case of Melnick-Needles syndrome. *Oral Maxillofac. Surg.* **15(2)**, 127–130.

Colmenero, C., Esteban, R., Albarino, A. R., Colmenero, B. (1991) Sleep apnoea syndrome associated with maxillofacial abnormalities. *J. Laryngol. Otol.* **105(2)**, 94–100.

Corral, J., Mogollon, M. V., Sánchez-Quiroga, M. Á., Gómez de Terreros, J., Romero, A., Caballero, C., Teran-Santos, J., Alonso-Álvarez, M. L., Gómez-García, T., González, M., López-Martínez, S., de Lucas, P., Marin, J. M., Romero, O., Díaz-Cambriles, T., Chiner, E., Egea, C., Lang, R. M., Mokhlesi, B., Masa, J. F.; Spanish Sleep Network (2018) Echocardiographic changes with non-invasive ventilation and CPAP in obesity hypoventilation syndrome. *Thorax* **73(4)**, 361–368.

Danks, D. M., Mayne, V. (1974) Frontometaphyseal dysplasia: A progressive disease of bone and connective tissue. *Birth Defects Orig. Artic. Ser.* **10(12)**, 57–60.

de Wit, M. C., Kros, J. M., Halley, D. J., de Coo, I. F., Verdijk, R., Jacobs, B. C., Mancini, G. M. (2009) Filamin A mutation, a common cause for periventricular heterotopia, aneurysms and cardiac defects. *J. Neurol. Neurosurg. Psychiatry* **80(4)**, 426–428.

Donnenfeld, A. E., Conard, K. A., Roberts, N. S., Borns, P. F., Zackai, E. H. (1987) Melnick-Needles syndrome in males: A lethal multiple congenital anomalies syndrome. *Am. J. Med. Genet.* **27(1)**, 159–173.

Edey, J., Soleimani-Nouri, P., Dawson-Kavanagh, A., Imran Azeem, M. S., Episkopou, V. (2023) X-linked neuronal migration disorders: Gender differences and insights for genetic screening. *Int. J. Dev. Neurosci.* **83(7)**, 581–599.

Feng, Y., Walsh, C. A. (2004) The many faces of filamin: A versatile molecular scaffold for cell motility and signalling. *Nat. Cell Biol.* **6(11)**, 1034–1038.

Feng, Y., Chen, M. H., Moskowitz, I. P., Mendonza, A. M., Vidali, L., Nakamura, F., Kwiatkowski, D. J., Walsh, C. A. (2006) Filamin A (*FLNA*) is required for cell-cell contact in vascular development and cardiac morphogenesis. *Proc. Natl. Acad. Sci. U. S. A.* **103(52)**, 19836–19841.

Fennell, N., Foulds, N., Johnson, D. S., Wilson, L. C., Wyatt, M., Robertson, S. P., Johnson, D., Wall, S. A., Wilkie, A. O. (2015) Association of mutations in *FLNA* with craniosynostosis. *Eur. J. Human Genet.* **23(12)**, 1684–1688.

Foley, C., Roberts, K., Tchrakian, N., Morgan, T., Fryer, A., Robertson, S. P., Tubridy, N. (2010) Expansion of the spectrum of *FLNA* mutations associated with Melnick-Needles syndrome. *Mol. Syndromol*. **1(3)**, 121–126.

Fox, J. W., Lamperti, E. D., Ekşioğlu, Y. Z., Hong, S. E., Feng, Y., Graham, D. A., Scheffer, I. E., Dobyns, W. B., Hirsch, B. A., Radtke, R. A., Berkovic, S. F., Huttenlocher, P. R., Walsh, C. A. (1998) Mutations in filamin 1 prevent migration of cerebral cortical neurons in human periventricular heterotopia. *Neuron* **21(6)**, 1315–1325.

Fulgent Genetics (2025) *Melnick-Needles Syndrome (FLNA Single Gene Test*). Available at: https://www.fulgentgenetics.com/Melnick-Needles-Syndrome

Goldstein, B. I., Birmaher, B., Carlson, G. A., DelBello, M. P., Findling, R. L., Fristad, M., Kowatch, R. A., Miklowitz, D. J., Nery, F. G., Perez-Algorta, G., Van Meter, A., Zeni, C. P., Correll, C. U., Kim, H. W., Wozniak, J., Chang, K. D., Hillegers, M., Youngstrom, E. A. (2017) The International Society for Bipolar Disorders Task Force report on pediatric bipolar disorder: Knowledge to date and directions for future research. *Bipolar Disord*. **19(7)**, 524–543.

Gorlin, R. J., Cohen, M. M. Jr. (1969) Frontometaphyseal dysplasia. A new syndrome. *Am. J. Dis. Child.* **118(3)**, 487–494.

Gorlin, R. J., Langer, L. O. Jr. (1978) Melnick-Needles syndrome: Radiographic alterations in the mandible. *Radiology* **128(2)**, 351–353.

Gorlin, R. J., Knier, J. (1982) X-linked or autosomal dominant, lethal in the male, inheritance of the Melnick-Needles (osteodysplasty) syndrome? A reappraisal. *Am. J. Med. Genet*. **13(4)**, 465–467.

Harper, D., Bloom, D. A., Rowley, J. A., Soubani, A., Smith, W. L. (2006) The high-resolution chest CT findings in an adult with Melnick-Needles syndrome. *Clin. Imaging* **30(5)**, 350–353.

Hauptman, J. S., Bollo, R., Damerla, R., Gibbs, B., Lo, C., Katz, A., Greene, S. (2018) Coincident myelomeningocele and gastroschisis: Report of 2 cases. *J. Neurosurg. Pediatr*. **21(6)**, 574–577.

Hino, R., Yamada, A., Chiba, Y., Yoshizaki, K., Fukumoto, E., Iwamoto, T., Maruya, Y., Otsu, K., Harada, H., Saito, K., Fukumoto, S. (2020) Melnick-Needles syndrome associated molecule, filamin-A regulates dental epithelial cell migration and root formation. *Pediatr. Dent. J.* **30(3)**, 208–214.

IVAMI (2025) *Genetic Testing – Otopalatodigital types 1 and 2, … syndrome (syndrome otopalatodigital types 1 and 2) – Gen FLNA*. Available at: https://www.ivami.com/en/genetic-testing-human-gene-mutations-diseases-neoplasias-and-pharmacogenetics/4218-genetic-testing-otopalatodigital-types-1-and-2-syndrome-syndrome-otopalatodigital-types-1-and-2-gen-flna

Katz, L. A., Schultz, R. E., Semina, E. V., Torfs, C. P., Krahn, K. N., Murray, J. C. (2004) Mutations in *PITX2* may contribute to cases of omphalocele and VATER-like syndromes. *Am. J. Med. Genet. A* **130A(3)**, 277–283.

Kelley, P., Mata, C., Da Silveira, A. (2010) Chronic temporomandibular joint dislocation by mandibular distraction in a patient with Melnick-Needles syndrome. *J. Craniofac. Surg*. **21(1)**, 174–176.

Klint, R. B., Agustsson, M. H., McAlister, W. H. (1977) Melnick-Needles osteodysplasia associated with pulmonary hypertension, obstructive uropathy and marrow hypoplasia. *Pediatr. Radiol*. **6(1)**, 49–51.

Krajewska-Walasek, M., Winkielman, J., Gorlin, R. J. (1987) Melnick-Needles syndrome in males. *Am. J. Med. Genet*. **27(1)**, 153–158.

Kristiansen, M., Knudsen, G. P., Søyland, A., Westvik, J., Ørstavik, K. H. (2002) Phenotypic variation in Melnick-Needles syndrome is not reflected in X inactivation patterns from blood or buccal smear. *Am. J. Med. Genet*. **108(2)**, 120–127.

Kunishima, S., Ito-Yamamura, Y., Hayakawa, A., Yamamoto, T., Saito, H. (2010) *FLNA* p.V528M substitution is neither associated with bilateral periventricular nodular heterotopia nor with macrothrombocytopenia. *J. Hum. Genet*. **55(12)**, 844–846.

Lauritzen, C., Lilja, J., Jarlstedt, J. (1986) Airway obstruction and sleep apnea in children with craniofacial anomalies. *Plast. Reconstr. Surg*. **77(1)**, 1–6.

Lian, G., Kanaujia, S., Wong, T., Sheen, V. (2017) FilaminA and Formin2 regulate skeletal, muscular, and intestinal formation through mesenchymal progenitor proliferation. *PLoS One* **12(12)**, e0189285.

Lord, A., Shapiro, A. J., Saint-Martin, C., Claveau, M., Melançon, S., Wintermark, P. (2014) Filamin A mutation may be associated with diffuse lung disease mimicking bronchopulmonary dysplasia in premature newborns. *Respir. Care* **59(11)**, e171–e177.

Lowe, A. A., Santamaria, J. D., Fleetham, J. A., Price, C. (1986) Facial morphology and obstructive sleep apnea. *Am. J. Orthod. Dentofacial Orthop*. **90(6)**, 484–491.

Luo, X., Yang, Z., Zeng, J., Chen, J., Chen, N., Jiang, X., Wei, Q., Yi, P., Xu, J. (2023) Mutation of *FLNA* attenuating the migration of abdominal muscles contributed to Melnick-Needles syndrome (MNS) in a family with recurrent miscarriage. *Mol. Genet. Genomic Med*. **11(5)**, e2145.

Lykissas, M. G., Crawford, A. H., Shufflebarger, H. L., Gaines, S., Permal, V. (2013) Correction of spine deformity in patients with Melnick-Needles syndrome: Report of 2 cases and literature review. *J. Pediatr. Orthop*. **33(2)**, 170–174.

Maas, S. M., Kayserili, H., Lam, J., Apak, M. Y., Hennekam, R. C. (2004) Further delineation of Frank-ter Haar syndrome. *Am. J. Med. Genet. A* **131(2)**, 127–133.

Masurel-Paulet, A., Haan, E., Thompson, E. M., Goizet, C., Thauvin-Robinet, C., Tai, A., Kennedy, D., Smith, G., Khong, T. Y., Solé, G., Guerineau, E., Coupry, I., Huet, F., Robertson, S., Faivre, L. (2011) Lung disease associated with periventricular nodular heterotopia and an *FLNA* mutation. *Eur. J. Med. Genet*. **54(1)**, 25–28.

MedlinePlus (2019) *Otopalatodigital syndrome type 1*. Available at: https://medlineplus.gov/genetics/condition/otopalatodigital-syndrome-type-1/

Melnick, J. C., Needles, C. F. (1966) An undiagnosed bone dysplasia. A family study of 4 generations and 3 generations. *Am. J. Roentgenol. Radium Ther. Nucl. Med*. **97(1)**, 39–48.

Molina, F., Morales, C., Taylor, J. A. (2008) Mandibular distraction osteogenesis in a patient with Melnick-Needles syndrome. *J. Craniofac. Surg*. **19(1)**, 277–279.

Moutton, S., Fergelot, P., Naudion, S., Cordier, M.-P., Solé, G., Guerineau, E., Hubert, C., Rooryck, C., Vuillaume, M. L., Houcinat, N., Deforges, J., Bouron, J., Devès, S., Le Merrer, M., David, A., Geneviève, D., Giuliano, F., Journel, H., Megarbane, A., Faivre, L., Chassaing, N., Francannet, C., Sarrazin, E., Stattin, E. L., Vigneron, J., Leclair, D., Abadie, C., Sarda, P., Baumann, C., Delrue, M. A., Arveiler, B., Lacombe, D., Goizet, C., Coupry, I. (2016) Otopalatodigital spectrum disorders: Refinement of the phenotypic and mutational spectrum. *J. Hum. Genet.* **61(8)**, 693–699.

National Library of Medicine (2022) *Melnick-Needles syndrome*. Available at: https://www.ncbi.nlm.nih.gov/medgen/6292

National Library of Medicine (2025) *Oto-palato-digital syndrome, type II*. Available at: https://www.ncbi.nlm.nih.gov/medgen/337064

Naudion, S., Moutton, S., Coupry, I., Sole, G., Deforges, J., Guerineau, E., Hubert, C., Deves, S., Pilliod, J., Rooryck, C.,

Abel, C., Le Breton, F., Collardeau-Frachon, S., Cordier, M. P., Delezoide, A. L., Goldenberg, A., Loget, P., Melki, J., Odent, S., Patrier, S., Verloes, A., Viot, G., Blesson, S., Bessières, B., Lacombe, D., Arveiler, B., Goizet, C., Fergelot, P. (2016) Fetal phenotypes in otopalatodigital spectrum disorders. *Clin. Genet*. **89(3)**, 371–377.

Nickol, A. H., Hart, N., Hopkinson, N. S., Moxham, J., Simonds, A., Polkey, M. I. (2005) Mechanisms of improvement of respiratory failure in patients with restrictive thoracic disease treated with non-invasive ventilation. *Thorax* **60(9)**, 754–760.

Oh, C. H., Lee, C. H., Kim, S. Y., Lee, S.-Y., Jun, H. H., Lee, S. (2020) A family of Melnick-Needles syndrome: A case report. *BMC Pediatr.* **20(1)**, 391.

Parrini, E., Ramazzotti, A., Dobyns, W. B., Mei, D., Moro, F., Veggiotti, P., Marini, C., Brilstra, E. H., Dalla Bernardina, B., Goodwin, L., Bodell, A., Jones, M. C., Nangeroni, M., Palmeri, S., Said, E., Sander, J. W., Striano, P., Takahashi, Y., Van Maldergem, L., Leonardi, G., Wright, M., Walsh, C. A., Guerrini, R. (2006) Periventricular heterotopia: Phenotypic heterogeneity and correlation with filamin A mutations. *Brain* **129(Pt 7)**, 1892–1906.

Pocket Dentistry (2018) *Orthognathic surgery in Melnick-Needles-Syndrome. Case report and review of the literature*. Available at: https://pocketdentistry.com/orthognathic-surgery-in-melnick-needles-syndrome-case-report-and-review-of-the-literature/

Poznanski, A. K. (1984) *The Hand in Radiologic Diagnosis*, 2nd Edition. W. B. Saunders, Philadelphia.

Protic, D., Polli, R., Bettella, E., Usdin, K., Murgia, A., Tassone, F. (2024) Somatic instability leading to mosaicism in fragile X syndrome and associated disorders: Complex mechanisms, diagnostics, and clinical relevance. *Int. J. Mol. Sci*. **25(24)**, 13681–13681.

Riccio, M. P., D'Andrea, G., Sarnataro, E., Marino, M., Bravaccio, C., Albert, U. (2021) Bipolar disorder with Melnick-Needles syndrome and periventricular nodular heterotopia: Two case reports and a review of the literature. *J. Med. Case Rep.* **15(1)**, 495.

Richards, S., Aziz, N., Bale, S., Bick, D., Das, S., Gastier-Foster, J., Grody, W. W., Hegde, M., Lyon, E., Spector, E., Voelkerding, K., Rehm, H. L. (2015) Standards and guidelines for the interpretation of sequence variants: A joint consensus recommendation of the American College of Medical Genetics and Genomics and the Association for Molecular Pathology. *Genet. Med*. **17(5)**, 405–424.

Robertson, S. P. (2007) Otopalatodigital syndrome spectrum disorders: Otopalatodigital syndrome types 1 and 2, frontometaphyseal dysplasia and Melnick-Needles syndrome. *Eur. J. Hum. Genet*. **15(1)**, 3–9.

Robertson, S. (2015) *Orphanet: Melnick-Needles syndrome*. Available at: https://www.orpha.net/en/disease/detail/2484

Robertson, S. (2019) *X-Linked Otopalatodigital Spectrum Disorders*. Available at: https://ern-ithaca.eu/wp-content/uploads/2020/12/Robertson_OPDs_Genereviews2019.pdf

Robertson, S., Gunn, T., Allen, B., Chapman, C., Becroft, D. (1997) Are Melnick-Needles syndrome and oto-palato-digital syndrome type II allelic? Observations in four-generation kindred. *Am. J. Med. Genet*. **71(3**), 341–347.

Robertson, S. P., Twigg, S. R. F., Sutherland-Smith, A. J., Biancalana, V., Gorlin, R. J., Horn, D., Kenwrick, S. J., Kim, C. A., Morava, E., Newbury-Ecob, R., Ørstavik, K. H., Quarrell, O. W. J., Schwartz, C. E., Shears, D. J., Suri, M., Kendrick-Jones, J., Wilkie, A. O. M. (2003) Localized mutations in the gene encoding the cytoskeletal protein filamin A cause diverse malformations in humans. *Nat. Genet*. **33(4)**, 487–491.

Robertson, S. P., Thompson, S., Morgan, T., Holder-Espinasse, M., Martinot-Duquenoy, V., Wilkie, A. O., Manouvrier-Hanu, S. (2006) Postzygotic mutation and germline mosaicism in the otopalatodigital syndrome spectrum disorders. *Eur. J. Hum. Genet*. **14(5)**, 549–554.

Rojewski, T. E., Schuller, D. E., Clark, R. W., Schmidt, H. S., Potts, R. E. (1984) Videoendoscopic determination of the mechanism of obstruction in obstructive sleep apnea. *Otolaryngol. Head Neck Surg*. **92(2)**, 127–131.

Santos, H. H., Garcia, P. P., Pereira, L., Leão, L. L., Aguiar, R. A., Lana, A. M., Carvalho, M. R., Aguiar, M. J. (2010) Mutational analysis of two boys with the severe perinatally lethal Melnick-Needles syndrome. *Am. J. Med. Genet. A* **152A(3)**, 726–731.

Sellars, S. L., Beighton, P. H. (1978) Deafness in osteodysplasty of Melnick and Needles. *Arch. Otolaryngol.* **104(4)**, 225–227.

Shah, S. M., Prabhu, S. S., Merchant, R. H. (2001) Mondini defect. *J. Postgrad. Med*. **47(4)**, 272–273.

Silverman, F. N. (1985) *Caffey's Pediatric X-ray Diagnosis*, 8th Edition. Year Book Medical Publishers, Chicago.

Spencer, C., Lombaard, H., Wise, A., Krause, A., Robertson, S. P. (2018) A recurrent mutation causing Melnick-Needles syndrome in females confers a severe, lethal phenotype in males. *Am. J. Med. Genet. A* **176(4)**, 980–984.

Stratton, R. F., Bluestone, D. L. (1991) Oto-palatal-digital syndrome type II with X-linked cerebellar hypoplasia/hydrocephalus. *Am. J. Med. Genet.* **41(2)**, 169–172.

Ter Haar, B., Hamel, B., Hendriks, J., de Jager, J. (1982) Melnick-Needles syndrome: Indication for an autosomal recessive form. *Am. J. Med. Genet*. **13(4)**, 469–477.

Tran, L., Cook, S. (2022) *Melnick-Needles Syndrome*. National Organization for Rare Disorders. Available at: https://rarediseases.org/rare-diseases/melnick-needles-syndrome/

Unal, V. S., Derici, O., Oken, F., Turan, S., Girgin, O. (2004) Fibular lengthening procedure: Treatment for lateral instability of the ankle caused by fibular insufficiency in Melnick-Needles syndrome. *J. Pediatr. Orthop. B* **13(2)**, 88–91.

van der Lely, H., Robben, S. G. F., Meradji, M., Derksen-Lubsen, G. (1991) Melnick-Needles syndrome (osteodysplasty) in an older male: Report of a case and a review of the literature. *Br. J. Radiol.* **64(764)**, 852–854.

Verloes, A., Lesenfants, S., Barr, M., Grange, D. K., Journel, H., Lombet, J., Mortier, G., Roeder, E. (2000) Fronto-otopalatodigital osteodysplasia: Clinical evidence for a single entity encompassing Melnick-Needles syndrome, otopalatodigital syndrome types 1 and 2, and frontometaphyseal dysplasia. *Am. J. Med. Genet*. **90(5)**, 407–422.

Zanga, S. M., Bicaba, D., Nagalo, K., Konané, S. G., Napon, A. M., Nikiéma, Z., Diallo, O., Sorgho, C., Cissé, R. (2023) Melnick Needles syndrome: Computed imaging and management difficulties. *Open J. Radiol*. **13(03)**, 146–154.

Zenker, M., Rauch, A., Winterpacht, A., Tagariello, A., Kraus, C., Rupprecht, T., Sticht, H., Reis, A. (2004) A dual phenotype of periventricular nodular heterotopia and frontometaphyseal dysplasia in one patient caused by a single *FLNA* mutation leading to two functionally different aberrant transcripts. *Am. J. Hum. Genet*. **74(4)**, 731–737.

Zou, J., Zhang, Y., Liu, Y., Xue, A., Yan, L., Li, H. (2023) Clinical characteristics and genetic analysis of a fetus with Melnick-Needles syndrome due to variant of *FLNA* gene. *Zhonghua Yi Xue Yi Chuan Xue Za Zhi* **40(5)**, 582–587. (in Chinese)

Effects of Stroke on Electromyographic Activity, Respiratory Muscle Strength, and Pulmonary Function

Camila Roza Gonçalves[1], Marcelo Palinkas[1,2], Gabriel Pádua da Silva[1], Robson Felipe Tosta Lopes[1], Edson Donizetti Verri[1], Isabella Cícero de Souza[1], Guilherme Gallo Costa Gomes[1], Evandro Marianetti Fioco[1], Selma Siéssere[1,2], Simone Cecilio Hallak Regalo[1,2]

[1] Department of Basic and Oral Biology, School of Dentistry of Ribeirão Preto, University of São Paulo, São Paulo, Brazil;
[2] National Institute of Science and Technology, Translational Medicine, São Paulo, Brazil

Received March 13, 2025; Accepted November 21, 2025.

Key words: Stroke – Respiratory muscle – Electromyography – Manovacuometry – Spirometry

Abstract: Stroke is a condition characterized by the sudden onset of clinical signs and symptoms, with persistent neurological deficits lasting more than twenty-four hours. This disease causes changes in cerebral blood circulation, impairing brain function either focally or globally. This observational study aimed to evaluate the respiratory function of subjects who suffered an ischemic or hemorrhagic stroke more than five years ago and compare them to a without neurological disorder group. Twenty-four subjects aged between 30 and 80 years participated, divided into two groups: stroke (n=12) and without neurological disorder (n=12). All analyses were conducted with a 5% significance level (Student's *t*-test). The results indicated that the stroke group showed significant changes compared to without neurological disorder group, including increased activity of respiratory and accessory muscles, as well as reduced respiratory muscle strength. However, spirometric evaluation did not reveal significant differences between the groups. The authors suggest that subjects with stroke exhibit neuromuscular deficits, with changes in the electromyographic activity of respiratory and accessory muscles, reduced respiratory muscle strength, and impaired lung volumes and capacities.

This study was supported by the Foundation for Research Support of the State of São Paulo (FAPESP) and the National Institute of Technology – Translational Medicine (INCT.TM).

Mailing Address: Prof. Marcelo Palinkas, PhD., School of Dentistry of Ribeirão Preto, University of São Paulo, Avenida do Café s/n, Bairro Monte Alegre CEP 14040-904, Ribeirão Preto, São Paulo, Brazil; e-mail: palinkas@usp.br

https://doi.org/10.14712/23362936.2025.31

Prague Medical Report / Vol. 126 (2025) No. 4, p. 193–200

Introduction

A stroke is a condition characterized by the reduction or complete interruption of blood flow in a specific brain region. It is the second leading cause of death, and the third leading cause of death and disability combined worldwide (da Silva et al., 2022; Feigin et al., 2025). This condition can be classified into two types: ischemic and hemorrhagic (Gomes et al., 2022; Hilkens et al., 2024).

The distinction between these types lies in the nature of the brain injury. The ischemic type results from the infarction or blockage of a cerebral artery, which restricts blood flow to the brain. In contrast, the hemorrhagic type occurs due to the leakage of blood from a cerebral artery (Duncan et al., 2021).

This condition presents with spastic hypertonia as a pathophysiological feature, making it possible to observe increased muscle tone and heightened deep tendon reflexes (Jian et al., 2017). In addition, age and gender are also important factors in the diagnosis of the disease, with males aged between 55 and 60 years being more susceptible to stroke development (Lisabeth et al., 2018).

Neurological conditions can be directly linked to respiratory dysfunctions, and stroke is a pathology that significantly affects the quality of life of these patients. It can lead to impairments in electromyographic activity, respiratory muscle strength, and pulmonary function (Verheyden et al., 2009; Lopes et al., 2023). Respiratory changes are frequently described in the literature among post-stroke patients, characterized by compromised lung mechanics and reduced respiratory muscle strength, along with impaired lung function. These changes result in respiratory weakness, alterations in respiratory patterns, and reductions in respiratory volumes and flows, leading to frequent respiratory complications and recurrent hospitalizations (Menezes et al., 2016).

This study aimed to evaluate the electromyographic activity of respiratory and accessory muscles, respiratory muscle strength, and pulmonary function in subjects with a clinical diagnosis of ischemic or hemorrhagic stroke and to establish parameters for comparison with healthy subjects. These results can provide healthcare professionals with a better understanding of the potential changes in the respiratory and accessory muscles of subjects with stroke. If the null hypothesis is confirmed, it would indicate that subjects with ischemic or hemorrhagic stroke do not exhibit changes in the electromyographic activity of the primary and accessory breathing muscles, inspiratory and expiratory muscle strength, or pulmonary function.

Material and Methods

This observational study was approved by the ethics committee (process # 92222318.8.0000.5419). Informed consent was obtained from all subjects participating in this study.

Sample selection

The sample size calculation was conducted using the *a priori* test through the G*Power software (version 3.1.9.2; Franz Faul, Kiel University, Kiel, Germany). This calculation considered a global population of 26 million cases of cerebrovascular diseases, as reported by the Brazilian Society of Cerebrovascular Diseases (Schimmel et al., 2017). The sample size was estimated with a statistical power of 80% to detect a 20% difference between groups, adopting a 90% confidence interval, resulting in a required sample of 12 subjects per group.

The study included 24 subjects aged between 30 and 80 years, with normal occlusion and no temporomandibular dysfunction according to the Research Diagnostic Criteria for Temporomandibular Disorders (Axis I and II). They were divided into two groups: stroke (n=12) and the without neurological disorders (n=12). The subjects selected for the study had a confirmed diagnosis of ischemic or hemorrhagic stroke, with more than five years having passed since the event. The groups were matched individually by sex, age, and body mass index. Among

Table 1: Sample characteristics and subject-to-subject matching criteria

Characteristics	P-value	Groups	
		stroke	without neurological disorder
Sex	–	6 (male)/6 (female)	6 (male)/6 (female)
Stroke types	–	6 (hemorrhagic)/6 (ischemic)	–
Cerebral hemisphere affected	–	9 (right)/3 (left)	–
Age	0.71	56.10 ± 4.00	54.00 ± 3.90
Body mass index	0.95	28.65 ± 1.04	28.54 ± 1.44

the stroke group, six subjects had ischemic stroke and six had hemorrhagic stroke, all confirmed by medical reports. All subjects underwent evaluation of the electromyographic activity of respiratory and accessory muscles, respiratory muscle strength, and lung function (Table 1).

Inclusion criteria included a confirmed clinical diagnosis of ischemic or hemorrhagic stroke, age between 30 and 80 years (with no prior history of pulmonary impairment), a diagnosis time exceeding five years, absence of diagnosed degenerative and/or functional alterations, non-smokers, and being under clinical treatment. Both sexes were included. Subjects were excluded if they had cognitive impairments or ulcerations, open wounds, or skin hypersensitivity.

Assessment of respiratory electromyographic activity

The MyoSystem BR1 P84 (DataHominis; Uberlândia, MG, Brazil), a twelve-channel, portable electromyography device, was used to collect electromyography signals. All surface electrodes were positioned by the same trained and qualified examiner (Hermens et al., 2000). To ensure the correct localization of the muscles, specific maneuvers of maximum voluntary muscle contraction and digital palpation were performed (De Luca, 1997). Before placing the electrodes, skin asepsis was performed using 70% alcohol to reduce impedance. The electrodes were fixed a few minutes after this procedure (Di Palma et al., 2017).

During the recording of electromyographic activity, the environment was kept calm and quiet, with the subject seated in a comfortable chair, maintaining an upright posture and upper limbs positioned parallel to the body. The hips, knees, and ankles were positioned at 90°. Additionally, the head was aligned to keep the Frankfurt horizontal plane parallel to the ground.

To assess the recruitment of respiratory muscle fibers, an experimental protocol involving electromyography recordings was applied at the following muscle sites: the right sternocleidomastoid (muscle belly), the right pectoralis major (midclavicular line, 5 cm below the clavicle), the right external intercostal (third intercostal space, 3 cm lateral to the body midline), the right portion of the diaphragm (seventh intercostal space, on the midclavicular line), the right serratus anterior (fifth rib on the midaxillary line), the right rectus abdominis (midpoint between the xiphoid process and umbilical scar, 3 cm lateral to the body midline), and the right external oblique (superior to the anterosuperior iliac spine, 15 cm lateral to the umbilical scar).

After the initiation of electromyography signal collection, the signals were normalized using the values obtained during the maneuver of inspiration and sustained maximum expiration (4 s) (Alonso et al., 2011). To prevent modifications or changes in the electromyography results, signal collection for these muscles was conducted exclusively on the right side of the body, as proposed by Hawkes et al. (2007), to avoid interference from the left side. This approach minimizes the risk of crosstalk caused by cardiac interference in the myoelectric signal (Abbaspour and Fallah, 2014).

The clinical conditions for electromyography data collection included the following: rest (10 s), respiratory cycle (deep breathing with inspiratory and expiratory phases) (10 s), maximal inspiration from residual volume (4 s), maximal expiration from total lung capacity (4 s), and maximum sustained inspiration (4 s) for normalization.

The raw electromyography signal was used to derive amplitude values, calculated by the root mean square method. This method was applied to measure respiratory muscle activity during rest, the respiratory cycle, maximal inspiration, and maximal expiration, where the envelope integral was used. The root mean square values obtained during maximum sustained inspiration were used to normalize the other clinical respiratory conditions.

Assessment of maximum respiratory muscle strength

An analog manometer (manometer with a three-way stopcock; CareFusion; San Diego, CA) was used to measure respiratory pressures: maximum inspiratory pressure and maximum expiratory pressure, with a range of ±150 cm H_2O, from Proarlife®, through a mouthpiece positioned between the lips. Before starting, subjects were informed about all stages of the assessment, and the first measurement was performed to facilitate learning.

For data collection, the subject was seated in a chair in Fowler's position, as comfortably as possible, with the upper limbs aligned at the sides of the body and the lower limbs flexed at a 90° angle. The device's mouthpiece was adapted according to the subject's oral cavity, with the nose occluded using a nose clip. A single evaluator was responsible for providing verbal instructions, advising the subjects to exhale completely, emptying their lungs as much as possible, and then inhale deeply and quickly through the mouth. Maximum inspiratory pressure (MIP) was then measured from the residual volume. This first test was repeated three times, with a one-minute interval between each measurement, and the highest value was considered valid.

Next, the device's mouthpiece was again attached to the subject's mouth, with the nose occluded by a nose

Prague Medical Report / Vol. 126 (2025) No. 4, p. 193–200

clip. The subject was instructed to inhale completely, filling their lungs as much as possible, and then exhale forcefully and quickly through the mouth. Maximum expiratory pressure (MEP) was then measured from the total lung capacity. This second test was also repeated three times, with a one-minute interval between each measurement, and the highest value was considered valid. The procedures were performed by a single evaluator throughout all stages of the research to prevent research bias.

Respiratory pressure data were analyzed after collecting at least three and at most five measurements, with a one-minute rest between them. The measurements were considered acceptable if there was a difference of 10% or less between them. The highest value obtained was used for statistical analysis and compared to predicted values (Costa et al., 2010).

Assessment of pulmonary function

A digital spirometer (Koko®, PFT type, nSpireHealth Inc., CO, USA) was used in a climate-controlled room maintained between 22 and 24 °C, following technical procedures, acceptability, and reproducibility criteria according to the American Thoracic Society/European Respiratory Society standards (Miller, 2005).

Subjects were instructed to eat beforehand but avoid heavy meals, and to refrain from consuming coffee, tea, alcohol, or smoking on the day of the exam. During the test, the subjects remained seated with a nose clip and received instructions on the procedures before performing the respective maneuvers. A mouthpiece was fitted to their lips to prevent air leakage, and they were asked to take a deep breath followed by a rapid and forced expiration for as long as possible. At the end of this, a deep inspiration was performed. Throughout the maneuvers, continuous and repetitive encouragement from the technician responsible for the examination was essential.

At least three forced expiratory curves were obtained to measure forced vital capacity and forced expiratory volume in the first second. Although spirometry allows the assessment of numerous

Table 2: Differences in the mean values (± standard error) of normalized electromyographic activity of respiratory muscles between the stroke and non-neurological disorder groups

Tasks	Muscles respiratory	Groups		P-value
		stroke	without neurological disorder	
Respiratory rest	right sternocleidomastoid	0.14 ± 0.03	0.15 ± 0.05	0.79
	right pectoralis major	0.23 ± 0.07	0.55 ± 0.09	0.01
	right external intercostal	0.89 ± 0.08	1.00 ± 0.12	0.40
	right portion diaphragm	0.70 ± 0.09	0.56 ± 0.11	0.39
	right serratus anterior	0.77 ± 0.12	0.80 ± 0.08	0.84
	right rectus abdominis	0.53 ± 0.13	0.74 ± 0.14	0.29
	right external oblique	0.33 ± 0.05	0.92 ± 0.16	0.00
Maximum inspiration	right sternocleidomastoid	0.70 ± 0.16	0.40 ± 0.08	0.11
	right pectoralis major	0.35 ± 0.06	0.49 ± 0.10	0.28
	right external intercostal	0.96 ± 0.08	0.97 ± 0.11	0.95
	right portion diaphragm	0.88 ± 0.12	0.66 ± 0.12	0.21
	right serratus anterior	0.65 ± 0.10	1.05 ± 0.14	0.03
	right rectus abdominis	0.40 ± 0.06	0.68 ± 0.07	0.01
	right external oblique	0.40 ± 0.06	0.71 ± 0.11	0.03
Maximum expiration	right sternocleidomastoid	0.44 ± 0.08	0.39 ± 0.10	0.71
	right pectoralis major	0.24 ± 0.05	0.47 ± 0.11	0.11
	right external intercostal	0.92 ± 0.06	1.03 ± 0.11	0.43
	right portion diaphragm	1.00 ± 0.11	0.66 ± 0.13	0.05
	right serratus anterior	0.78 ± 0.12	0.94 ± 0.15	0.43
	right rectus abdominis	0.52 ± 0.08	0.68 ± 0.11	0.27
	right external oblique	0.46 ± 0.06	0.72 ± 0.12	0.08
Respiratory cycle	right sternocleidomastoid	0.86 ± 0.10	0.57 ± 0.15	0.14
	right pectoralis major	0.47 ± 0.07	1.48 ± 0.32	0.00
	right external intercostal	2.01 ± 0.17	2.33 ± 0.24	0.30
	right portion diaphragm	1.76 ± 0.17	1.70 ± 0.42	0.89
	right serratus anterior	1.20 ± 0.18	2.78 ± 0.43	0.00
	right rectus abdominis	0.77 ± 0.12	1.59 ± 0.28	0.01
	right external oblique	1.09 ± 0.14	1.99 ± 0.31	0.01

parameters, the most relevant for the purposes of this study were forced vital capacity, forced expiratory volume in one second, and the forced expiratory volume in one second/forced vital capacity ratio, which exhibit lower inter- and intra-subject variability (Carvalho-Pinto et al., 2021).

Statistical analysis

Statistical analyses were conducted using IBM SPSS software, version 26.0 (IBM SPSS Inc., Chicago, IL, USA). Data normality was evaluated through the Shapiro-Wilk test. For comparisons between independent samples, the *t*-test was applied, considering a significance level of 95%.

Results

Table 2 presents the results of electromyographic analyses for both respiratory and accessory muscles during respiratory rest, maximal inspiration, maximal expiration, and the respiratory cycle. During the electromyographic analysis of respiratory rest, statistically significant differences were observed in the right pectoralis major (P=0.01) and right external oblique (P=0.00) muscles. For maximal inspiration, the analysis revealed significant results for the right serratus anterior and right external oblique muscles (P=0.03), as well as for the right rectus abdominis (P=0.01) and right external oblique (P=0.03) muscles. In the case of maximal expiration, significant differences were observed between the groups for the right portion of the diaphragm muscle (P=0.05). Finally, the analysis of the respiratory cycle revealed significant values for the right pectoralis major (P=0.01), right serratus anterior (P=0.00), right rectus abdominis (P=0.01), and right external oblique (P=0.00) muscles.

Regarding the analysis of average respiratory muscle strength, the stroke group exhibited lower averages for maximum inspiratory pressure and maximum expiratory pressure. Significant differences were found for both MIP and MEP (P<0.01) (Table 3).

In the pulmonary function assessment, the stroke group demonstrated higher average values for the Tiffeneau index (forced expiratory volume in one second/forced vital capacity), but lower averages for forced expiratory volume in one second and forced vital capacity. However, these results did not reach statistical significance (P<0.05) (Table 4).

Discussion

The null hypothesis was rejected, as significant differences were observed between the groups, indicating that subjects with ischemic or hemorrhagic stroke do exhibit changes in the electromyographic activity of the primary and accessory muscles of breathing, as well as in inspiratory and expiratory muscle strength. The main results found in the stroke group compared to the group without neurological disorders were higher electromyographic averages, with significant results for all conditions analysed,

Table 3: Differences in the mean values (± standard error) in maximum inspiratory (MIP) and expiratory (MEP) pressures, for the respiratory muscles strength in the stroke and non-neurological disorder groups

Pressures	Groups		P-value
	stroke	without neurological disorder	
MIP	–70.00 ± 7.33	–115.41 ± 10.72	0.00
MEP	65.41 ± 6.94	105.41 ± 7.00	0.00

Table 4: Differences in the mean values (± standard error) of pulmonary function of forced vital capacity (FVC), forced expiratory volume in one second (FEV1) and Tiffeneau index (FEV1/FVC) in the stroke and non-neurological disorder groups

Function	Groups		P-value
	stroke	without neurological disorder	
FVC	3.13 ± 0.18	3.16 ± 0.22	0.91
FEV1	2.51 ± 0.15	2.57 ± 0.23	0.82
FEV1/FVC	0.80 ± 0.01	0.79 ± 0.03	0.88

Prague Medical Report / Vol. 126 (2025) No. 4, p. 193–200

except for the condition of maximum muscle expiration; a significant reduction in respiratory muscle strength; and no significant differences in lung volumes and capacities between the groups.

Subjects who have had a stroke may experience changes in the affected hemibody, such as alterations in muscle tone, changes in trunk stability, and, as a result, they may maintain an asymmetrical posture, which affects the respiratory muscles and leads to respiratory dysfunction (Okumuş et al., 2025). These deficits occur due to damage to the upper motor neurons, which control skeletal muscles in coordination with the respiratory muscles and also assist in trunk movement (Laufer et al., 2005; Marcucci et al., 2007).

In this study, electromyographic analysis of the clinical condition during respiratory rest revealed that the muscles – the right pectoralis major and the right external oblique – showed lower averages with significant values in the stroke group when compared to the group without neurological disorders. The pectoralis major muscle functions in internal rotation and shoulder flexion, while the external oblique muscle is responsible for lateral flexion and trunk flexion. These findings suggest that changes in electromyographic activity may be related to the posture adopted after a stroke.

According to the study by Chen et al. (2015), post-stroke posture misalignment occurs due to muscle atrophy resulting from paralysis of the affected hemibody. Additionally, the study by Santos et al. (2019) describes that the posture adopted by subjects after chronic stroke includes increased scapular prostration, homolateral flexion, anterior trunk flexion, and reduced elbow extension, all of which can interfere with daily living activities.

Several studies have observed that after a stroke, there is a reduction in the activation of the thoracoabdominal muscles and, consequently, a change in the position of the rib cage, which typically remains in the inspiratory position. As a result, hemiparetic and hemiplegic subjects experience impairments in respiratory function (Marcucci et al., 2007). In this study, significant values were observed for the right pectoralis major muscle, right portion of the diaphragm, and right anterior serratus muscle in the conditions of respiratory rest, maximum inspiration, and the respiratory cycle in the stroke group. The pectoralis major muscle plays a role during forced inspiration, the diaphragm is involved in both inspiration and expiration, and the serratus anterior muscle has an accessory role in the inspiratory phase.

There is a correlation between motor and respiratory disorders in stroke because trunk muscles are related to both postural control and breathing control (Howard et al., 2001; Lanini et al., 2003). When evaluating electromyographic activity in the clinical condition of maximal expiration, the right sternocleidomastoid and right diaphragm muscles showed higher activity, likely as an adaptation to reach the expiratory reserve volume. According to the study by Li et al. (2022), negative changes in skeletal muscle associated with aging can occur after a stroke due to the loss of type I muscle fibers, which can lead to muscle deficiencies not only in the affected hemibody but also in the contralateral limb, ultimately resulting in reduced physical performance.

The results of this study showed significant reductions in both inspiratory and expiratory muscle strength in post-stroke subjects compared to the group without neurological disorders when evaluating respiratory muscle strength. When performing a literature review, we observed that subjects who have suffered ischemic and hemorrhagic strokes tend to experience reductions in inspiratory and expiratory muscle strength, as well as pulmonary function. Studies show significant and effective results when respiratory muscle training is performed, with improvements in inspiratory and expiratory strength, lung function, and dyspnea, leading to consequent benefits in daily living activities (Menezes et al., 2018). The study by Yang et al. (2015) aimed to investigate the effects of respiratory muscle training combined with the abdominal retraction maneuver in reducing the activity and function of respiratory muscles in post-stroke subjects. The results showed activation of the diaphragm and external intercostal muscles during peak inspiratory efforts, suggesting that respiratory muscle training, in conjunction with the abdominal retraction maneuver, may improve lung function in post-stroke subjects.

Menezes et al. (2016) conducted a systematic review of randomized clinical trials involving post-stroke subjects with respiratory muscle weakness. They concluded that respiratory muscle training, performed for 30 minutes, five times a week, over 5 weeks, can increase respiratory muscle strength in fragile post-stroke subjects and reduce the risk of respiratory complications. Liaw et al. (2020) concluded that inspiratory and expiratory respiratory muscle training performed over 6 weeks is essential for post-stroke subjects to improve levels of fatigue, respiratory muscle strength, lung volume, and respiratory flow.

When analysing the spirometric results, no significant changes in pulmonary capacities were observed. However, it was noted that the post-stroke subjects had lower average forced expiratory volume in one second, forced vital capacity, and the Tiffeneau index (forced expiratory volume in one second/forced vital capacity) compared to the group without neurological

disorders. In total, seven post-stroke subjects with right hemiparesis had a restrictive ventilatory disorder, representing 58.33% of the sample. The results of this study corroborate the findings of Rattes et al. (2018), who analysed the effects of stretching the respiratory muscles on the ventilatory pattern, as well as total and compartmental volumes through plethysmography, in post-stroke subjects with right hemiparesis. Their study found restrictive pulmonary function in some subjects, and after the intervention involving respiratory muscle stretching, there was an improvement in chest wall expansion, respiratory muscle compliance, and increases in tidal volume, minute ventilation, and inspiratory and expiratory flow.

On the other hand, the study by Ptaszkowska et al. (2019) aimed to observe the effect of a single session of proprioceptive neuromuscular facilitation on the respiratory parameters of 60 post-stroke subjects. The study concluded that the proprioceptive neuromuscular facilitation method produced positive results, contributing only to an increase in the Tiffeneau index.

There were some limitations in this study, such as limitations in the selection of subjects for the sample composition due to diagnostic variability within the stroke group, difficulties in controlling the evaluation period, and the absence of evaluative scales for spasticity and the degree of sarcopenia to confirm the diagnostic hypotheses related to electromyographic activity.

Conclusion

Subjects who have had a stroke experience neuromuscular deficit, with significant changes in the electromyographic activity of respiratory and accessory muscles, in addition to a reduction in respiratory muscle strength and lung volumes and capacities. Therefore, it is recommended to implement early respiratory muscle training for these subjects, combined with motor rehabilitation, due to the involvement of the entire musculoskeletal system caused by the pathology, with the goal of achieving complete and adequate rehabilitation for this population.

References

Abbaspour, S., Fallah, A. (2014) A combination method for electrocardiogram rejection from surface electromyogram. *Open Biomed. Eng. J.* **8**, 13–19.

Alonso, J. F., Mañanas, M. A., Rojas, M., Bruce, E. N. (2011) Coordination of respiratory muscles assessed by means of nonlinear forecasting of demodulated myographic signals. *J. Electromyogr. Kinesiol.* **21**, 1064–1073.

Carvalho-Pinto, R. M., Cançado, J. E. D., Pizzichini, M. M. M., Fiterman, J., Rubin, A. S., Cerci Neto, A., Cruz, Á. A., Fernandes, A. L. G., Araujo, A. M. S., Blanco, D. C., Cordeiro Junior, G., Caetano, L. S. B., Rabahi, M. F., Menezes, M. B., Oliveira, M. A., Lima, M. A., Pitrez, P. M. (2021) 2021 Brazilian Thoracic Association recommendations for the management of severe asthma. *J. Bras. Pneumol.* **47**, e20210273.

Chen, Y. K., Qu, J. F., Xiao, W. M., Li, W. Y., Weng, H. Y., Li, W., Liu, Y. L., Luo, G. P., Fang, X. W., Ungvari, G. S., Xiang, Y. T. (2015) Poststroke fatigue: Risk factors and its effect on functional status and health-related quality of life. *Int. J. Stroke* **10**, 506–512.

Costa, D., Gonçalves, H. A., Lima, L. P., Ike, D., Cancelliero, K. M., Montebelo, M. I. (2010) New reference values for maximal respiratory pressures in the Brazilian population. *J. Bras. Pneumol.* **36**, 306–312.

da Silva, G. P., Verri, E. D., Palinkas, M., Gonçalves, C. R., Gonçalves, P. N., Lopes, R. F. T., Gomes, G. G. C., Regalo, I. H., Siéssere, S., Regalo, S. C. H. (2022) Impact of hemorrhagic stroke on molar bite force: A prospective study. *Prague Med. Rep.* **123(3)**, 181–187.

De Luca, C. J. (1997) The use of surface electromyography in biomechanics. *J. Appl. Biomech.* **13**, 135–163.

Di Palma, E., Tepedino, M., Chimenti, C., Tartaglia, G., Sforza, C. (2017) Effects of the functional orthopaedic therapy on masticatory muscles activity. *J. Clin. Exp. Dent.* **9**, e886–e891.

Duncan, P. W., Bushnell, C., Sissine, M., Coleman, S., Lutz, B. J., Johnson, A. M., Radman, M., Pvru Bettger, J., Zorowitz, R. D., Stein, J. (2021) Comprehensive stroke care and outcomes: Time for a paradigm shift. *Stroke* **52**, 385–393.

Feigin, V. L., Brainin, M., Norrving, B., Martins, S. O., Pandian, J., Lindsay, P., Grupper, M. F., Rautalin, I. (2025) World Stroke Organization: Global stroke fact sheet 2025. *Int. J. Stroke* **20**, 132–144.

Gomes, G. G. C., Palinkas, M., da Silva, G. P., Gonçalves, C. R., Lopes, R. F. T., Verri, E. D., Fabrin, S. C. V., Fioco, E. M., Siéssere, S., Regalo, S. C. H. (2022) Bite force, thickness, and thermographic patterns of masticatory muscles post-hemorrhagic stroke. *J. Stroke Cerebrovasc. Dis.* **31**, 106173.

Hawkes, E. Z., Nowicky, A. V., McConnell, A. K. (2007) Diaphragm and intercostal surface EMG and muscle performance after acute inspiratory muscle loading. *Respir. Physiol. Neurobiol.* **155**, 213–219.

Hermens, H. J., Freriks, B., Disselhorst-Klug, C., Rau, G. (2000) Development of recommendations for SEMG sensors and sensor placement procedures. *J. Electromyogr. Kinesiol.* **10**, 361–374.

Hilkens, N. A., Casolla, B., Leung, T. W., de Leeuw, F. E. (2024) Stroke. *Lancet* **403**, 2820–2836.

Howard, R. S., Rudd, A. G., Wolfe, C. D., Williams, A. J. (2001) Pathophysiological and clinical aspects of breathing after stroke. *Postgrad. Med. J.* **77**, 700–702.

Jian, C., Wei, M., Luo, J., Lin, J., Zeng, W., Huang, W., Song, R. (2017) Multiparameter electromyography analysis of the masticatory muscle activities in subjects with brainstem stroke at different head positions. *Front. Neurol.* **8**, 1–10.

Lanini, B., Bianchi, R., Romagnoli, I., Coli, C., Binazzi, B., Gigliotti, F., Pizzi, A., Grippo, A., Scano, G. (2003) Chest wall kinematics in subjects with hemiplegia. *Am. J. Respir. Crit. Care Med.* **168**, 109–113.

Laufer, Y., Schwarzmann, R., Sivan, D., Sprecher, E. (2005) Postural control of subjects with hemiparesis: Force plates measurements

based on the clinical sensory organization test. *Physiother. Theory Pract*. **21**, 163–171.

Li, S., Gonzalez-Buonomo, J., Ghuman, J., Huang, X., Malik, A., Yozbatiran, N., Magat, E., Francisco, G. E., Wu, H., Frontera, W. R. (2022) Aging after stroke: How to define post-stroke sarcopenia and what are its risk factors? *Eur. J. Phys. Rehabil. Med*. **58**, 683–692.

Liaw, M. Y., Hsu, C. H., Leong, C. P., Liao, C. Y., Wang, L. Y., Lu, C. H., Lin, M. C. (2020) Respiratory muscle training in stroke subjects with respiratory muscle weakness, dysphagia, and dysarthria – A prospective randomized trial. *Medicine (Baltimore)* **99**, e19337.

Lisabeth, L. D., Baek, J., Morgenstern, L. B., Zahuranec, D. B., Case, E., Skolarus, L. E. (2018) Prognosis of midlife stroke. *J. Stroke Cerebrovasc. Dis*. **27**, 1153–1159.

Lopes, R. F. T., Palinkas, M., Pádua da Silva, G., Verri, E. D., Regalo, I. H., Gonçalves, C. R., Hallak, J. E. C., Costa Gomes, G. G., Regalo, S. C. H., Siéssere, S. (2023) Stroke: An electromyographic approach to the masseter and temporal muscles, orofacial soft tissue pressure, and occlusal force. *PLoS One* **18**, e0282362.

Marcucci, F. C. I., Cardoso, N. S., Berteli, K. D. S., Garanhani, M. R., Cardoso, J. R. (2007) Electromyographic alterations of trunk muscle of subjects with post-stroke hemiparesis. *Arq. Neuropsiquiatr*. **65**, 900–905. (in Portuguese)

Menezes, K. K. P., Nascimento, L. R., Ada, L., Polese, J. C., Avelino, P. R., Teixeira-Salmela, L. F. (2016) Respiratory muscle training increases respiratory muscle strength and reduces respiratory complications after stroke: A systematic review. *J. Physiother.* **62**, 138–144.

Menezes, K. K. P., Nascimento, L. R., Avelino, P. R., Alvarenga, M. T. M., Teixeira-Salmela, L. F. (2018) Efficacy of interventions to improve respiratory function after stroke. *Respir. Care* **63**, 920–933.

Miller, M. R. (2005) Standardisation of spirometry. *Eur. Respir. J*. **26**, 319–338.

Okumuş, B., Akıncı, B., Aytutuldu, G. K., Baran, M. S. (2025) Impact of upper extremity robotic rehabilitation on respiratory parameters, functional capacity and dyspnea in subjects with stroke: A randomized controlled study. *Neurol. Sci*. **46**, 1257–1266.

Ptaszkowska, L., Ptaszkowski, K., Halski, T., Taradaj, J., Dymarek, R., Paprocka-Borowicz, M. (2019) Immediate effects of the respiratory stimulation on ventilation parameters in ischemic stroke survivors: A randomized interventional study (CONSORT). *Medicine (Baltimore)* **98**, e17128.

Rattes, C., Campos, S. L., Morais, C., Gonçalves, T., Sayão, L. B., Galindo-Filho, V. C., Parreira, V., Aliverti, A., Dornelas de Andrade, A. (2018) Respiratory muscles stretching acutely increases expansion in hemiparetic chest wall. *Respir. Physiol. Neurobiol*. **254**, 16–22.

Santos, G. L. D., Silva, E. S. M. D., Desloovere, K., Russo, T. L. (2019) Effects of elastic tape on kinematic parameters during a functional task in chronic hemiparetic subjects: A randomized sham-controlled crossover trial. *PLoS One* **14**, e0211332.

Schimmel, M., Voegeli, G., Duvernay, E., Leemann, B., Müller, F. (2017) Oral tactile sensitivity and masticatory performance are impaired in stroke subjects. *J. Oral Rehabil*. **44**, 163–171.

Verheyden, G., Vereeck, L., Truijen, S., Troch, M., Lafosse, C., Saeys, W., Leenaerts, E., Palinckx, A., De Weerdt, W. (2009) Additional exercises improve trunk performance after stroke: A pilot randomized controlled trial. *Neurorehabil. Neural Repair*. **23**, 281–286.

Yang, D. J., Park, S. K., Kim, J. H., Heo, J. W., Lee, Y. S., Uhm, Y. H. (2015) Effect of changes in postural alignment on foot pressure and walking ability of stroke subjects. *J. Phys. Ther. Sci*. **27**, 2943–2945.

Impact of Age and Gender on Mean QT and QTc Intervals Measured with Ambulatory Electrocardiogram Monitoring

Oleksii Skakun[1], Ihor Vandzhura[2], Yaroslava Vandzhura[2], Roksolana Denina[2]

[1] St. Luke's Clinic, Ivano-Frankivsk, Ukraine;
[2] Department of Internal Medicine No. 2 and Nursing, Ivano-Frankivsk National Medical University, Ivano-Frankivsk, Ukraine

Received December 4, 2024; Accepted November 21, 2025.

Key words: Age – Sex – Gender – QT interval – QTc interval – Ambulatory ECG

Abstract: Although the impact of age and gender on QT and QTc intervals on conventional electrocardiogram (ECG) has been well studied, the impact of these factors on mean QT and QTc intervals measured with ambulatory ECG monitoring has not been studied. The aim of this study was to assess the impact of age and gender on mean QT and QTc intervals measured with ambulatory ECG monitoring. Recordings of ambulatory ECG monitoring from 380 patients without significant cardiac abnormalities were analysed. The mean QT interval was longer in women (390.5 [373.0–405.0] ms) than in men (380.0 [366.0–397.5] ms) ($p<0.001$). The mean QTc interval was also longer in women (439.0 [429.0–447.5] ms) than in men (428.5 [417.0–441.0] ms) ($p<0.001$). The normal (2.5–97.5 percentiles) mean QTc interval measured with ambulatory ECG monitoring ranged from 393 to 466 ms in men and from 411 to 471 ms in women. QT and QTc intervals increased with age ($p<0.001$). There was a positive correlation between age and QT interval ($r=0.474$, $p<0.001$) as well as between age and QTc interval ($r=0.263$, $p<0.001$). Thus, female gender is associated with longer mean QT and QTc intervals measured with ambulatory ECG monitoring. QT and QTc intervals become longer with age.

Mailing Address: Oleksii Skakun, MD., PhD., St. Luke's Clinic, Garbarska Str. 22, Ivano-Frankivsk, 76019, Ukraine; e-mail: olexiy109921@ukr.net

https://doi.org/10.14712/23362936.2025.32

Prague Medical Report / Vol. 126 (2025) No. 4, p. 201–206

Introduction

The QT interval on the electrocardiogram (ECG) reflects the depolarization and repolarization of the ventricles (Locati et al., 2017). It's calculated as the distance from the first deflection of the QRS complex to the end of the T wave (Monitillo et al., 2016). As heart rate has a significant effect on the QT interval, a corrected form of the QT interval is generally used. A Bazett's formula is the most commonly used to measure the corrected QT interval (QTc interval) (Rezuş et al., 2015).

In healthy individuals, the QTc interval measured by conventional ECG ranges from 350 to 450 ms for men and from 360 to 460 ms for women (Zhang et al., 2011). Both shortened and prolonged QTc intervals are associated with an increased risk of cardiovascular mortality (Straus et al., 2006; Rezuş et al., 2015).

It's known that age and gender influence the QTc interval (Annamalai et al., 2014; Khaleel et al., 2014). However, all studies compared QT and QTc intervals with conventional ECG, while normal ranges of these intervals measured with ambulatory ECG monitoring and the impact of age and gender on these intervals are poorly studied.

This study aims to assess the impact of age and gender on mean QT and QTc intervals measured with ambulatory ECG monitoring.

Material and Methods

Study design

This was cross-sectional study. Ambulatory 24-hour ECG recordings were analysed.

Setting

The study included all ambulatory ECG monitoring recordings performed between October 2022 and December 2024 from 380 patients, except for those who met the exclusion criteria. The recordings were extracted from St. Luke's Clinic database. Each recording was analysed using Labtech Cardiospy software.

Participants

Recordings from 380 patients were included in the study. Presence of any factor that may impact QT interval was an exclusion criterion.

Inclusion criterion:

- Ambulatory ECG recordings from individuals of both genders.

Exclusion criteria:

- Any episode of atrial fibrillation or atrial flutter;
- More than 1,000 premature atrial or ventricular contractions;
- Average heart rate <55 bpm or >100 bpm;
- Any episode of type 2 sinus exit block or sinus arrest;
- Maximum PR interval ≥250 ms;
- ≥10 episodes of second-degree atrioventricular block, Mobitz-I;
- Second-degree atrioventricular block, Mobitz-II;
- Complete atrioventricular block;
- QRS complex width ≥120 ms (left or right bundle branch block or non-specific ventricular conduction delay);
- Any type of implanted cardiac pacemaker;
- Wolff-Parkinson-White syndrome;
- Previously diagnosed long QT syndrome;
- Any abnormality of ST segment or T wave;
- Known moderate/severe valvar abnormalities, ventricular hypertrophy or dilation;
- Previously diagnosed coronary artery disease;
- Known use of drugs that prolong the QT interval.

Variables

Mean QT interval, mean QTc interval and percentage of monitoring time with QT/QTc interval above 450 ms were analysed. The Bazett's formula was used to calculate the QTc interval.

Statistical methods

Statistical processing was performed using MS Excel and MedCalc. The distribution of variables was assessed using Shapiro-Wilk test. Data with an abnormal distribution are presented as the median value with lower and upper quartiles. Mann-Whitney U test, Kruskal-Wallis with post-hoc Dunn test, Jonckheere-Terpstra test and Spearman correlation were used. Linear regression analysis was carried out. A p-value < 0.05 was considered to be significant.

Results

Descriptive data

The median age of the patients was 42.0 (31.0–59.0) years. There were 188 (49.5%) males and 192 (50.5%) females. The mean heart rate was 78.5 (72.5–85.0) bpm. Characteristics of the QT and QTc intervals in all included recordings are shown in Table 1.

Gender differences

Mean QT and QTc intervals were compared between men and women (Table 2). QT interval ($p<0.001$) and QTc interval ($p<0.001$) were higher in women than in men. Also, the percentage of monitoring time with QT interval above 450 ms ($p<0.001$) and percentage

of monitoring time with QTc interval above 450 ms ($p<0.001$) were higher in women than in men.

Age differences

QT and QT interval lengthened with age (Table 3). According to the Jonckheere-Terpstra test, there was an increasing trend in both the mean QT interval ($p<0.001$) and the mean QTc interval ($p<0.001$) with age. There was positive correlation between age and QT interval ($r=0.474$, $p<0.001$) as well as between age and QTc interval ($r=0.263$, $p<0.001$). Figure 1 shows the regression analysis of age and

Table 1: Percentiles of QT and QTc intervals in all enrolled patients

Parameter	Percentiles				
	2.5	25	median	75	97.5
Mean QT interval, ms	344.00	369.0	384.5	400.0	455.0
Mean QTc interval, ms	400.00	421.0	433.5	444.0	467.0
Percentage of monitoring time with QT interval above 450 ms, %	0.00	0.0	0.0	3.6	53.8
Percentage of monitoring time with QTc interval above 450 ms, %	1.01	6.2	15.1	32.7	86.1

Table 2: Percentiles of QT and QTc intervals in men and women

Parameter		Percentiles				
		2.5	25	median	75	97.5
Men	Mean QT interval, ms	342.4	366.0	380.0	397.5	432.2
	Mean QTc interval, ms	393.0	417.0	428.5	441.0	466.0
	Percentage of monitoring time with QT interval above 450 ms, %	0.0	0.0	0.0	0.4	32.8
	Percentage of monitoring time with QTc interval above 450 ms, %	0.7	4.9	9.8	24.9	77.3
Women	Mean QT interval, ms	348.0	373.0	390.5	405.0	458.0
	Mean QTc interval, ms	411.3	429.0	439.0	447.5	470.8
	Percentage of monitoring time with QT interval above 450 ms, %	0.0	0.0	0.0	7.3	57.7
	Percentage of monitoring time with QTc interval above 450 ms, %	1.2	9.0	22.5	42.9	91.8

Table 3: QT and QTc intervals in different age groups

Age, years	<25 (n=39)[1]	25–39 (n=135)[2]	40–54 (n=88)[3]	55–69 (n=95)[4]	≥70 (n=23)[5]	p
Mean QT interval, ms	373.0 (358.8–383.5)	376.0 (361.0–392.8)	381.0 (369.0–396.0)	400.0 (390.0–415.0)	401.0 (391.3–425.8)	Kruskal-Wallis test: $p<0.001$ Post-hoc Dunn test: $p_{1-4}<0.05$ $p_{1-5}<0.05$ $p_{2-4}<0.05$ $p_{2-5}<0.05$ $p_{3-4}<0.05$ $p_{3-5}<0.05$
Mean QTc interval, ms	429.0 (419.3–437.0)	431.0 (417.3–441.0)	436.5 (426.0–447.0)	441.0 (429.3–449.0)	442.0 (422.0–453.3)	Kruskal-Wallis test: $p<0.001$ Post-hoc Dunn test: $p_{1-3}<0.05$ $p_{1-4}<0.05$ $p_{2-4}<0.05$

Prague Medical Report / Vol. 126 (2025) No. 4, p. 201–206

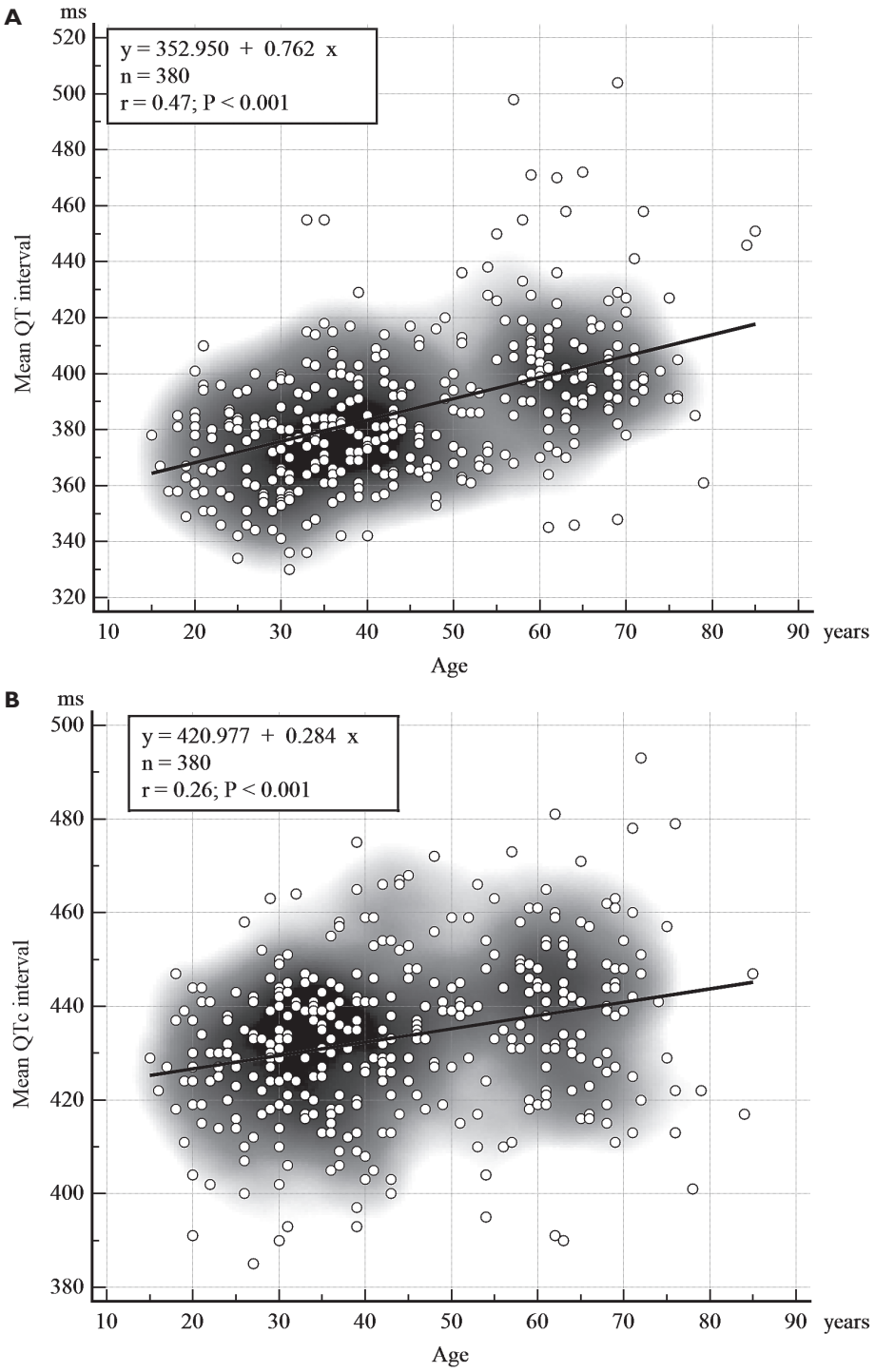

Figure 1: Regression analysis showing the relationship between age and mean QT interval (A) as well as age and mean QTc interval (B).

QT/QTc interval. There were following coefficients of determination R^2: 0.225 for QT interval and age, 0.069 for QTc interval and age.

Discussion

Our study didn't include patients with significant cardiac abnormalities and factors that may affect the QT interval. According to our study, the normal mean QTc interval measured by ambulatory ECG monitoring ranged from 393 to 466 ms in men and from 411 to 471 ms in women (2.5–97.5 percentiles). These results are somewhat controversial as the upper limit of the norm for the QTc interval on conventional ECG is considered to be 450 ms in men and 460 ms in women (Viskin, 2009). However, these values may be revised as 10–20% of otherwise healthy individuals

have values of QTc interval outside the normal range (Rezuş et al., 2015).

Although a range of smart devices can measure the QT interval (Utomo et al., 2021; Hoek et al., 2023; Alam et al., 2024), the normal mean QT/QTc interval measured by ambulatory ECG monitoring has been poorly studied. Lutfullin et al. (2013) studied the QT/QTc interval in athletes using ambulatory ECG monitoring; athletes without left ventricular hypertrophy had a mean QT interval of 422.0 ± 12.6 ms and a QTc interval of 412.0 ± 20.3 ms, which is similar to our data.

We have found that mean QT and QTc intervals measured with ambulatory ECG monitoring are 2.8 and 2.5% longer, respectively, in women than in men. Several studies have found that women have longer QT/QTc intervals on conventional ECG than men (Burke et al., 1997; Rautaharju et al., 2014; Rabkin, 2015), which is consistent with our findings on ambulatory ECG monitoring. However, one study with a small number of patients showed the opposite result – male gender was associated with a longer QT/QTc interval (Satpathy et al., 2018).

It was found that QT interval prolongation is associated with increased all-cause mortality (Schouten et al., 1991; Adabag et al., 2024). Many non-cardiac conditions are associated with prolongation of QT and QTc intervals: Graves's disease (Lee et al., 2015; Kirac et al., 2023), hyperglycaemia (Ninkovic et al., 2016), liver cirrhosis (Tsiompanidis et al., 2018), cerebral contusion (Yavuz et al., 2023), acidosis (Yenigun et al., 2016), hypothermia (Khan et al., 2010), electrolyte abnormalities and medications (TeBay et al., 2022). However, a 10-ms increase in the QTc interval was significantly greater associated with an increased mortality risk in men compared to women (4.6 vs. 2.4%) (Williams et al., 2012).

Also, some studies found that QT/QTc interval on conventional ECG increases with age (Rautaharju et al., 2014; Rabkin et al., 2016). Our study shows a similar tendency: QT and QTc intervals positively correlate with age. Specifically, the QT interval increases by 0.762 ms for every 1 year of age, and the QTc interval increases by 0.284 ms for every 1 year of age.

To minimize bias at the upper normal limits, some age- and gender-specific criteria for QT prolongation based on rate correction formulas were proposed (Rautaharju et al., 2014). However, their clinical relevance has been poorly established.

Our study has several limitations. First, all enrolled patients were Caucasian, so extrapolation of the results to other ethnicities should be cautious. Due to a higher burden of comorbidities, older patients were more likely to meet the exclusion criteria and their proportion in our study was lower. Minimal and maximal QT/QTc intervals were not studied, as these parameters are more sensitive to heart rate and artefacts.

Conclusion

Female gender is associated with longer mean QT and QTc intervals measured with ambulatory ECG monitoring. QT and QTc intervals become longer with ageing. The percentage of monitoring time with a QT/QTc interval above 450 ms appears to be of little value because of the very wide range in healthy individuals.

References

Adabag, S., Gravely, A., Kattel, S., Buelt-Gebhardt, M., Westanmo, A. (2024) QT prolongation predicts all-cause mortality above and beyond a validated risk score. *J. Electrocardiol.* **83**, 1–3.

Alam, R., Aguirre, A., Stultz, C. M. (2024) Detecting QT prolongation from a single-lead ECG with deep learning. *PLOS Digit. Health* **3**, e0000539.

Annamalai, N., Revathi, M., Palaniappan, A., Rajajeyakumar, M. (2014) Impact of age and gender on QTc interval – A retrospective study. *Int. J. Appl. Basic Med. Sci.* **4**, 308–312.

Burke, J. H., Ehlert, F. A., Kruse, J. T., Parker, M. A., Goldberger, J. J., Kadish, A. H. (1997) Gender-specific differences in the QT interval and the effect of autonomic tone and menstrual cycle in healthy adults. *Am. J. Cardiol.* **79**, 178–181.

Hoek, L. J., Brouwer, J. L. P., Voors, A. A., Maass, A. H. (2023) Smart devices to measure and monitor QT intervals. *Front. Cardiovasc. Med.* **10**, 1172666.

Khaleel, Y. M., Al-Selevany, B. K., Mahmood, M. F. (2014) Effect of age and gender on corrected QT interval in healthy adults. *J. Bahrain Med. Soc.* **25**, 24–28.

Khan, J. N., Prasad, N., Glancy, J. M. (2010) QTc prolongation during therapeutic hypothermia: Are we giving it the attention it deserves? *Europace* **12**, 266–270.

Kirac, C. O., Sirikci, V., Findikli, H. A. (2023) Evaluation of the Tpeak-Tend interval as an arrhythmogenicity index in Graves' disease. *Galician Med. J.* **30**, E202324.

Lee, Y. S., Choi, J. W., Bae, E. J., Park, W. I., Lee, H. J., Oh, P. S. (2015) The corrected QT (QTc) prolongation in hyperthyroidism and the association of thyroid hormone with the QTc interval. *Korean J. Pediatr.* **58**, 263–266.

Locati, E. T., Bagliani, G., Padeletti, L. (2017) Normal ventricular repolarization and QT interval: Ionic background, modifiers, and measurements. *Card. Electrophysiol. Clin.* **9**, 487–513.

Lutfullin, I. Y., Kim, Z. F., Bilalova, R. R., Tsibulkin, N. A., Almetova, R. R., Mudarisova, R. R., Ahmetov, I. I. (2013) A 24-hour ambulatory ECG monitoring in assessment of QT interval duration and dispersion in rowers with physiological myocardial hypertrophy. *Biol. Sport* **30**, 237–241.

Monitillo, F., Leone, M., Rizzo, C., Passantino, A., Iacoviello, M. (2016) Ventricular repolarization measures for arrhythmic risk stratification. *World J. Cardiol.* **8**, 57–73.

Ninkovic, V. M., Ninkovic, S. M., Miloradovic, V., Stanojevic, D., Babic, M., Giga, V., Dobric, M., Trenell, M. I., Lalic, N., Seferovic, P. M., Jakovljevic, D. G. (2016) Prevalence and risk factors for prolonged QT interval and QT dispersion in patients with type 2 diabetes. *Acta Diabetol*. **53**, 737–744.

Rabkin, S. W. (2015) Impact of age and sex on QT prolongation in patients receiving psychotropics. *Can. J. Psychiatry* **60**, 206–214.

Rabkin, S. W., Cheng, X. J., Thompson, D. J. (2016) Detailed analysis of the impact of age on the QT interval. *J. Geriatr. Cardiol*. **13**, 740–748.

Rautaharju, P. M., Mason, J. W., Akiyama, T. (2014) New age- and sex-specific criteria for QT prolongation based on rate correction formulas that minimize bias at the upper normal limits. *Int. J. Cardiol*. **174**, 535–540.

Rezuş, C., Moga, V. D., Ouatu, A., Floria, M. (2015) QT interval variations and mortality risk: Is there any relationship? *Anatol. J. Cardiol.* **15**, 255–258.

Satpathy, S., Satpathy, S., Nayak, P. K. (2018) Effect of age and gender on QT interval. *Natl. J. Physiol. Pharm. Pharmacol.* **8**, 224–227.

Schouten, E. G., Dekker, J. M., Meppelink, P., Kok, F. J., Vandenbroucke, J. P., Pool, J. (1991) QT interval prolongation predicts cardiovascular mortality in an apparently healthy population. *Circulation* **84**, 1516–1523.

Straus, S. M., Kors, J. A., De Bruin, M. L., van der Hooft, C. S., Hofman, A., Heeringa, J., Deckers, J. W., Kingma, J. H., Sturkenboom, M. C., Stricker, B. H., Witteman, J. C. (2006) Prolonged QTc interval and risk of sudden cardiac death in a population of older adults. *J. Am. Coll. Cardiol.* **47**, 362–367.

TeBay, C., Hill, A. P., Windley, M. J. (2022) Metabolic and electrolyte abnormalities as risk factors in drug-induced long QT syndrome. *Biophys. Rev.* **14**, 353–367.

Tsiompanidis, E., Siakavellas, S. I., Tentolouris, A., Eleftheriadou, I., Chorepsima, S., Manolakis, A., Oikonomou, K., Tentolouris, N. (2018) Liver cirrhosis-effect on QT interval and cardiac autonomic nervous system activity. *World J. Gastrointest. Pathophysiol.* **9**, 28–36.

Utomo, T. P., Nuryanim, N., Nugroho, A. S. (2021) A new automatic QT-interval measurement method for wireless ECG monitoring system using smartphone. *J. Biomed. Phys. Eng.* **11**, 641–652.

Viskin, S. (2009) The QT interval: Too long, too short or just right. *Heart Rhythm* **6**, 711–715.

Williams, E. S., Thomas, K. L., Broderick, S., Shaw, L. K., Velazquez, E. J., Al-Khatib, S. M., Daubert, J. P. (2012) Race and gender variation in the QT interval and its association with mortality in patients with coronary artery disease: Results from the Duke Databank for Cardiovascular Disease (DDCD). *Am. Heart J.* **164**, 434–441.

Yavuz, A. Y., Baskurt, O., Kurtulus, Y., Avci, I. (2023) Prognostic significance of prolonged corrected QT interval in cerebral contusion. *Indian J. Med. Res*. **158**, 175–181.

Yenigun, E. C., Aypak, C., Turgut, D., Aydin, M. Z., Dede, F. (2016) Effect of metabolic acidosis on QT intervals in patients with chronic kidney disease. *Int. J. Artif. Organs* **39**, 272–276.

Zhang, Y., Post, W. S., Blasco-Colmenares, E., Dalal, D., Tomaselli, G. F., Guallar, E. (2011) Electrocardiographic QT interval and mortality: A meta-analysis. *Epidemiology* **22**, 660–670.

Long-term Graft Patency of Saphenous Vein Grafts after Endoscopic Harvest in Aortocoronary Bypass Surgery

Okaikor Okantey[1,3], Tomáš Jonszta[2,3], Lubomír Pavliska[4], Jiří Sieja[1,3], Miriam Kende[1,3], Radim Brát[1,3]

[1] Department of Cardiac Surgery, University Hospital Ostrava, Ostrava, Czech Republic;
[2] Department of Radiology, University Hospital Ostrava, Ostrava, Czech Republic;
[3] Faculty of Medicine, University of Ostrava, Ostrava, Czech Republic;
[4] Department of Science and Research, University Hospital Ostrava, Ostrava, Czech Republic

Received November 20, 2024; Accepted November 21, 2025.

Key words: Graft patency – Endoscopic vein harvest – Coronary artery bypass grafting – Saphenous vein

Abstract: Endoscopic vein harvest of the greater saphenous vein for aortocoronary bypass grafting presents a relatively newer and less invasive mode of vein harvest that has become a more popular approach used in the field of cardiac surgery. This study aimed to compare the long-term patency of saphenous vein grafts and clinical outcomes (a minimum of 10 years) after endoscopic harvest with open vein harvest in patients after isolated surgical myocardial revascularization. Fifty patients (25 after endoscopic and 25 after open harvest) who underwent isolated myocardial revascularization between 2009 and 2011 assessed. The study comprised two phases: completion of questionnaires assessing recurring symptoms of ischemic heart disease and visualisation of vein grafts via coronary computed tomography angiography to assess graft patency. The primary outcome showed higher patency rates after open vein harvest (76.1 vs. 68.8%); without significant statistical difference (p=0.873). Differences in clinical outcomes were not statistically significant regarding recurring angina (28% endoscopic group, 32% open group, p=0.519), dyspnea (24 vs. 16%, p=0.817) and myocardial infarctions with catheter-based revascularization of vein grafts (8% endoscopic group, 16% open, p=0.734). Redo surgery was not reported in neither group. Endoscopic and open vein harvest yielded comparable long-term patency rates both angiographically and clinically. That strenghtens endoscopic approach as a non-inferior mode to the traditional approach in patients undergoing surgical myocardial revascularization.

This study was supported by the Ministry of Health of the Czech Republic – conceptual development of research organization (FNOs/2020).

Mailing Address: Okaikor Okantey, MD., Department of Cardiac Surgery, University Hospital Ostrava, 17. listopadu 1790/5, 70852 Ostrava, Czech Republic; Mobile Phone: +420 732 890 200; e-mail: okaikor.okantey@fno.cz

https://doi.org/10.14712/23362936.2025.33

Prague Medical Report / Vol. 126 (2025) No. 4, p. 207–214

Introduction

Coronary artery bypass grafting (CABG) refers to a surgical treatment modality for ischemic heart disease that resolves obstructive coronary artery disease by re-routing and restoring optimal oxygenated blood flow to compromised parts of the myocardium. The ultimate goal of surgical revascularization of the myocardium is to achieve long-term improvement of the quality of life of patients with chronic or acute ischemic heart disease, symptomatic or asymptomatic with hemodynamically significant stenotic or totally occluded coronary arteries, with respect to the elimination of the occurrence or recurrence of angina pectoris, prevention of acute myocardial infarction, prevention of life-threatening ischemia-related ventricular arrhythmias, improving exercise tolerance, and preventing sudden death (Ivaniuk et al., 2016). Arterial or venous graft patency plays an important role in achieving long-term clinical outcomes of CABG. The greater saphenous vein (GSV) is widely known to be one of the most common and readily accessible conduits employed in surgical myocardial revascularization. Currently, two common approaches to vein harvest exist: the traditional open vein harvest (OVH) and the more recently introduced endoscopic vein harvest (EVH). Unlike conventional OVH, which requires a long incision corresponding to the length of the needed graft, EVH is a minimally invasive video-assisted approach for harvesting the. Since the inception of EVH, extensive comparative studies of leg wound morbidity between OVH and EVH have been conducted, has been proven to manifest significantly lower leg-wound morbidity rates after CABG (Aziz et al., 2005; Chiu et al., 2006; Yokoyama et al., 2021). However, few studies have evaluated long-term graft patency after EVH with its associated clinical outcomes. Some studies have documented an association between EVH and a higher incidence of early graft failure via vascular endothelial damage, triggering an inflammatory response and the subsequent activation of the coagulation cascade, thus facilitating early graft failure.

This study aimed to angiographically assess and compare the long-term graft patency, a minimum of 10 years after CABG, between saphenous vein grafts (SVGs) after EVH and OVH, and also comparing the clinical outcomes after bypass surgery.

Material and Methods

Study design

This was an observational, retrospective single-centre study approved by the local ethics Committee of the University Hospital; ethical approval number: 402/2020, project protocol number: 01/RVO-FNOs/2020. All cohorts were selected in chronological order from the date of CABG via the database of the Department of Cardiac Surgery, University Hospital Ostrava. This study retrospectively examined patients to assess vein graft patency via radiological imaging and subsequent clinical outcomes at a minimum follow-up time of 10 years after CABG.

Inclusion criteria

Adult patients between the ages of 18–85 years who had undergone isolated CABG from 2009 to 2011 with at least one saphenous vein graft and consenting participants.

Exclusion criteria

Moderate to severe chronic renal impairment as a relative contraindication for application of intravenous contrast material for radiographic imaging methods, non-consenting patients, deceased patients, conversion of EVH to OVH, and CABG with only arterial grafts, including MIDCAB (minimally invasive direct coronary artery bypass) procedure, a minimally-invasive method of myocardial revascularization of the left anterior descending artery (in some cases, diagonal branches of the left anterior descending [LAD] artery) via left-sided anterolateral thoracotomy within the fourth or fifth intercostal space.

Through telephone contacts extracted from the hospital database, the purpose of the study was extensively explained to the patients or relatives, and an invitation for examination was extended to free willing participants.

Methods

Two hundred and eighty-three patients who underwent isolated CABG, regardless of the urgency of surgery, from November 2009 to March 2011 were enrolled from the departmental surgery records in chronological order. After CABG, all patients were encouraged to use a combination of antiaggregation therapy (for at least 1 year) and cholesterol-lowering drugs. Fifty-eight patients were confirmed to have died by relatives and from the hospital database. Ninety-six patients refused follow-up examinations, and 74 could not be traced. Fifty-five patients agreed to be examined and were enrolled in the study (28 OVH and 27 EVH). Two written consent forms were required and signed by all cohorts for: enrolment into the study and radiological examination using coronary computed tomography angiography (CCTA). One patient in the OVH group was excluded from the study because of refusal of administration of intravenous contrast material upon arrival. Blood

Table 1: Pre- and perioperative patient characteristics and demographics

		Endoscopic vein harvest (n=25)	Open vein harvest (n=25)	P-value
Age in years (mean ± SD)		72.9 ± 7.33	72.8 ± 6.08	0.950
Gender	male, n (%)	19 (76)	21 (84)	0.981
	female, n (%)	6 (24)	4 (16)	0.817
BMI > 30 kg/m^2, n (%)		9 (36)	5 (20)	0.519
LV EF < 55%, n (%)		9 (36)	7 (28)	0.882
COPD, n (%)		5 (20)	8 (32)	0.666
Previous MI, n (%)		10 (40)	9 (36)	–
Diabetes mellitus, n (%)		13 (52)	12 (48)	–
Hypertension, n (%)		24 (96)	24 (96)	–
Dyslipidemia, n (%)		21 (84)	21 (84)	–
Tobacco use	non-smokers, n (%)	11 (44)	9 (36)	0.909
	ex-smokers, n (%)	8 (32)	9 (36)	–
	current smokers, n (%)	6 (24)	7 (28)	–
Use of ECC, n (%)		21 (84)	18 (72)	0.883
Urgency of surgery	planned, n (%)	24 (96)	16 (64)	0.463
	urgent, n (%)	1 (4)	5 (20)	0.265
	emergent, n (%)	0 (0)	4 (16)	0.158

SD – standard deviation; BMI – body mass index; LV EF – left ventricular ejection fraction; COPD – chronic obstructive pulmonary disease; MI – myocardial infarction; ECC – extracorporeal circulation

was drawn to complete renal function tests of all study cohorts upon arrival. Two patients from each group were excluded because of elevated creatinine levels upon completion of renal function tests before CCTA. The total study population comprised of 50 patients. Baseline patient characteristics and preoperative and perioperative demographics are highlighted in Table 1. During this period, EVH was performed using VirtuoSaph® Plus Endoscopic Harvest System coupled with a Terumo® endoscope (Terumo Cardiovascular Systems Corporation, MI, USA). At the time of surgery, EVH approach was via a 2–3 cm incision at the medial aspect of the knee above the GSV identified and marked using ultrasound prior to surgery. OVH was performed using a traditional surgical incision from the medial aspect of the ankle, above the saphenous vein. All vein grafts were always interrupted at least 5 minutes after systemic administration of heparin intravenously. All side branches of the vein grafts were either ligated or clipped off, dilated with a mixture of heparinized Ringer's solution and subsequently preserved and the same solution at room temperature pending anastomosis either as single or sequential grafts. Both modes of harvesting were performed by experienced cardiac surgeons with over two years experience in EVH. The cohorts, who were selected in chronological order of the date of surgery, were categorised into two groups: 25 patients (48 total vein grafts) after EVH and 25 patients (46 total vein grafts) after OVH. All patients in the EVH group underwent complete endoscopic harvesting of the SVG, without conversion to OVH. The study comprised of two phases. The first phase involved filling out questionnaires that assessed the clinical outcomes of patients with respect to angina symptoms and subsequent treatment, medical or surgical, indicative of ischemic heart disease, and risk factors of ischemic heart disease. The second phase involved the assessment of vein graft patency using CCTA as an imaging method of choice to quantify the degree of stenosis, CCTA being preferred because of its reliability, usage of low-dose radiation and noninvasiveness (Richards and Obaid, 2019). Patients were examined at a mean follow-up time of 10.67 years. We defined significant stenosis of the vein grafts as luminal occlusion greater than 49% of the total graft thrombosis.

Coronary computed tomography angiography

Computed tomography (CT) imaging was performed using a Siemens Somatom Force, double-source CT scanner with 66 ms temporal resolution and EKG-gated scanning. The software employed for image reconstruction and evaluation was Syngovia, Siemens Healthcare GmbH, CT cardiac dedicated software, and coronary vessel evaluation for semiautomatic

Prague Medical Report / Vol. 126 (2025) No. 4, p. 207–214

vessel course identification. A virtual line along the long axis of the center of the bypass graft was created, which allowed for the evaluation of vessel length, diameter, plaque size, residual lumen diameter and area.

Image analysis: All CT examinations were evaluated twice by the same radiologist for using the operative protocol to confirm the revascularized target vessels.

Statistical analysis

Results were calculated using standard statistical methods for continuous variables (*t*-test, Kruskal-Wallis test – for categorical variables using the chi-square test). Continuous variables are expressed as mean ± standard deviation, and categorical variables are expressed as percentages. Statistical significance was set at $p<0.05$.

Results

Approximately 26% of the recruited cohorts were untraceable putting the estimated survival rate at least 53.36% (34.98% OVH vs. 18.37% EVH). All-cause mortality accounted for at least 20.49%. Angiographic findings estimated the overall vein graft patency within the study population at a minimum follow-up time of 10 years at 72.3%. The primary outcome showed higher patency rates in the OVH group (76.1%) than in the EVH group (68.8%), but with no statistically significant difference at a follow-up of a minimum of 10 years after CABG within both groups (p=0.873) (Table 2).

Similarly, the secondary endpoints (Table 3), with respect to the clinical manifestations of ischemic heart disease, were as follows:

Recurring angina symptoms CCS (Canadian Cardiovascular Society) III–IV were comparable between the groups (p=0.519). Two patients in each group with totally occluded grafts did not present with recurrent angina symptoms. Recurring dyspnea on exertion were comparable in both groups p=0.058. Non-fatal myocardial infarctions after CABG were observed in 12% (6 of 50 patients) of the study cohorts, with double rates occurring within the OVH group, 16% (4 of 25 patients) than in the EVH group (2 of 25 patients), and comparable rates in both groups (p=0.734). The same figures were accounted for with respect to patients undergoing percutaneous coronary intervention (PCI) in both groups. In fact, the patients who suffered myocardial infarctions (MIs) resultant of vein graft occlusion were the same as those who underwent PCI of the grafts. With respect to individual grafts, PCI rates within OVH were 11.6% (5 of 46 grafts) versus EVH 4.35% (2 of 48 grafts), but with no statistically significant difference (p=0.256). In-stent restenosis was present in the vein graft of one patient in each group. None of the patients included in the study required repeat CABG at the time of the examination. It is important to note that all patients after CABG were treated with antiaggregation therapy (a minimum of one year) and cholesterol-lowering drugs many statins. At the time of examination, one patient in each group reported discontinuation of statins (the patient in the EVH group also reported discontinuation of

Table 2: Angiographic findings by coronary computed tomography angiography assessing saphenous vein graft occlusion at a minimum of 10 years after surgical myocardial revascularization

	Endoscopic vein harvest (n=48)	Open vein harvest (n=46)	P-value
0–49% graft stenosis, n (%)	33 (68.8)	35 (76.1)	0.873
≥ 50% – total graft thrombosis, n (%)	15 (31.2)	11 (23.9)	0.706

Table 3: Clinical outcomes of isolated surgical myocardial revascularization after a minimum of 10 years

	Endoscopic vein harvest (n=25)	Open vein harvest (n=25)	P-value
Angina pectoris CCS III–IV, n (%)	7 (28)	8 (32)	0.519
Dyspnea, NYHA III–IV, n (%)	6 (24)	4 (16)	0.817
MI with catheter-based revascularization of vein grafts, n (%)	2 (8)	4 (16)	0.734
Redo surgical myocardial revascularization, n (%)	0 (0)	0 (0)	–

NYHA – New York Heart Association; CCS – Canadian Cardiovascular Society; MI – myocardial infarction

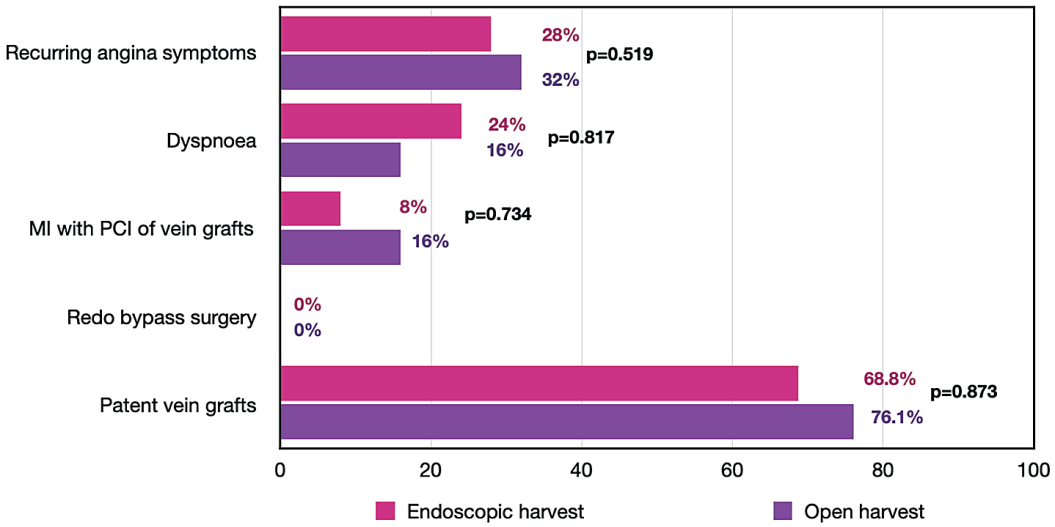

Figure 1: Summary illustrating the primary and secondary outcomes evaluated at a minimum of 10 years after surgical myocardial revascularization. MI – myocardial infarction; PCI – percutaneous coronary intervention.

antiaggregation and/or anticoagulation therapy); both patients had patent SVGs with no recurring angina symptoms. Discontinuation of antiaggregation therapy in one patient after OVH reported with thrombosis of the SVG. The category of patients who reported the use of anticoagulation therapy instead of the antiaggregation concomitantly with statins (5 of EVH and 3 of OVH) all had patent SVGs. The clinical and angiographic outcomes were not influenced by the administration of statins and antiaggregation therapy. Figure 1 summarises of the primary and secondary outcomes of this study.

Discussion

The SVG a commonly used conduit in surgical myocardial revascularization. From an evidence-based standpoint, the overall occlusion rate of the SVG after CABG is estimated to be approximately 8% after surgery, 13% at 1 year, 20% at 5 years, 41% at 10 years, and 45% at more than 11.5 years (Fitzgibbon et al., 1996; Motwani and Topol, 1998). Long-term patency rates at a minimum of 10 years, according to a review analysis, accounts for 50–60% (Gaudino et al., 2017). It is well documented that SVGs are generally more susceptible to accelerated development of atherosclerosis than native coronary arteries, subsequently limiting the duration of patency with possible poor long-term clinical outcomes after CABG. Risk factors influencing SVG disease after CABG, similar to those involved in the development of atherosclerosis in native coronary arteries, include dyslipidemia with increased LDL (low-density lipoproteins) levels and lower HDL (high-density lipoproteins) levels, cigarette smoking, hypertension, and diabetes mellitus.

Long- or short-term patency, whether of arterial of vein grafts, after surgical myocardial revascularization cumulatively depends on several intrinsic and extrinsic determinants, such as patient characteristics and the patients' compliance to treatment regimes after myocardial revascularization, surgeon's experience of both conduit harvest and construction of coronary-graft anastomosis, quality of the target vessels, and development of new hemodynamically significant occlusive lesions of the native coronary arteries after CABG etc. This opens an extensive discussion ranging from patient characteristics, lifestyle, and technical surgical factors to radical treatment strategies to decelerate the atherosclerotic processes of SVGs after CABG. Since the inception of EVH, there has been widespread speculation of relatively more frequent endothelial damage during vein harvest associated with early graft failure compared to OVH. However, every mode of harvest is associated with some degree of shear vascular wall stress from mechanical manipulation and increased distension pressure; hence, some level of endothelial damage is expected. These speculations are however not supported by sufficient clinical trials powered solely to assess long-term vein graft patency following EVH. Without sufficient evidence, a reasonable consensus regarding the safety and efficacy of EVH compared to the traditional approach of vein harvesting cannot be reached. Development and improvement of operators' skills of endoscopic vein harvest has been linked with a steep learning curve during which graft injuries arising from

Prague Medical Report / Vol. 126 (2025) No. 4, p. 207–214

thermal assault by the cautery device causing avulsion to the vasa vasorum and adventitia of the saphenous venous subsequently causing segmental vein necrosis (Krishnamoorthy et al., 2016). Overcoming this curve is crucial to reducing graft-related injuries.

According to a conducted study (Manchio et al., 2005), a strong and direct correlation was established between endothelial integrity and graft patency. After comparative histological examination of the grafts after OVH and EVH, thrombosed grafts exhibited higher rates of compromised endothelial integrity than patent vein grafts (Manchio et al., 2005). However, the difference between endothelial disruption and subsequent vein graft failure (VGF) due to thrombosis discovered within the EVH (51.24%) and OVH (49.23%) subgroups was not statistically significant. Hence, early vein graft failure could not be solely attributed to a specific mode of harvest. A histological and immunohistochemical analysis of vein grafts, showed higher rates of endothelial damage within the EVH group than in the OVH group, without any statistical significance (Aboollo et al., 2022).

A more recent follow-up study, initially powered to assess leg-wound morbidity after EVH, evaluated the patency of the SVG at a mean duration of 6.3 years using CCTA. This study showed an increased vein graft failure rate after EVH compared to OVH (p=0.001). However, there were comparable rates of recurrent angina symptoms (p=0.44), myocardial infarction (p=0.11), and all-cause mortality (p=0.15) (Andreasen et al., 2015). In this study, angiographic findings did not correlate with overall clinical outcomes. This could imply that with time following CABG, graft patency alone is not a single significant predictive factor for recurrent clinical manifestations of ischemic heart disease.

Another follow-up study from the PREVENT IV trial (Hess et al., 2014), a multicenter randomized controlled trial, powered to evaluate the effects of types of vein graft preservation solutions on graft patency after one year and subsequent clinical outcomes after 5 years, reported that EVH was associated with increased rates of vein graft failure at 12–18 months evaluated angiographically, thereby presenting an independent predictive factor in occlusive graft disease with poor clinical outcomes with regards to acute ischemic cardiac events, repeat CABG, and death. Interestingly, there was a significant difference in terms of race, that is, there were more people of African descent than Hispanics and a higher number of hypertensive patients enrolled in the EVH group than in the OVH group. This is not a coincidence, as it has been documented that the incidence of hypertension is higher among people of African descent. This may further emphasise the influence of hemodynamic pathophysiology on graft patency, with hypertension being one of the risk factors accelerating the development of atherosclerosis rather than the mode of harvest. At 3 years, EVH was also associated with poor clinical outcomes associated with EVH with respect to higher rates of myocardial infarction and repeat CABG. The PREVENT IV trial has however been associated with the poor overall graft patency therefore so many questions can be raised about attributing graft failure solely to EVH.

Results from the ROOBY trial (Zenati et al., 2011), primarily powered to compare the efficacy of on-pump and off-pump bypass grafting at 1-year angiographic follow-up, showed that grafts after EVH were associated with a higher incidence of SVG occlusion in at least one vein graft (43.1 vs. 28% after OVH, p<0.0001). However, the 30-day composite outcomes (repeat revascularization, cardiac arrest, and stroke) were comparable between the groups (p=0.60). The 1-year composite outcome showed no statistically significant difference between the cohorts that underwent OVH and EVH (p=0.061). However, the repeat revascularization rates were higher in the EVH group (p=0.033). Similar to the follow-up of the PREVENT IV trial, the clinical outcomes did not correlate with the angiographic findings, further emphasising that long-term clinical outcomes do not depend on graft patency alone.

Results from a study (Jarrett et al., 2023) showed that at 5 years, ischemia-driven revascularization of the myocardium was significantly higher in the EVH group (11.5 vs. 6.7%, p=0.047). However, the graft occlusion rates (9.7 vs. 5.4%, p=0.054) and the composite of death, myocardial infarction, and stroke (17.4 vs. 20.9%, p=0.27) at 5 years were similar between the OVH and EVH groups.

Angiogenesis of collateral blood supply or the presence of LIMA grafts, which significantly or partially compensates for occluded grafts, is capable of relieving angina symptoms to some extent in cases where new hemodynamically significant stenosis of the native coronary arteries is absent. This could partially explain why some patients with total thrombosis of the SVGs do not present with recurrent angina symptoms. On the other hand, new atherosclerotic plaques of the coronary arteries causing significant obstructive flow could account for the recurring symptoms of ischemic heart disease in patients with fully patent grafts after CABG. Reduction in the intensity of physical exertion due to old age could also mask angina symptoms in patients with new atherosclerotic plaques.

As mentioned earlier, another important and uncontrollable factor, which is patient compliance to treatment regimens with a combination of

hypolipidemics such as statins, antiaggregation therapy and antihypertensives, adequate management of other co-morbidities, lifestyle changes such as cessation of smoking that aim at controlling the rate of thrombogenesis, and atherosclerosis play a crucial role in ensuring long-term graft patency, arterial or venous. Over the years, technological enhancements in various EVH systems have facilitated the improvement of perioperative surgical conditions and outcomes of CABG. Moreover, EVH is skill-dependent with a steep learning curve. A study conducted assessing the impact of the learning curve of EVH on graft quality and early graft failure (Desai et al., 2011) showed that inexperienced technicians performing EVH are more likely to cause intimal and deep vessel injury to the SVG, increasing graft failure risk and concluded that growing surgical experience in the EVH might be associated with better outcomes.

Vein graft patency is closely linked to the target artery caliber and the lesion complexity reflected in the SYNTAX score (Ong et al., 2006). A higher SYNTAX score (>33) is associated with more diffuse and complex coronary artery disease (CAD), CABG requiring multiple vein grafts to achieve complete revascularization offers superior long-term outcomes compared to PCI. The SYNTAX study also showed that SVG to the LAD have higher failure rates compared to arterial grafts in the same position, whereas vein grafts to the right coronary artery or obtuse marginal branches often have relatively better patency rates largely attributed to differences in vessel caliber, flow dynamics, and competitive flow (Ong et al., 2006). These factors must be considered when selecting the optimal revascularization strategy, reinforcing the importance of individualized surgical planning.

Conclusion

Despite speculations regarding EVH causing endothelial damage, thereby influencing early and/or late graft failure, at a minimum follow-up time of 10 years, no significant difference in graft patency rates between EVH and OVH was found. Similarly, the long-term clinical outcomes were comparable between the two groups. Considering the multiple factors that influence overall graft patency, it would be erroneous to attribute reduced long-term graft patency solely to a specific mode of harvest. Based on the results of this study, considering the added advantages of lower leg wound morbidity EVH over OVH, we conclude that EVH, if performed carefully with minimal structural damage to the SVG, is a non-inferior method of vein harvest, comparable to the long-term graft patency rates of vein grafts after OVH. We propose that for aortocoronary anastomoses, EVH should be considered, especially in diabetic and obese patients who fall into the high-risk group for general surgical wound complications and higher leg-wound morbidity rates.

Study limitations

All patients after isolated CABG were initially not followed up routinely with the intention of assessing graft patency and/or clinical outcomes after EVH; therefore, many patients were eventually lost to follow-up after 10 years. This study size was not optimal. Follow-up of patients, especially after 10 years, is was quite demanding. A number of patients died of unknown causes due to the inability to access the database of other hospitals so exact percentages of all-cause mortality and cardiovascular-related deaths could not be estimated. A significant number of patients refused follow-up examination likely due to being addled with old age and limiting comorbidities.

Data availability

The data of this research is only accessible within the University Hospital Ostrava servers in accordance with patient privacy laws of the Czech Republic. However, anonymized data can be extracted and made available by the corresponding author upon reasonable request.

References

Aboollo, M. F., Awadallah, K. M., Elsharkawy, T., Abd, E. M. E, Hafez, B. A. (2022) Endoscopic versus conventional vein harvest technique: Histological and immunohistochemical evaluation of venous wall integrity. *Heart Surg. Forum* **25(4)**, 520–524.

Andreasen, J. J., Vadmann, H., Oddershede, L., Tilsted, H. H., Frøkjær, J. B., Jensen, S. E. (2015) Decreased patency rates following endoscopic vein harvest in coronary artery bypass surgery. *Scand. Cardiovasc. J.* **49(5)**, 286–292.

Aziz, O., Athanasiou, T., Panesar, S. S., Massey-Patel, R., Warren, O., Kinross, J., Purkayastha, S., Casula, R., Glenville, B., Darzi, A. (2005) Does minimally invasive vein harvesting technique affect the quality of the conduit for coronary revascularization? *Ann. Thorac. Surg.* **80(6)**, 2407–2414.

Chiu, K. M., Lin, T. Y., Wang, M. J., Chu, S. H. (2006) Reduction of carbon dioxide embolism for endoscopic saphenous vein harvesting. *Ann. Thorac. Surg.* **81(5)**, 1697–1699.

Desai, P., Kiani, S., Thiruvanthan, N., Henkin, S., Kurian, D., Ziu, P., Brown, A., Patel, N., Poston, R. (2011) Impact of the learning curve for endoscopic vein harvest on conduit quality and early graft patency. *Ann. Thorac. Surg.* **91(5)**, 1385–1391; discussion 1391–1392.

Fitzgibbon, G. M., Kafka, H. P., Leach, A. J., Keon, W. J., Hooper, G. D., Burton, J. R. (1996) Coronary bypass graft fate and patient outcome: Angiographic follow-up of 5,065 grafts related to survival

and reoperation in 1,388 patients during 25 years. *J. Am. Coll. Cardiol*. **28(3)**, 616–626.

Gaudino, M., Antoniades, C., Benedetto, U., Deb, S., Di Franco, A., Di Giammarco, G., Fremes, S., Glineur, D., Grau, J., He, G. W., Marinelli, D., Ohmes, L. B., Patrono, C., Puskas, J., Tranbaugh, R., Girardi, L. N., Taggart, D. P.; ATLANTIC (Arterial Grafting International Consortium) Alliance (2017) Mechanisms, consequences, and prevention of coronary graft failure. *Circulation* **136(18)**, 1749–1764.

Hess, C. N., Lopes, R. D., Gibson, C. M., Hager, R., Wojdyla, D. M., Englum, B. R., Mack, M. J., Califf, R. M., Kouchoukos, N. T., Peterson, E. D., Alexander, J. H. (2014) Saphenous vein graft failure after coronary artery bypass surgery: Insights from PREVENT IV. *Circulation* **130(17)**, 1445–1451.

Ivaniuk, N. B., Zharinov, O. J., Mikhaliev, K. O., Yepanchintseva, O. A., Todurov, B. M. (2016) Factors determining quality of life of patients with ischemic cardiomyopathy selected for revascularization procedures. *Cardiac. Surg. Interv. Cardiol*. **3**, 21–29. (in Ukrainian)

Jarrett, C. M., Pelletier, M., Abu-Omar, Y., Baeza, C., Elgudin, Y., Markowitz, A., Vega, P. R., Dressler, O., Kappetein, A. P., Serruys, P. W., Stone, G. W., Sabik, J. F. 3rd (2023) Endoscopic vs open vein harvest in drug-eluting stents or bypass surgery for left main disease trial. *Ann. Thorac. Surg*. **115(1)**, 72–78.

Krishnamoorthy, B., Critchley, W. R., Venkateswaran, R. V., Barnard, J., Caress, A., Fildes, J. E., Yonan, N. (2016) A comprehensive review on learning curve associated problems in endoscopic vein harvesting and the requirement for a standardised training programme. *J. Cardiothorac. Surg*. **11**, 45.

Manchio, J. V., Gu, J., Romar, L., Brown, J., Gammie, J., Pierson, R. N. 3rd, Griffith, B., Poston, R. S. (2005) Disruption of graft endothelium correlates with early failure after off-pump coronary artery bypass surgery. *Ann. Thorac. Surg*. **79(6)**, 1991–1998.

Motwani, J. G., Topol, E. J. (1998) Aortocoronary saphenous vein graft disease: Pathogenesis, predisposition, and prevention. *Circulation* **97(9)**, 916–931.

Ong, A. T. L., Serruys, P. W., Mohr, F. W., Morice, M. C., Kappetein, A. P., Holmes, D. R. Jr., Mack, M. J., van den Brand, M., Morel, M. A., van Es, G. A., Kleijne, J., Koglin, J., Russell, M. E. (2006) The SYNergy between percutaneous coronary intervention with TAXus and cardiac surgery (SYNTAX) study: Design, rationale, and run-in phase. *Am. Heart J*. **151(6)**, 1194–1204.

Richards, C. E., Obaid, D. R. (2019) Low-dose radiation advances in coronary computed tomography angiography in the diagnosis of coronary artery disease. *Curr. Cardiol. Rev*. **5(1)**, 56–64.

Yokoyama, Y., Shimamura, J., Takagi, H., Kuno, T. (2021) Harvesting techniques of the saphenous vein graft for coronary artery bypass: Insights from a network meta-analysis. *J. Card. Surg*. **36(11)**, 4369–4375.

Zenati, M. A., Shroyer, A. L., Collins, J. F., Hattler, B., Ota, T., Almassi, G. H., Amidi, M., Novitzky, D., Grover, F. L., Sonel, A. F. (2011) Impact of endoscopic versus open saphenous vein harvest technique on late coronary artery bypass grafting patient outcomes in the ROOBY (Randomized On/Off Bypass) Trial. *J. Thorac. Cardiovasc. Surg*. **141(2)**, 338–344.

Radiological Analysis of Interhemispheric Fissure: A Comprehensive Study

Prabhjot Singh[1], Renu Gupta[2], Ashish K. Nayyar[2], Surajit Ghatak[2], Sarbesh Tiwari[3], Jaskaran Singh Gosal[4], Kumar Sambhav[1]

[1] Department of Anatomy, All India Institute of Medical Sciences, Bilaspur, Himachal Pradesh, India;
[2] Department of Anatomy, All India Institute of Medical Sciences, Jodhpur, Rajasthan, India;
[3] Department of Diagnostic and Interventional Radiology, All India Institute of Medical Sciences, Jodhpur, Rajasthan, India;
[4] Department of Neurosurgery, All India Institute of Medical Sciences, Jodhpur, Rajasthan, India

Received February 5, 2025; Accepted November 21, 2025.

Key words: MRI – Interhemispheric fissure – Neuroimaging – Morphometry

Abstract: Interhemispheric fissure is the midline groove present between the cerebral hemispheres. It provides access to corpus callosum, lateral ventricles and third ventricle during interhemispheric approach in neurosurgery. The knowledge and established data about its morphometry are limited. 90 participants who underwent magnetic resonance imaging scans were studied. The data was divided into 4 age groups (25–45, 45–65, 65–85 and >85 years) as well as among males and females. The depth of interhemispheric fissure was measured from 6 predetermined reference points from the superomedial border of cerebral hemisphere to the floor of corpus callosum which is formed by corpus callosum. Mean along with standard deviation and confidence interval were calculated. Unpaired *t*-test and ANOVA was used to analyse the statistical difference between various age groups. The mean value of depth of interhemispheric fissure from frontal pole to genu is 35.08 ± 3.20 mm, at the level of coronal suture is 35.64 ± 4.27 mm, 1 cm anterior to coronal suture is 35.50 ± 3.27 mm, 1 cm posterior to coronal suture is 34.38 ± 4.95 mm. The depth from superomedial border at the level of parietooccipital sulcus is 43.72 ± 3.63 mm and at the level of calcarine sulcus is 54.13 ± 5.96 mm. This data is useful for neurosurgeons in order to perform interhemispheric approach.

Mailing Address: Prabhjot Singh, MD., Department of Anatomy, All India Institute of Medical Sciences, Kangra-Shimla National Highway – 205, Kothipura, Bilaspur, Himachal Pradesh, 174037, India; e-mail: sprabhjot74@yahoo.com

https://doi.org/10.14712/23362936.2025.34

Prague Medical Report / Vol. 126 (2025) No. 4, p. 215–222

Introduction

The interhemispheric fissure (IHF) is a deep midline groove situated between the left cerebral hemisphere (LCH) and the right cerebral hemisphere (RCH). IHF is also known as longitudinal cerebral fissure/ longitudinal fissure and medial longitudinal fissure. The location of this fissure is self-explanatory i.e., it is present in between both the hemispheres of the cerebrum. IHF does not completely separate the RCH and LCH, RCH and LCH remain in connection with one another both anatomically and functionally through the thick band of white matter known as the corpus callosum (CC) (Kalaiselvi et al., 2016).

The mid sagittal plane divides the cerebrum into RCH and LCH, hereby coinciding with the IHF (Stegmann et al., 2005).

Though IHF is a fissure, it contains numerous anatomical structures viz falx cerebri, corpus callosum at depth and importantly anterior cerebral artery and veins which drain this particular area (Macori and Di Muzio, 2015). The brain is covered with 3 layered meninges from outside to inside namely; dura mater, arachnoid mater and pia mater. Dura mater further forms reflections like falx cerebri, falx cerebelli, tentorium cerebelli and diaphragmatic sellae in the cranial cavity. Out of these, falx cerebri is present in between two cerebral hemispheres in the IHF (Fernandez-Miranda, 2016). At the depth of IHF below the falx cerebri, CC is situated i.e., the floor of IHF is formed by CC (Ribas, 2016).

Interestingly, IHF divides the cerebral hemispheres into two unequal parts. For instance, planum temporale is the area which represents Wernicke's area and is found to be larger in the left hemisphere (Becker, 2002). Caudate nucleus, which is the part of the basal ganglia of the brain, is found to be larger on the right side (Watkins et al., 2001). IHF contains falx cerebri, anterior cerebral artery (ACA) and the CC at its depth (Kasowski and Piepmeier, 2001).

IHF as a natural corridor between RCH and LCH, plays a key role in various neurosurgeries. Transcallosal approach is one such approach which is carried out through IHF. It is aimed towards removal of tumours of the third ventricle, post thalamic tumours (Kasowski and Piepmeier, 2001). Corpus callosotomy is a palliative surgery which is performed through IHF in patients irresponsive to medical management and whose seizures are intractable despite all possible medical management (Aboitiz et al., 1992).

Thorough knowledge of the anatomy of interhemispheric fissure, bridging cortical veins, ACA and corpus callosum is essential to perform the transcallosal approach safely and effectively in neurosurgery. Apart from corpus callosotomy (used for refractory seizure control) (Asadi-Pooya et al., 2008), the interhemispheric transcallosal approach is also used for addressing tumours and vascular malformations of CC like callosal gliomas and arteriovenous malformations of (AVM) (Pabaney et al., 2016; Forster et al., 2020). Also, different tumours of the lateral and third ventricle are excised via this approach (Kasowski and Piepmeier, 2001). The interhemispheric approach (without transgressing the CC) is also used for the surgical management of medial hemispheric gliomas, vascular malformations like cavernomas and falcine meningiomas (Malekpour and Cohen-Gadol, 2015; Das et al., 2017).

The transcallosal approach is of 2 types – anterior and posterior. Anterior is performed anterior to coronal suture and posterior is formed posterior to coronal suture (Cohen-Gadol, 2016). The frontal interhemispheric approach provides access to a range of midline brain pathologies. Originally developed as the anterior interhemispheric approach for treating anterior communicating artery aneurysms, it has since become a widely adopted neurosurgical technique. This approach not only reveals interhemispheric structures but also allows exposure of lesions in the suprasellar and prechiasmatic cisterns, including craniopharyngiomas and midline meningiomas such as those located at the olfactory groove, planum sphenoidale, or tuberculum sellae. The frontal interhemispheric approach (FIA) can also be used to access cingulate and callosal lesions (Aftahy et al., 2021).

An extension of this technique, the frontobasal interhemispheric approach (FBIA), offers a broader view of the anterior skull base, spanning from the crista galli to the tuberculum sellae in the anteroposterior direction and from the midline to the sphenoid wing laterally. This approach is considered safe, particularly with respect to preserving visual and pituitary stalk function, and it provides a more subfrontal exposure.

Further posteriorly, the parietooccipital interhemispheric approach (PIA) allows for the removal of lesions in the peritrigonal or periatrial regions. However, this technique is more complex due to the depth of the target area and the presence of critical anatomical structures.

Since coronal suture is the demarcating landmark between anterior and posterior approaches, coronal suture is chosen as the reference point of this study (Cohen-Gadol, 2016). This study aims to access the shortest possible route to reach corpus callosum from the supero-medial margin of cerebral hemisphere.

Material and Methods

Type of study and duration

This study is non interventional, retrospective, single centric study which was done for the period of 3 years from 2021 to 2023.

The depth of IHF from the surface up to the level of CC along with measurements of dimensions of CC were studied with the help of magnetic resonance imaging (MRI) at the department of Diagnostic and Interventional Radiology. The equipment used was General Electronics Discovery 370 – equipped with 3 Tesla magnets and the 3D sequences were used. 90 participants were analysed in this study.

The depth of IHF was measured from the superomedial border of cerebral hemisphere to the floor of IHF, which is formed by CC. The depth of IHF was measured from the following reference points (Figure 1):

1) At the level of coronal suture to the trunk of CC (CS)
2) 1 cm anterior to coronal suture to the trunk of CC (A-CS)
3) 1 cm posterior to coronal suture to the trunk of CC (P-CS)
4) From frontal pole to genu of CC (FP)
5) From the point where parieto-occipital suture reaches superomedial border to splenium of CC (PO)
6) From the point where calcarine suture reaches superomedial border to splenium of CC (Cal)

90 participants were studied with the mean age of 63.04 ± 17.29 years. The sample was divided in 4 age groups (Table 1).

Table 1: Classification of sample in various age groups

Serial number	Age group	Number of participants
1	25–45	17
2	45–65	20
3	65–85	47
4	>85	6

Out of 90 participants, 57 were males with mean age of 60.58 ± 18.08 years and 33 were females with the mean age of 67.30 ± 15.17.

The sample was segregated based on gender and hence, gender-based analysis was also done.

Statistical analysis

The data was compared and analysed using SPSS version 21. Mean along with standard deviations was evaluated and the comparison of depth between various age groups and gender was performed using unpaired *t*-test and ANOVA. The 95% confidence interval was also calculated to express the data of this study over the whole population.

Results

The findings of the study without any age or gender segregation are represented in Table 2.

Age based analysis

Comparative analysis was performed between the various groups. Unpaired *t*-test was used to compare

Figure 1: Representation of various reference points chosen for the measurement of depth of interhemispheric fissure, frontal pole to genu, anterior and posterior to the coronal suture and at the occipital pole. FP – frontal pole; PO – parieto-occipital suture; Cal – calcarine sulcus; CS – coronal suture; A-CS – anterior to CS; P-CS – posterior to CS.

Prague Medical Report / Vol. 126 (2025) No. 4, p. 215–222

Table 2: Summary of mean values and SD of depth of IHF without age or gender – based segregation

Serial number	Reference point	Mean ± SD
1	FP	35.08 ± 3.20
2	CS	35.64 ± 4.27
3	A-CS	35.50 ± 3.27
4	P-CS	34.38 ± 4.95
5	PO	43.72 ± 3.63
6	Cal	54.13 ± 5.96

SD – standard deviation; IHF – interhemispheric fissure; FP – mean depth from FP to CC (corpus callosum); CS – mean depth of IHF from coronal suture to the floor of IHF; A-CS – mean depth from point A-CS (1 cm anterior to coronal suture); P-CS – mean depth from point P-CS (1 cm posterior to coronal suture); PO – mean depth of IHF through parieto-occipital suture; Cal – mean depth of IHF through calcarine suture. All the measurements are in mm. All the values are in mm and rounded off up to 2 decimal places

one parameter (e.g., depth at point FP) between two age groups and ANOVA was used to compare the same parameter across all age groups at once.

Graphical representation of mean and standard deviation for various age groups is shown in Figure 2. The minimum and maximum depth of interhemispheric fissure among various age groups in given in Table 3; the upper and lower limits of 95% confidence intervals is given in Table 4.

Finding of unpaired *t*-test:

1) Significant difference (p-value ≤ 0.05) in the depth of IHF from point FP between the age groups of 25–45 years versus 65–85 years (p-value = 0.01) and 25–45 years versus >85 years (p-value = 0.02).
2) Significant difference (p-value ≤ 0.05) in the depth of IHF from point A-CS (1 cm anterior to coronal suture) between the age groups of 25–45 years versus 65–85 years (p-value = 0.01), 25–45 years versus >85 years (p-value = 0.04), 45–65 versus 65–85 years (p-value = 0.001) and 45–65 versus >85 years (p-value = 0.01).
3) Significant difference (p-value ≤ 0.05) in the depth of IHF from point P-CS (1 cm posterior to coronal suture) between the age groups of 45–65 versus 65–85 years (p-value = 0.04).
4) No significant difference was noted while comparing other parameters and age groups.

ANOVA revealed the following:

1) Significant difference (p-value ≤ 0.05) in the depth of IHF from point FP (p-value = 0.03), A-CS (1 cm anterior to coronal suture) (p-value = 0.00090) among various age groups.

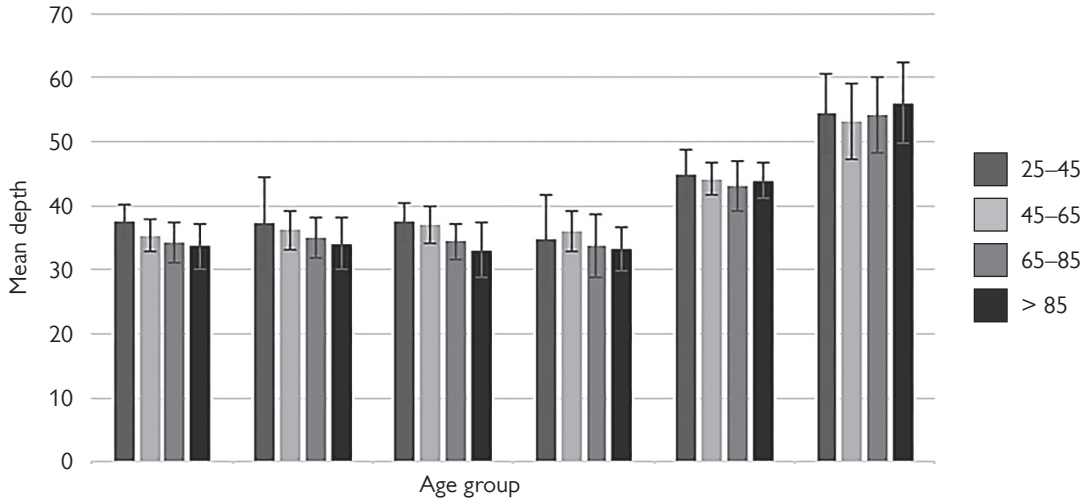

	FP	CS	A-CS	P-CS	PO	Cal
25–45	37.49	37.32	37.42	34.65	44.89	54.44
45–65	35.31	36.22	37.02	35.99	44.20	53.16
65–85	34.29	34.98	34.47	33.74	43.07	54.20
> 85	33.65	34.08	33.07	33.30	43.95	56.00

Figure 2: Representation of mean and SD of depth of IHF among various age groups. SD – standard deviation; IHF – interhemispheric fissure; FP – mean depth from FP to CC (corpus callosum); CS – mean depth of IHF from coronal suture to the floor of IHF; A-CS – mean depth from point A-CS (1 cm anterior to coronal suture); P-CS – mean depth from point P-CS (1 cm posterior to coronal suture); PO – mean depth of IHF through parieto-occipital suture; Cal – mean depth of IHF through calcarine suture.

Table 3: Minimum and maximum depths of IHF in various age groups

Serial number	Reference point	Minimum depth				Maximum depth			
		Age group (years)				Age group (years)			
		25–45	45–65	65–85	>85	25–45	45–65	65–85	>85
1.	FP	31.5	28.7	24.8	28.4	42.2	38.7	39.7	37.6
2.	CS	10.6	31.2	28.1	27.6	43.1	41.2	44.7	39.6
3.	A-CS	31.6	32.7	29.9	28.4	41.2	42.3	46.5	40.4
4.	P-CS	10.1	31.2	10.1	28.1	41.2	41.7	41.9	37.0
5.	PO	37.0	39.5	33.6	39.1	51.5	49.3	50.8	47.6
6.	Cal	38.8	45.0	42.5	44.0	65.1	66.2	63.4	61.4

IHF – interhemispheric fissure; FP – mean depth from FP to genu of CC (corpus callosum); CS – mean depth of IHF of depth from coronal suture to the floor of IHF; A-CS – mean depth from point A-CS (1 cm anterior to coronal suture); P-CS – mean depth from point P-CS (1 cm posterior to coronal suture); PO – mean depth of IHF through parieto-occipital suture; Cal – mean depth of IHF through calcarine suture. All the measurements are in mm

Table 4: Lower and upper limits of 95% confidence interval (CI) for depth of IHF

Serial number	Reference point	Lower limit 95% CI				Upper limit 95% CI			
		Age group (years)				Age group (years)			
		25–45	45–65	65–85	>85	25–45	45–65	65–85	>85
1.	FP	36.17	34.13	33.34	29.90	38.81	36.49	35.24	37.40
2.	CS	33.63	34.81	34.06	29.78	41.00	37.63	35.90	38.39
3.	A-CS	35.84	35.70	33.64	28.62	39.00	38.34	35.29	37.51
4.	P-CS	31.07	34.50	32.32	29.74	38.22	37.47	35.16	36.86
5.	PO	42.87	43.01	41.91	41.02	46.91	45.39	44.23	46.88
6.	Cal	51.29	50.38	52.44	49.37	57.59	55.94	55.95	62.63

A 95% confidence interval suggests that the measurement of 95% population will lie within these limits. IHF – interhemispheric fissure; FP – mean depth from FP to genu of CC (corpus callosum); CS – mean depth of IHF of depth from coronal suture to the floor of IHF; A-CS – mean depth from point A-CS (1 cm anterior to coronal suture); P-CS – mean depth from point P-CS (1 cm posterior to coronal suture); PO – mean depth of IHF through parieto-occipital suture; Cal – mean depth of IHF through calcarine suture. All the measurements are in mm. All the values are in mm and rounded off up to 2 decimal places

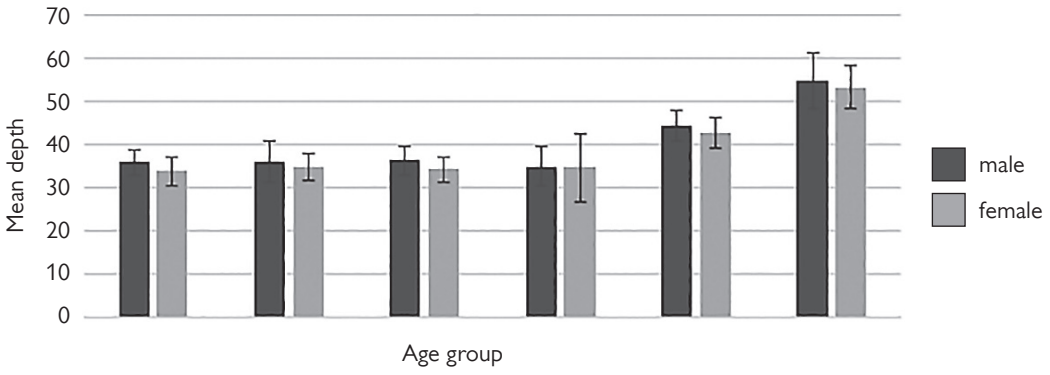

	FP	CS	A-CS	P-CS	PO	Cal
male	35.84	36.12	36.25	34.89	44.36	54.63
female	33.76	34.81	34.20	34.58	42.62	53.28

Figure 3: Representation of mean and SD of depth of IHF. SD – standard deviation; IHF – interhemispheric fissure; FP – mean depth from FP to CC (corpus callosum); CS – mean depth of IHF from coronal suture to the floor of IHF; A-CS – mean depth from point A-CS (1 cm anterior to coronal suture); P-CS – mean depth from point P-CS (1 cm posterior to coronal suture); PO – mean depth of IHF through parieto-occipital suture; Cal – mean depth of IHF through calcarine suture.

Prague Medical Report / Vol. 126 (2025) No. 4, p. 215–222

Table 5: Maximum and minimum depths of IHF along with lower and upper limits of 95% confidence interval (CI)

Serial number	Reference point	Minimum depth		Maximum depth		Lower limit 95% CI		Upper limit 95% CI	
		Male	Female	Male	Female	Male	Female	Male	Female
1.	FP	28.70	24.80	42.20	37.50	35.08	32.57	36.60	34.96
2.	CS	10.60	27.60	44.70	39.10	34.85	33.70	37.38	35.92
3.	A-CS	30.50	28.40	46.50	40.70	35.39	33.16	37.11	35.24
4.	P-CS	10.10	10.10	41.90	39.00	33.63	31.64	36.14	35.37
5.	PO	35.20	33.60	51.50	48.10	43.42	41.36	45.30	43.89
6.	Cal	38.80	44.00	66.20	61.10	52.90	51.56	56.36	54.99

IHF – interhemispheric fissure; FP – mean depth from FP to genu of CC (corpus callosum); CS – mean depth of IHF of depth from coronal suture to the floor of IHF; A-CS – mean depth from point A-CS (1 cm anterior to coronal suture); P-CS – mean depth from point P-CS (1 cm posterior to coronal suture); PO – mean depth of IHF through parieto-occipital suture; Cal – mean depth of IHF through calcarine suture. All the measurements are in mm and rounded off up to 2 decimal places

2) No significant difference was observed in other parameters across various age groups.

Gender based analysis

Comparative analysis was performed between the two groups using unpaired *t*-test.

Graphical representation of mean and standard deviation for both the genders is shown in Figure 3. The minimum and maximum depth of interhemispheric recorded in both genders along with upper and lower limits of 95% confidence interval is given in Table 5.

Finding of unpaired *t*-test:

1) Significant difference (p-value ≤ 0.05) in the depth of IHF at point FP (p-value = 0.025), point A-CS (1 cm anterior to coronal suture) (p-value = 0.03) and at point PO among male and female groups (p-value = 0.03).
2) No significant difference was noted while comparing other parameters.

Discussion

The interhemispheric fissure develops during early fetal development, typically around the 8th gestational week. It is formed when the dura mater forms the fold known as falx cerebri. As the cerebral hemispheres grow and increase in size the falx cerebri also grows and the depth of IHF increases. The formation of the interhemispheric fissure is a critical step in the development of the brain's structure and allows for proper hemispheric development and separation (Lewine, 1995; Vinurel et al., 2014).

In the current study with the increase in age, the depth of IHF from frontal pole to genu, at coronal suture and anterior to coronal suture decreased; whereas posterior to coronal suture, the depth of IHF increased and then decreased with age. From the occipital pole to the splenium at point "PO" depth decreased till the age of 85 followed by a slight increase; at point "Cal" depth decreased till the age of 65 and then increased.

In the past couple of studies have been performed to measure the depth of IHF on cadavers as well using MRI. In the past, only a few studies have been conducted on the morphometry of the interhemispheric fissure. These studies are summarized in Table 6. The depth of IHF through coronal suture, 1 cm anterior and 1 cm posterior to the coronal suture the depth has been measured in any of the previous studies.

From Table 6 it can be concluded that radiological studies validate the result of the cadaveric studies since there is no significant difference between results of cadaveric and MRI measurement. The findings of the radiological studies are crucial because neurosurgeons require the readings of IHF on the patients and not on the cadavers. The readings of the cadavers have their limitations as it cannot be applied to the operative patients since cadavers are formalin fixed which leads to shrinkage of the tissue.

The gender-based comparison was also carried out to reveal that the depth of IHF is more among males than females at all the reference points which were used for this study.

Conclusion

The knowledge gained about the depth of the interhemispheric fissure will be valuable for neurosurgeons performing surgeries through the IHF, such as corpus callosotomies. The depth of the

Table 6: Comparison of the results of the current study with those of the studies done previously

Serial no.	Study (year)	Cadaveric /radio-logical	Age	FP to genu	1 cm anterior to coronal suture	1 cm posterior to coronal suture	PO to splenium	
1	Anagnostopoulou et al. (2006)	Cadaveric		33.5			52.6	
2	Mourgela et al. (2007)	Radiological		31.6 ± 3.3			51.5 ± 4.8	
3	Patra et al. (2021)	Cadaveric		33.1 ± 2.9			56.5 ± 5.4	
4	Singh et al. (2023)	Cadaveric		35.00 ± 7.75	35.71 ± 5.61	40.46 ± 4.09	at parieto-occipital suture 46.54 ± 4.95	at calcarine suture 51.29 ± 6.83
5	Current study	Radiological		35.08 ± 3.20	35.50 ± 3.27	34.38 ± 4.95	43.72 ± 3.63	54.13 ± 5.96
			25–45	37.49 ± 2.57	37.42 ± 3.08	34.65 ± 6.95	44.89 ± 3.93	54.44 ± 6.13
			45–65	35.31 ± 2.53	37.02 ± 2.81	35.99 ± 3.18	44.20 ± 2.55	54.44 ± 5.93
			65–85	34.29 ± 3.23	34.47 ± 2.81	33.74 ± 4.84	43.07 ± 3.94	54.20 ± 5.98
			>85	33.65 ± 3.57	33.07 ± 4.24	33.30 ± 3.39	43.95 ± 2.79	56.00 ± 6.32

FP – mean depth from FP to genu of CC (corpus callosum); PO – mean depth from point where parieto-occipital suture reaches superomedial border to splenium of CC

IHF can help reduce dependence on neuronavigation equipment, enabling certain brain surgeries to be performed in centres where such equipment may be lacking.

This study has just focused on the population of the north western region of India, further studies are required in order to establish these findings for the populations of other origins.

References

Aboitiz, F., Scheibel, A. B., Fisher, R. S., Zaidel, E. (1992) Fiber composition of the human corpus callosum. *Brain Res*. **598(1–2)**, 143–153.

Aftahy, A. K., Barz, M., Wagner, A., Liesche-Starnecker, F., Negwer, C., Meyer, B., Gempt, J. (2021) The interhemispheric fissure – Surgical outcome of interhemispheric approaches. *Neurosurg. Rev*. **44(4)**, 2099–2110.

Anagnostopoulou, S., Mourgela, S., Katritsis, D. (2006) Morphometry of corpus callosum: An anatomical study. *Neuroanatomy* **5**, 20–23.

Asadi-Pooya, A. A., Sharan, A., Nei, M., Sperling, M. R. (2008) Corpus callosotomy. *Epilepsy Behav*. **13(2)**, 271–278.

Becker, J. B. (2002) *Behavioral Endocrinology*, 2nd Edition. MIT Press, Cambridge.

Cohen-Gadol, A. (2016) *Neurosurgical Atlas*. Available at: https://www.neurosurgicalatlas.com/

Das, K. K., Gosal, J. S., Sharma, P., Mehrotra, A., Bhaisora, K., Sardhara, J., Srivastava, A., Jaiswal, A. K., Kumar, R., Behari, S. (2017) Falcine meningiomas: Analysis of the impact of radiologic tumor extensions and proposal of a modified preoperative radiologic classification scheme. *World Neurosurg*. **104**, 248–258.

Fernandez-Miranda, J. C. (2016) Intracranial region. In: *Gray's Anatomy: The Anatomical Basis of Clinical Practice*, 41st Edition. Standring, S., Elsevier Limited, London.

Forster, M.-T., Behrens, M., Lortz, I., Conradi, N., Senft, C., Voss, M., Rauch, M., Seifert, V. (2020) Benefits of glioma resection in the corpus callosum. *Sci. Rep*. **10(1)**, 16630.

Kalaiselvi, T., Sriramakrishnan, P., Somasundaram, K. (2016) Brain abnormality detection from MRI of human head scans using the bilateral symmetry property and histogram similarity measures. In: *2016 International Computer Science and Engineering Conference (ICSEC)*, Chiang Mai, Thailand.

Kasowski, H., Piepmeier, J. M. (2001) Transcallosal approach for tumors of the lateral and third ventricles. *Neurosurg. Focus* **10(6)**, E3.

Lewine, J. D. (1995) Chapter 2 – Introduction to functional neuroimaging: Functional neuroanatomy. In: *Functional Brain Imaging* (Internet). Orrison, W. W., Lewine, J. D., Sanders, J. A., Hartshorne, M. F., pp. 13–95, Mosby. Available at: https://www.sciencedirect.com/science/article/pii/B9780815165095500060

Macori, F., Di Muzio, B. (2015) Interhemispheric fissure. Available at: https://radiopaedia.org/

Malekpour, M., Cohen-Gadol, A. A. (2015) Interhemispheric transfalcine approach and awake cortical mapping for resection of peri-atrial gliomas associated with the central lobule. *J. Clin. Neurosci*. **22(2)**, 383–386.

Mourgela, S., Anagnostopoulou, S., Sakellaropoulos, A., Gouliamos, A. (2007) An MRI study of sex- and age-related differences in the dimensions of the corpus callosum and brain. *Neuroanatomy* **6**, 63–65.

Pabaney, A. H., Ali, R., Kole, M., Malik, G. M. (2016) Arteriovenous malformations of the corpus callosum: Pooled analysis and systematic review of literature. *Surg. Neurol. Int*. **7(Suppl. 9)**, S228–S236.

Patra, A., Singla, R. K., Chaudhary, P., Malhotra, V. (2020) Morphometric analysis of the corpus callosum using cadaveric brain: An anatomical study. *Asian J. Neurosurg*. **15(2)**, 322–327.

Ribas, G. C. (2016) Cerebral hemispheres. In: *Gray's Anatomy: The Anatomical Basis of Clinical Practice*, 41st Edition. Standring, S., Elsevier Limited, London.

Singh, P., Gupta, R., Nayyar, A. K., Ghatak, S., Gosal, J. S., Varghese, R. (2023) Morphometry of depth of interhemispheric fissure on Indian cadaveric brain specimens. *Clin. Ter*. **174(3)**, 281–286.

Stegmann, M. B., Skoglund, K., Ryberg, C. (2005) Mid-sagittal plane and mid-sagittal surface optimization in brain MRI using a local symmetry measure. *Proceedings of SPIE* **5477**, 568–579.

Vinurel, N., Van Nieuwenhuyse, A., Cagneaux, M., Garel, C., Quarello, E., Brasseur, M., Picone, O., Ferry, M., Gaucherand, P., des Portes, V., Guibaud, L. (2014) Distortion of the anterior part of the interhemispheric fissure: Significance and implications for prenatal diagnosis. *Ultrasound Obstet. Gynecol*. **43(3)**, 346–352.

Watkins, K. E., Paus, T., Lerch, J. P., Zijdenbos, A., Collins, D. L., Neelin, P., Taylor, J., Worsley, K. J., Evans, A. C. (2001) Structural asymmetries in the human brain: A voxel-based statistical analysis of 142 MRI scans. *Cereb. Cortex* **11(9)**, 868–877.

Head and Neck Cancer Treatment with Mandibular Overdenture on Implants

José Guilherme Dalía Perocco, Daniela Micheline dos Santos, Marcelo Coelho Goiato

Department of Dental Materials and Prosthodontics, School of Dentistry, São Paulo State University (UNESP), São Paulo, Brazil

Received April 8, 2025; Accepted November 21, 2025.

Key words: Oncology – Overdenture – Dental implant – Radiotherapy

Abstract: Treatments with prostheses on implants must be very well planned and executed, in order to have adequate maintenance and longevity. Thus, the present work demonstrates, through a clinical case report, the making of an overdenture prosthesis on two implants previously installed in the mandible and a conventional complete denture in the upper arch, considering the biopsychosocial principles of the patient. Male patient, 74-year-old, who underwent radiotherapy treatment, attended the Oral Oncology Center – FOA UNESP, for oral rehabilitation, after treatment of squamous cell carcinoma, complaining mainly of masticatory inefficiency due to edentulism. Intraoral clinical examination revealed a healthy gingiva in its entirety. In the maxillary ridge, an adequate bone height of the ridge was observed, however, with a failure in the posterior region on the left side due to surgery performed in the previous oncological treatment. In the lower arch, it was possible to observe bone resorption of the ridges and two implants (S.I.N. Implant System) already installed, parallel and stabilized (monitored by a device named Osstell) in the anterior region of the mandible. The treatment plan was defined by the elaboration of two prostheses, making an upper conventional complete denture and a lower overdenture-type prosthesis, taking advantage of the two implants previously installed in the radiotherapy sessions. After the installation of the prostheses, it was possible to diagnose greater masticatory comfort, improvement in aesthetics and self-esteem, managing to promote quality and longevity in the treatment according to the patient's needs and age, restoring oral health and him.

Mailing Address: Prof. Marcelo Coelho Goiato, Department of Dental Materials and Prosthodontic, School of Dentistry, São Paulo State University (UNESP), José Bonifácio Street, 1193, Vila Mendonça – Araçatuba, 16015-050, São Paulo, Brazil; e-mail: m.goiato@unesp.br

https://doi.org/10.14712/23362936.2025.35

Prague Medical Report / Vol. 126 (2025) No. 4, p. 223–230

Introduction

Tooth loss reflects the care taken with oral health throughout life and cannot be considered merely a consequence of the presence of other oral health problems, such as dental caries and periodontal disease, but also a reflection of socioeconomic factors and/or levels of health education (Sônego et al., 2022).

In the United States, it is projected that by 2060, the number of older adults will exceed the number of children for the first time. The rate of edentulism is still significant, being greater than 17%, and may decrease by 3% by 2050 (Atanda et al., 2022).

This fact may be due to the legacy of a healthcare model based on invasive treatments resulting in an excessive number of extractions, with oral rehabilitation with complete dental prosthesis being the treatment of choice for this condition. Oral rehabilitation with complete dentures aims to restore chewing, phonetics, appearance and, above all, the patient's self-worth and dignity. In addition to restoring self-esteem, complete dentures aim to preserve the alveolar ridges and integrate the patient psychosocially into society. The complete denture with mucous membranes is used in completely edentulous areas and remains adhered to the fibromucosa by means of a saliva film and the adaptation between the edges of the prosthesis and the patient's surrounding tissues (Penitente et al., 2024).

The use of the lower complete dentures is typically less stable and more challenging to adapt than upper dentures. This is due to a lack of surface tension, causing instability of the lower complete denture due to anatomical changes such as reabsorption of the alveolar ridge and the location of muscles such as the orbicularis oris and the tongue muscles (de Caxias et al., 2018).

Therefore, the search for new treatment methods is necessary to ensure better acceptance of the prosthesis by patients. One such method is the use of overdenture-type complete dentures. Overdentures are implant-retained and mucous membrane-supported complete dentures designed to increase the retention, stability and comfort of conventional dentures, since the lack of retention and stability is normally presented by mandibular prostheses. O-rings are fitting systems composed of metal capsules that accommodate rubber or nylon rings, which are housed in the base of the denture and ball attachments, screwed onto the implants. They are relatively simple technically, low cost, restore lip support and allow easy cleaning, but require periodic maintenance to replace the internal ring (Sônego et al., 2017).

When it comes to rehabilitating patients with a history of head and neck cancer, there is still no consensus in the literature regarding this association, due to the involvement of radiotherapy and/or chemotherapy during treatment, which have side effects such as xerostomia, decreased vascular supply, difficulty opening the mouth and swallowing, and difficulty tolerating the prosthesis (Sankar and Xu, 2023).

Osteoradionecrosis can develop in previously irradiated sites where implants are installed, with a significant percentage (Goiato et al., 2010).

Proposal

Therefore, based on the above, a clinical case of a patient after treatment for head and neck cancer will be reported, with the need to perform rehabilitation with a complete lower denture, the overdenture type being chosen, retained by an O-ring retention system, since the patient had implants (S.I.N. Implant System) installed and parallel in the anterior region of the mandible and the production of a conventional complete upper denture, since he has a history of radiotherapy treatment in the head and neck region, with surgery to install implants being contraindicated.

Case report

A 74-year-old male patient, attended the clinic at the Oral Oncology Center of FOA-UNESP/Brazil for oral rehabilitation after treatment of squamous cell carcinoma of the tonsillar region and with extension to the soft palate, uvula, and lateral wall of the nasopharynx, due to the loss of teeth, which were extracted to begin radiotherapy treatment, without presenting any systemic problem worthy of note.

Extra and intraoral examination

The extraoral examination showed a visible loss of vertical dimension. A decrease in lip support was

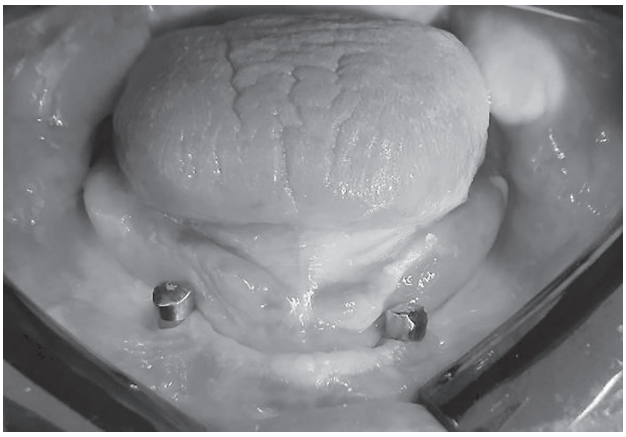

Figure 1: Jaw with healthy gums with two implants (S.I.N. Implant System) in the anterior region of the jaw.

Figure 2: Implant stability quotient value provided by the Osstell device. 76 implant stability.

observed due to the loss of the anterior elements (Figure 1). The intraoral examination did not detect any alteration of the oral mucosa, presence of torus, or any anomaly that would contraindicate the planning and programmed rehabilitation. Bone resorption of the residual jaw ridges was observed, but with a healthy gingiva in its entirety and the implants (S.I.N. Implant System, Brazil) in the anterior region of the jaw stabilized, due to the quality of the bone present (Types I and II). The stability of the implants was monitored by a device called Osstell (Osstell® Mentor, Goteborg, Sweden), which has the function of monitoring the stability of the implant by measuring the resonance of a transducer coupled to the implants at any stage of the treatment and observation period (Hayashi et al., 2010).

The average value on the ISQ scale (implant stability quotient) provided by Osstell was 76 (Figure 2), where the values range from 1 to 100. The manufacturer of the device states that ISQ greater than 70 represents high stability, ISQ between 60 and 69, medium stability and ISQ less than 60 is considered low stability. Therefore, the higher the ISQ, the greater the implant stability (Truhlar et al., 1997; Alsaadi et al., 2007).

In the maxillary ridge, we observed a favourable prognosis, with adequate bone height of the ridge, since the shape and size of the residual ridge are some of the factors that can influence masticatory efficiency, since the ability to fragment food is directly influenced by the stability and retention of the prosthesis. However, there is a defect in the posterior region on the left side due to surgery performed in the previous oncological treatment.

Radiographic examination

To confirm the clinical diagnosis and execute the treatment plan, a panoramic radiograph was requested (Figure 3), which confirmed considerable bone loss in the areas of the upper molars bilaterally and in the posterior areas of the lower edentulous teeth, and the presence of two implants (S.I.N. Implant System) installed, parallel in the anterior region of the mandible. Therefore, based on the radiograph presented, the creation of a complete denture of the mandibular overdenture type was planned, supported by individual O-ring systems on the implants (S.I.N. Implant System) already installed, selected for their bone implantation, considered to have favourable biomechanics, easy maintenance and cleaning, and a reduced potential for mucosal hyperplasia.

Study molding and functional molding

After the clinical examination and analysis of the panoramic radiograph, the study molding was performed using condensation silicone (Zetaplus – Zhermack, Italy). In view of the above, the individual mold was made in the laboratory, with the objective of performing the functional molding. It is important

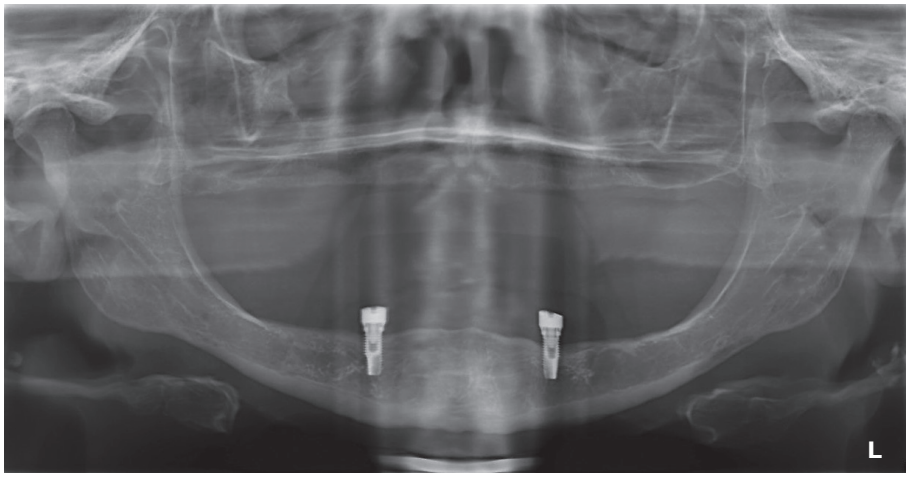

Figure 3: Panoramic radiograph.

Prague Medical Report / Vol. 126 (2025) No. 4, p. 223–230

to emphasize the importance of this phase, as it aims to reproduce the tissues of the capable area and determine the extension of the complete denture. This procedure aims to ensure stability and retention of the future prosthesis by sealing the entire periphery of the prosthesis, with the confinement of a thin film of saliva between the prosthesis and the fibromucosa, which in turn promotes lower atmospheric pressure, contributing to retention and, in addition, aims to ensure good seating of the prosthesis on the basal area, resulting in patient comfort by reducing the interposition of food between the prosthesis and the mucosa. In the upper arch, zinc enolic paste was used for internal molding and the addition of molding wax, melted to a liquid state and applied with a brush to the line of the hard palate and soft palate, to compress the area corresponding to the transition zone between the hard and soft palates, optimizing posterior locking, corroborating the retention of the prosthesis in the maxillary arch, since compression can occur in this region, due to the presence of resilient structures, with the sealing of the entry of air during the action of the tensor and levator muscles of the soft palate in physiological situations, such as swallowing and phonetics. Immediately in the mandibular arch, the implant transfer molding was performed with individual open molds with square transfers (Figure 4).

Corrective molding was performed with fluid silicone (Oranwash L Fluid – Zhermack, Italy), which after the polymerization time of the molding material with the transfer materials, these were captured during the removal of the mold and the analogues were immediately adapted to them to obtain the working model (de Moraes Melo Neto et al., 2023).

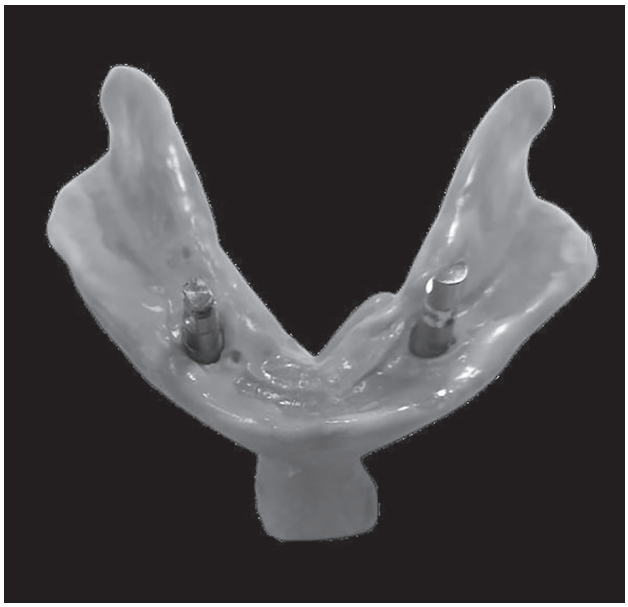

Figure 4: Functional impression of the jaw with square transfers.

Trial base and wax plane

The trial base and wax plane were made. The upper wax plane was oriented. Lip support was evaluated, with no need to reduce the volume of wax with the spatula 36 or increase it with a wax blade, also evaluating the buccal corridor and the exposure of wax at rest and smiling. Then, the parallelism was made with the fox ruler, positioning it parallel to the bipupillary line from the front of the patient and on the side, from the wing of the nose to the tragus, both were parallel to the prosthetic plane.

Assembling the facebow

In this step, the upper wax plane was adapted to the fork, by adapting a wax sheet over it. The plane was joined to the fork by depositing molten wax at the junction of the two on the palatal side. Once this was done, the assembly (wax plane and facebow fork) was taken to the patient's mouth and the facebow was connected to the assembly by inserting the fork into the "universal joint" of the facebow. Next, the olives (plastic parts at the ends of the facebow) were introduced into the external auditory canal and the patient was instructed to hold them with forward pressure. The next step consisted of adapting the nasal relators, which were attached to the facebow and placed against the nasal saddle. Once this was done, and with the trial base well attached to the support area, the screws were tightened. Then, the assembly was removed from the patient, loosening the lateral and central screws of the bow. The next step was to transfer the orientation plane to the articulator, with the model superimposed on the test base.

Recording the vertical dimension of occlusion (VDO) and defining the height of the lower plane

The method used to determine the patient's vertical dimension of occlusion was the two-point method. The patient was positioned in the dental chair in an upright position, forming a 90° angle. Two points were marked on the patient's skin, on the median line: one at the tip of the nose and the other at the base of the chin. Using a compass, the distance between these two points was measured, with the patient's mandible at rest. From the measurement obtained, 3 mm was subtracted, corresponding to the free functional space, thus determining the vertical dimension of occlusion. The reference lines were drawn, tracing the midline, canine line and high line of the upper lip, marking with the patient smiling and using a colour scale, the appropriate selection of teeth was performed. The upper wax plane was placed in the patient's mouth, already oriented (parallel to the prosthetic plane and the bipupillary line), with the occlusal surface isolated

with petroleum jelly. The lower wax plane was then plasticized and placed in the mouth, asking the patient to close it slowly.

The plasticized wax was being "kneaded" while it was observed when the tips of the compass coincided with the marks on the patient's skin. Given the above, the mandible was observed in the VDO position, and that the height of the lower plane was defined. Phonetic, physiognomic and functional tests were performed to certify that the VDO was correct (de Sousa Ervolino et al., 2023).

Recording of the central relation (CR) and subsequent fixation of the orientation planes and assembly of the lower model in the articulator

To reestablish the CR, the technique of coincidence between the lines marked between the maxillary and mandibular planes was used, in the midline region and in the canine region. The patient was asked to open and close the mouth with the antagonistic wax planes and if this coincidence between the 3 lines occurred there, the relationship in the horizontal mandibular direction would be determined and the patient's occlusion would be reestablished so that the teeth could be assembled in this position. The patient was then asked to remain firmly in the position and the planes were fixed together using metal clamps (one on each side), close to the level of the canines. The set was removed from the mouth and then transferred to the articulator. Since the upper model was already mounted on the articulator with the aid of the facial bow, the lower model was mounted. The indexing was performed on the articulator and the base was isolated with solid petroleum jelly, and then it was mounted with a sufficient amount of stone plaster (de Sousa Ervolino et al., 2023).

Mounting of artificial teeth

Once the mounting on the articulator was completed, the patient was sent to the prosthetist for the mounting of the artificial teeth (Figure 5). The teeth were selected according to the patient's profile, who has a longilinear body type and trapezoidal arch. Using the BIOTONE brand (Biotone Dentsply do Brasil) mold chart, the 2D – 2D – 30M – 30L model in colour 69 was chosen. The artificial teeth were fitted with a functional and aesthetic test, which was approved by the patient.

Installation of the conventional complete denture and the overdenture complete denture

After the acrylic hardening of the prostheses by the prosthetist, the prostheses were finally installed in the upper and lower arches (Figure 6). In the lower arch prosthesis, two male abutments, each 1.0 mm high, were screwed into the implants using 3.75/4.0 mm external hexagon connection implants (S.I.N. Implant System) with a more spherical projection and a torque of 25 N (Figure 7), with a narrower neck to fit into the female, which is attached to the base of the prosthesis. The female, composed of a metal capsule that has a recess called an internal cavity, which is where the rubber ring was fitted. After fitting the lower

Figure 5: Front view of teeth mounted on ASA articulator.

Figure 6: Acrylic mandibular overdenture with the O-rings in position.

Prague Medical Report / Vol. 126 (2025) No. 4, p. 223–230

Figure 7: Screwing the O-rings with a torque of 25 N into the implants.

prosthesis, the upper complete denture was installed, the brakes and bridles were evaluated, checking the seating of the prosthetic base on the support area, the occlusal contact, the aesthetic and phonetic evaluation, observing an excellent adaptation, retention and aesthetics, which left the patient very satisfied. After the installation was done, the patient was instructed on hygiene and care of the prosthesis. After 7 days, the patient returned for prosthesis control, requiring the application of compression-evidencing paste on the lower prosthesis, with the need to wear a thin internal layer of the base of the lower prosthesis that was exposed by removing the paste. After the occlusal adjustment and minimal wear on the internal base of the lower prosthesis, a harmony of the occlusal contacts was observed and absence of evidence of compression. Therefore, another appointment was scheduled to check the prosthesis, and the patient attended with no complaints about the prosthesis.

Discussion

As a treatment option for edentulism, the conventional complete denture represents a viable and safe alternative for most elderly patients. A large part of this population characterizes this type of rehabilitation as satisfactory. However, there are those who are dissatisfied due to difficulties with adaptation, especially in relation to the mandibular complete denture. In these cases, rehabilitation with implant-retained complete dentures is a treatment modality that can minimize this dissatisfaction. An implant-supported mandibular complete denture allows for better masticatory efficiency and quality of life compared to the conventional mandibular complete denture. Thus, since the patient already had the implants (S.I.N. Implant System) installed and parallel in the anterior region of the mandible, the O-ring system was chosen given the most commonly used retention systems in overdentures. This retention system was chosen because it offers advantages such as ease of manufacture, as it does not require more complex and costly technical procedures, such as casting a metal structure (bar), simplifying both the laboratory and clinical processes. Its cleaning system is simpler for the patient to perform when compared to the bar-clip system. Since the patient was elderly, motor coordination is closely related to the quality of cleaning of the prosthetic device, and this type of prosthesis became the most recommended, also due to the visual acuity observed, and with the isolated implants, cleaning is easier for the patient (Goiato et al., 2017a).

An analysis of the biomechanics of the ring system was studied, an *in vitro* study on the O-ring system showed the lowest number of high-intensity stresses in the photoelastic image and strain gauge analysis compared to the other retention systems with the bar clip. The O-ring retention system has good retention and optimum biomechanical distribution of axial and lateral forces on the implants, which contributes to their maintenance, masticatory efficiency and social interaction, and is more comfortable than conventional complete dentures. Electromyography evaluation of masseter and temporalis, bite force, and quality of life in elderly patients during the adaptation of mandibular implant-supported overdentures (Goiato et al., 2017b; Sônego et al., 2017).

The better distribution of stress when overdentures are subjected to compressive loads can be explained by the rubber O-ring on the female component, which absorbs and reduces deformations (Goiato et al., 2017b).

Therefore, this case proved to be an efficient treatment option, using implants (S.I.N. Implant System) already installed, stabilized and in a parallel situation for perfect insertion and removal of the overdenture prosthesis. This approach offered enhanced chewing efficiency, increased bite force, and, therefore, greater confidence in using the prosthesis, which was particularly important since the patient had no prior experience with dentures use (Sônego et al., 2017).

Since it was impossible to make prosthesis on implants in the patient's upper arch, due to his history of radiotherapy treatment, which contraindicated implant installation surgery, the conventional complete denture was successfully made. Its functions were performed correctly, respecting all the manufacturing steps according to the literature, especially the step that requires the greatest attention from the

dentist in the making of the prosthesis, which is the determination of the vertical dimension of occlusion, as it will influence the final result of the treatment (Sônego et al., 2017).

Dental implants placed in the irradiated area of the head and neck region have a good survival rate, but rigorous follow-up is necessary to avoid complications and thus reduce potential failures. However, since many irradiated patients are rehabilitated with implant-supported prostheses, clinical risk assessment is important. The results showed a large variation in the total dose of radiation received, which can be detrimental to the installation of implants and can cause osteoradionecrosis (Granström, 2005; Smith Nobrega et al., 2016). The use of hyperbaric oxygen therapy (HBO) would be indicated, as this treatment improves bone repair and aids the osseointegration process through stimulation of the irradiated tissues and a significant increase in oxygen content in areas prone to osteoradionecrosis. Another important factor is the waiting time between the last radiotherapy session and implant surgery, which can be up to 240 months (Granström, 2005; Smith Nobrega et al., 2016).

To obtain the ISQ value, it is measured at four points on the SmartPeg (mesial, distal, vestibular and lingual/palatal) and has an average value. According to Osstell guidelines, for ISQ values below 60 (low stability), the implant should be monitored, because ISQ < 60 may suggest the possibility of osseointegration failure. In this situation, ISQ values above 65 (medium-high stability) or with an ISQ value of 70 or higher (high stability) mean that the implant has very good stability and osseointegration, as seen in the clinical case in question with an ISQ value of 76, confirming successful osseointegration for prosthetic rehabilitation with an overdenture (do Vale Souza et al., 2021; The Evidence-based Osstell ISQ Scale – Clinical Guidelines – available at: https://www.osstell.com/clinical-guidelines/ [accessed January 10, 2025]).

This measure determines the correct reestablishment, returning the stomatognathic system to a harmonious function of the muscles of the lower third of the face, improving facial appearance, restoring the patient's chewing, speech and swallowing functions, providing a better quality of life.

Conclusion

In view of the above, it can be concluded that implant-supported overdentures were an adequate alternative for the oral rehabilitation of a patient who had undergone radiation in the head and neck region, since the patient had previously installed implants. They have the following positive aspects: minimization of bone resorption, sensory feedback, stability and distribution of forces, in addition to having an optimistic effect on the patient's psychological well-being, since they will not be edentulous. Therefore, on the day of the installation, the patient was given adequate instructions on oral hygiene, diet, such as eating soft foods cut into small pieces and chewing them bilaterally, and the need to maintain the overdenture prosthesis, annual evaluation of the central screws of the implants (torque check, since one of the causes of screw loosening is the removable characteristic of the overdenture) and finally, regular replacement of the rubber rings at the base of the overdenture due to wear observed according to use, aiming at the longevity of the work performed and improving the patient's quality of life.

References

Alsaadi, G., Quirynen, M., Michiels, K., Jacobs, R., van Steenberghe, D. (2007) A biomechanical assessment of the relation between the oral implant stability at insertion and subjective bone quality assessment. *J. Clin. Periodontol*. **34(4)**, 359–366.

Atanda, A. J., Livinski, A. A., London, S. D., Boroumand, S., Weatherspoon, D., Iafolla, T. J., Dye, B. A. (2022) Tooth retention, health, and quality of life in older adults: A scoping review. *BMC Oral Health* **22(1)**, 185.

de Caxias, F. P., Dos Santos, D. M., Goiato, M. C., Bitencourt, S. B., da Silva, E. V. F., Laurindo-Junior, M. C. B., Turcio, K. H. L. (2018) Effects of mouth rehabilitation with removable complete dentures on stimulus perception and the electromyographic activity of the orbicularis oris muscle. *J. Prosthet. Dent*. **119(5)**, 749–754.

de Moraes Melo Neto, C. L., dos Santos, D. M., Goiato, M. C. (2023) Complete denture – Border molding technique using a laboratory condensation silicone putty: Review. *Prague Med. Rep*. **124(4)**, 359–379.

de Sousa Ervolino, I. C., Goiato, M. C., de Moraes Melo Neto, C. L., de Caxias, F. P., da Silva, E. V. F., Túrcio, K. H. L., Dos Santos, D. M. (2023) Clinical reproducibility of different centric relation recording techniques in edentulous individuals: An observational cross-sectional study. *J. Prosthodont.* **32(6)**, 497–504.

do Vale Souza, J. P., de Moraes Melo Neto, C. L., Piacenza, L. T., Freitas da Silva, E. V., de Melo Moreno, A. L., Penitente, P. A., Brunetto, J. L., Dos Santos, D. M., Goiato, M. C. (2021) Relation between insertion torque and implant stability quotient: A clinical study. *Eur. J. Dent*. **15(4)**, 618–623.

Goiato, M. C., Dos Santos, D. M., Rondon, B. C. S., Moreno, A., Baptista, G. T., Verri, F. R., Dekon, S. F. (2010) Care required when using bisphosphonates in dental surgical practice. *J. Craniofac. Surg*. **21(6)**, 1966–1970.

Goiato, M. C., de Medeiros, R. A., da Silva, E. V. F., Sônego, M. V., Dos Santos, D. M. (2017a) Biomechanical evaluation of spring system for implant-supported prosthesis: Analysis by photoelasticity and extensometry. *J. Med. Eng. Technol*. **41(4)**, 309–313.

Goiato, M. C., Matheus, H. R., de Medeiros, R. A., Dos Santos, D. M., Bitencourt, S. B., Pesqueira, A. A. (2017b) A photoelastic and strain

gauge comparison of two attachments for obturator prostheses. *J. Prosthet. Dent*. **117(5)**, 685–689.

Granström, G. (2005) Osseointegration in irradiated cancer patients: An analysis with respect to implant failures. *J. Oral Maxillofac. Surg*. **63(5)**, 579–585.

Hayashi, M., Kobayashi, C., Ogata, H., Yamaoka, M., Ogiso, B. (2010) A no-contact vibration device for measuring implant stability. *Clin. Oral Implants Res*. **21(9)**, 931–936.

Penitente, P. A., Onuki, V. T. L. P., Goiato, J. C. V., da Silva, E. V. F., de Moraes Melo Neto, C. L., Turcio, K. H. L., de Magalhães Bertoz, A. P., Dos Santos, D. M., Goiato, M. C. (2024) Influence of new complete dentures on the touch perception threshold and quality of life of edentulous patients. *Gerodontology* **41(4)**, 570–575.

Sankar, V., Xu, Y. (2023) Oral complications from oropharyngeal cancer therapy. *Cancers (Basel)* **15(18)**, 4548.

Smith Nobrega, A., Santiago, J. F. Jr., de Faria Almeida, D. A., Dos Santos, D. M., Pellizzer, E. P., Goiato, M. C. (2016) Irradiated patients and survival rate of dental implants: A systematic review and meta-analysis. *J. Prosthet. Dent*. **116(6)**, 858–866.

Sônego, M. V., Dos Santos, D. M., Goiato, M. C. (2017) Electromyography evaluation of masseter and temporalis, bite force, and quality of life in elderly patients during the adaptation of mandibular implant-supported overdentures. *Clin. Oral Implants Res*. **28(10)**, e169–e174.

Sônego, M. V., de Moraes Melo Neto, C. L., Dos Santos, D. M., de Magalhães Bertoz, A. P., Goiato, M. C. (2022) Quality of life, satisfaction, occlusal force, and halitosis after direct and indirect relining of inferior complete dentures. *Eur. J. Dent*. **16(1)**, 215–222.

Truhlar, R. S., Lauciello, F., Morris, H. F., Ochi, S. (1997) The influence of bone quality on Periotest values of endosseous dental implants at stage II surgery. *J. Oral Maxillofac. Surg*. **55**, 55–61.

Plastic of Smile: Adhesive Fixed Dental Prosthesis, Fiberglass Post Restoration, and Direct Veneers in Resin Composite

Cláudio Eufrásio Medeiros Lins[1], Amina Kadja Martins Cahu[1], Marlon Ferreira Dias[2], Glaucia Danielle Ferreira da Silva[1], Natália Gomes de Oliveira[3], Luís Felipe Espíndola-Castro[4]

[1] School of Dentistry, Centro Universitário Brasileiro (UNIBRA), Recife, Brazil;
[2] School of Dentistry, Universidade de São Paulo (UNESP), São Paulo, Brazil;
[3] School of Dentistry, Universidade de Pernambuco (UPE), Recife, Brazil;
[4] School of Dentistry, Universidade Federal de Pernambuco (UFPE), Recife, Brazil

Received September 23, 2024; Accepted November 21, 2025.

Key words: Resin composites – Fiberglass post – Dental veneers – Adhesive fixed dental prosthesis – Dental esthetics

Abstract: Tooth loss, darkened teeth, and disproportionate shape and size of teeth can compromise the way an individual sees themselves and their interpersonal relationships. The present study aims to report a case report of a plastic smile. After initial clinical examinations, it was proposed to perform an adhesive-fixed dental prosthesis, fiberglass post-restoration, and direct veneers in resin composite. For tooth 11, which had extensive coronary damage, a fiberglass post-restoration was performed. The fiberglass post was cemented with dual resin cement and the tooth was sculpted using the indirect resin composite technique. For the tooth loss (13), an adhesive fixed dental prosthesis was made of fiberglass, with wear of the abutment teeth (12 and 14) to support the prosthesis. From teeth 14 to 24, wear to veneers was performed. The veneers were implemented with resin composed by the direct hands-free technique. Treatment was completed with occlusal adjustments, finishing, and polishing. Rehabilitation treatment performed emphasizes the importance of associating adequate planning, dentist dexterity, and the choice of materials and techniques used.

Mailing Address: Luís Felipe Espíndola-Castro, DDS., MSc., PhD., Departamento de Prótese e Cirurgia Buco Facial, Av. Prof. Moraes Rego, 1235, Cidade Universitária, 50670-901, Recife – PE, Brazil; e-mail: luis.espindola@ufpe.br

https://doi.org/10.14712/23362936.2025.36

Prague Medical Report / Vol. 126 (2025) No. 4, p. 231–237

Introduction

Direct restorative treatments aim to restore form, function, and aesthetics with conservative tooth wear (Espíndola-Castro et al., 2019). Materials can be used to repair and improve the appearance of healthy teeth, such as composite resins. These materials have excellent aesthetic properties, due to biomimetic and functional characteristics similar to dental tissues (Espíndola-Castro et al., 2019). In addition, they are very versatile, which can be used in direct or indirect restorations (Dias et al., 2020).

However, in situations with significant coronal destruction, resin composite restorations may not have sufficient adhesion areas. Fiberglass posts (FGP) are indicated for rehabilitation to promote intraradicular retention in cases of fractured teeth or coronary loss (Goracci and Ferrari, 2011). FGPs have a modulus of elasticity close to dentin, reducing the possibility of fractures and a clear colour, which is easily masked by the composite resin restoration (Ruschel et al., 2018).

Furthermore, in the case of unitary dental absences, a therapeutic option is adhesive prostheses. The main advantage of this treatment is that can be performed in a short clinical period, besides that, this technique also has a lower cost and good durability (Wolff et al., 2018).

The durability of resin composite restorations is still considered inferior when compared to ceramic restorations (Fan et al., 2021). However, resin composites are excellent options that require less preparation time, do not require laboratory steps, are repairable, and have a lower cost (Korkut and Özcan, 2022). They therefore present a viable alternative for use in public services or when the patient does not have the financial means to pay for a longer-lasting treatment.

Thus, the present study aims to report a clinical case of aesthetic rehabilitation that was performed with a fiberglass post restoration, an adhesive fixed dental prosthesis, and composite resin veneers.

Case report

A 38-year-old male with a non-remarkable medical history and no known drug allergies came to the dentistry clinic complaining of dissatisfaction with his smile (Figure 1A). After clinical and radiographic examinations, unsatisfactory restorations of tooth 21, absence of tooth 13, and significant coronal destruction of tooth 11 were observed (Figure 1B and C).

After clinical examinations, the proposed treatment was approved by the patient and was divided into four clinical sessions.

Session 1: Replacements of unsatisfactory restorations

Restorative treatment was started with the removal of unsatisfactory restorations (teeth 21 and 22), followed by rubber dam isolation (Figure 1D). Due to unsatisfactory restoration overcontouring and gingival inflammation, the restorations were initially replaced to induce periodontal healing. The teeth were restored using the direct technique of composite resin layering.

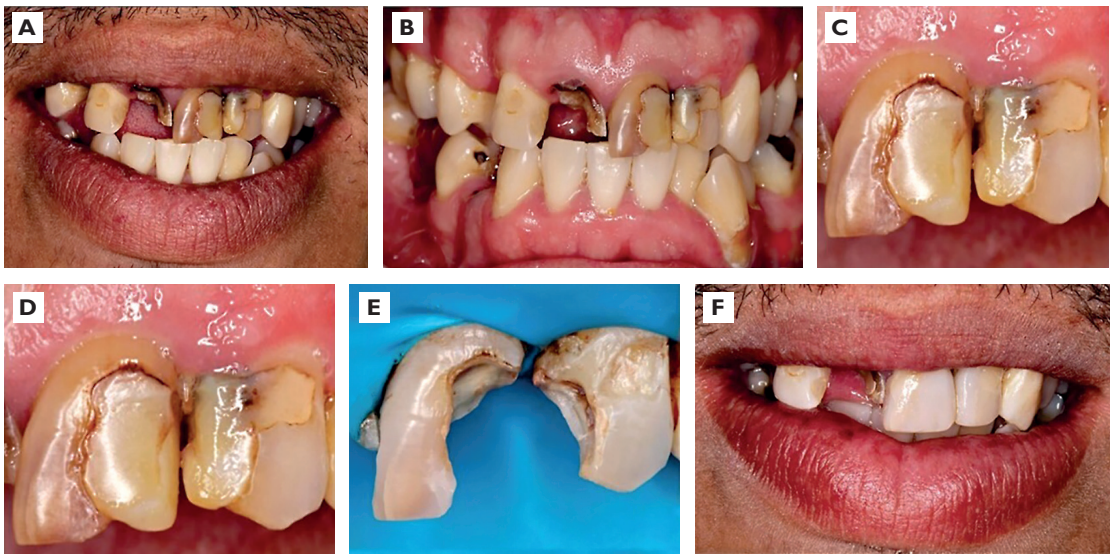

Figure 1: Initial stages. (A) Clinical appearance of the smile. (B) Detailed view of dental structures. (C) Unsatisfactory restorations. (D) Removal of restorations and rubber dam isolation. (E) Confection of resin composite restorations. (F) Immediate final clinical appearance.

The finishing and polishing protocol was performed at the end (Figure 1E).

Session 2: Fiberglass post restoration

For tooth 11, the root canal was opened with gates and largo drills, preserving 4 mm of apical obturator material (Figure 2A). Then, fiberglass post was proved in root canal and was cut in half of the clinical crown (Figure 2B and C). After stages, the conduit was cleaned with pumice paste, conditioned with 37% phosphoric acid, washed with water and completely dried. The fiberglass post surface was cleaned with 37% phosphoric acid, treated with silane for a minute (Figure 2D), and a thin layer of universal adhesive was applied, followed by light cured (Figure 2E). For the fiberglass post cementation process, self-adhesive dual cement was used (Figure 2F). Subsequently, the post was covered with resin composite, and a single crown wear was performed.

Session 3: Adhesive fixed dental prosthesis

For this step, after rubber dam isolation, proximal occlusal wear was performed on teeth 12 and 14 using diamond tips #3131 to adapt and fix the reinforced glass fiber (Figure 3A).

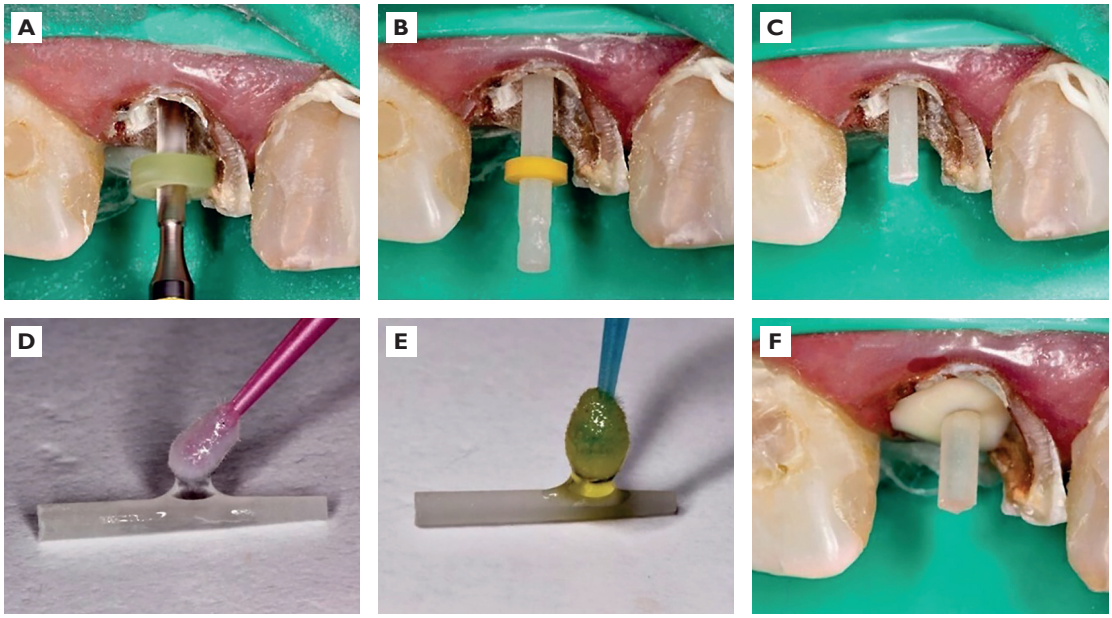

Figure 2: Fiberglass post restoration. (A) Removal of gutta-percha with gattes drills. (B) Proof of stability of the selected pin. (C) Cut of the post at the height of half of the clinical crown. (D) Silanization for 1 minute. (E) Application of universal adhesive. (F) Cementation with dual resin cement.

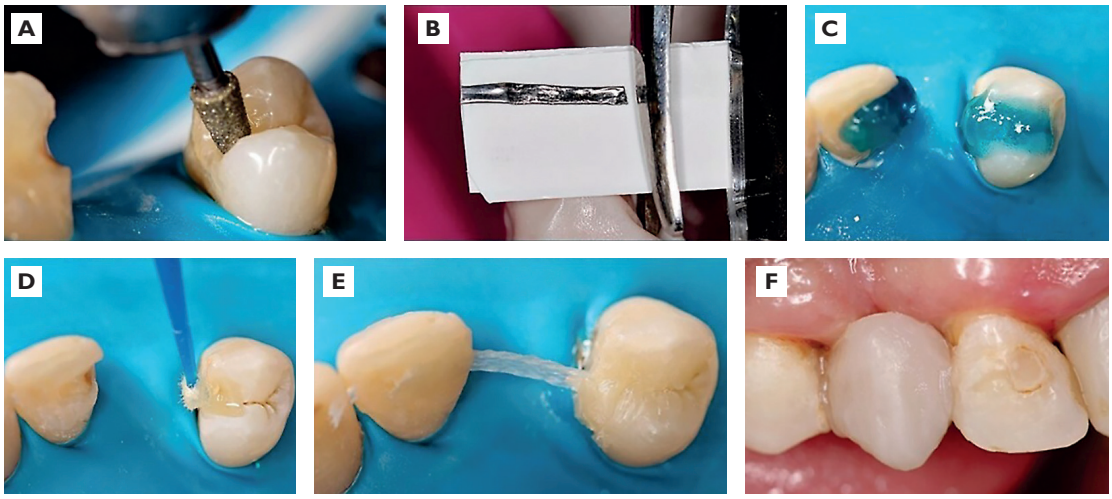

Figure 3: Adhesive fixed dental prosthesis. (A) Dental wear to supports with diamond tip #3131. (B) Measurement of the size of the fiberglass with lead film (radiographic film). (C) Acid etching. (D) Adhesive system application. (E) Fixing the fiberglass with resin composite. (F) Fabrication of the pontic with resin composite.

Prague Medical Report / Vol. 126 (2025) No. 4, p. 231–237

After the support teeth were worn out, the fiberglass size was measured with a lead sheet (radiographic film). The lead sheet was placed over the fiber package and cut with scissors (Figure 3B). Prophylaxis was performed in the cavities with pumice paste. Etching was performed with 37% phosphoric acid for 30 seconds (Figure 3C). After washing and drying, the universal adhesive was applied and light cured for 40 seconds each (Figure 3D). For the adaptation and fixation of the glass fiber-reinforced, a nanoparticulate resin composite was used (Figure 3E). The tooth 13 was sculpted in composite resin over fiberglass using a freehand direct technique with nanoparticulate resin composite (Figure 3F).

Session 4: Direct veneers in resin composite

The teeth 14 to 24 were prepared for resin composite veneers using the silhouette technique. Initially, the marginal channel delineation in the cervical and proximal areas was performed with a spherical diamond tip #1014 (Figure 4A). Vertical channels were made with the cylindrical diamond tip #1141 (Figure 4B). The appearance after this wear can be seen in Figure 4C. All grooves were marked with a graphite pencil (Figure 4D) to level the entire preparation using the #3080 conical diamond tip (Figure 4E). The proximal contacts were removed to adjust for tooth width differences (Figure 4F).

To perform the direct veneers in resin composite, modified rubber dam isolation was performed, and a #000 retractor wire was inserted into the gingival sulcus (Figure 5A). Prophylaxis was performed with pumice stone paste, and acid etching was performed for 30 seconds (Figure 5B). After washing and drying with a light air jet, the adhesive was applied and light cured for 40 seconds (Figure 5C).

For faceting using the direct technique, the palatal shells were made with a high translucency resin composite (Trans) (Figure 5D). Then, a layer of resin composite with high opacity (dentin to bleaching teeth) was applied to the buccal surface, followed by the mamelus sculpture (Figure 5E). Finally, a resin layer with translucency compatible with enamel was applied (Figure 5F).

Finishing with sanding discs was followed, and polishing was performed with felt discs impregnated with a polishing paste (Figure 6A and B). The final clinical appearance can be seen in Figure 6C and D.

Discussion

In the case presented, procedures were proposed using resin as the main restorative material. Dental reanatomization with resin composite using the direct technique is considered a simple technique with less clinical time, low cost, and satisfactory aesthetic results (Araújo et al., 2018; Espíndola-Castro et al., 2019).

To obtain the clinical success of direct composite restorations, the correct execution of the adhesive procedure is essential (Collares et al., 2017). Current dental adhesive systems can be classified according to the strategy that they bond to dental tissues in etch-and-rinse or self-etch adhesives, which do not require prior treatment (Cardoso et al., 2019). Universal or multimode adhesives are supposed to promote

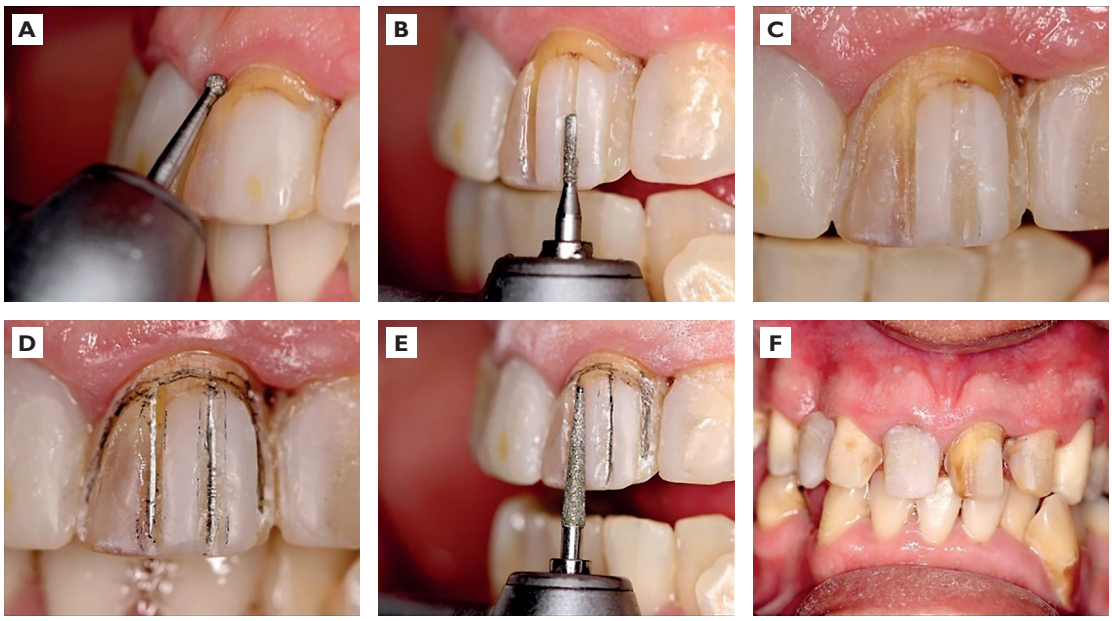

Figure 4: Wear for direct veneers. (A) Marginal channel delineation. (B) Vertical channels delineation. (C) Finished channels. (D) Marking the channels with a graphite pencil. (E) Level the entire preparation. (F) Finished wear.

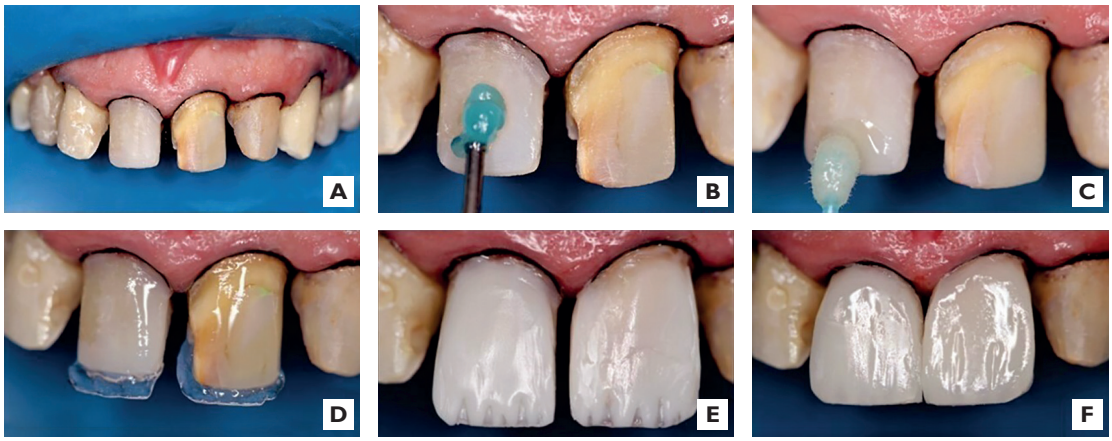

Figure 5: Production of direct veneers in resin composite. (A) Modified rubber dam isolation. (B) Acid etching. (C) Application of the adhesive. (D) Production of the palatal shell with extremely translucent resin. (E) Application of resin with high opacity. (F) Insertion of composite resin with enamel translucency.

Figure 6: Final clinical appearance. (A) Immediate clinical aspect. (B) Characterizations, finishing and polishing. (C) Final profile appearance. (D) Final clinical appearance of the smile.

adhesion to various restorative substrates, including fiberglass posts (Collares et al., 2017; El-Safty et al., 2024). These materials can also be applied to dentin as two-step, etch-and-rinse, or one-step self-etch bonding agents (Perdigão et al., 2013).

Fiberglass post posts are an excellent alternative for endodontically treated tooth restoration (Soares et al., 2012). Despite the possibility of using universal adhesive as a pretreatment for FGP, due to the presence of silane in its composition (Cadore-Rodrigues et al., 2020), in the present case, silane was used as a pretreatment before the adhesive. Some studies show that the application of silane does not influence the bond strength to the fiberglass post, therefore, this step may be optional (Robles et al., 2020; Oliveira et al., 2021).

Traditionally, posts can be classified based on the elastic modulus, with metallic, ceramic, carbon fiber, and fiberglass posts (Soares et al., 2012). A recent systematic review showed that fiberglass posts induce less stress in endodontically treated teeth when compared to other posts (Badami et al., 2022). In this case, a fiberglass post was used; this protocol is widely used to replace metallic pins due to excellent aesthetic properties (Gallo et al., 2002).

The large loss of coronal structure of tooth 11 (Figure 1) may cause concern regarding the longevity of the treatment. However, post-restorations can

Prague Medical Report / Vol. 126 (2025) No. 4, p. 231–237

be an alternative to tooth extraction. In a systematic review that evaluated the effect of the ferrule on the fracture resistance of teeth restored with posts, a greater fracture resistance was observed when the ferrule existed (Skupien et al., 2016). However, no difference in clinical longevity was observed when restorations were performed on anterior teeth without a ferrule. The authors concluded that the presence of the ferrule is responsible for an improvement in the fracture resistance of the restoration; however, other clinical factors besides the ferrule may be associated with survival in anterior teeth and need to be further investigated. Thus, there is no consensus in the literature on the contraindication of restorations with fiber posts in anterior teeth when the ferrule does not exist, which is why we indicate it in the present case.

After the implantation of the fiberglass post and the crown, composite adhesive fixed dental prostheses were fabricated with a double fixation system. This type of prosthesis represents a low-cost option for the rehabilitation of missing teeth and is considered minimally invasive (Ahmed et al., 2017). In some systematic reviews that evaluated the survival of adhesive fixed dental prostheses, there is an estimated average survival of 5 years (Ahmed et al., 2017; Thoma et al., 2017; Santos et al., 2023). However, technical complications such as detachment and minor chipping were frequent (Santos et al., 2023). These findings suggest that the technique used may be an alternative to more complex treatments such as implants or removable prostheses.

To make the direct facets, a composite nanoparticle resin was used. This type of composite has excellent surface smoothness that favours high clinical performance in this type of aesthetic procedure (Khurshid et al., 2015). All these favourable characteristics associated with good planning were evidenced in this case report, which proved to be a very viable procedure for interventions that seek the harmony of the smile as the main objective. In a systematic review that evaluated the longevity of resin composite veneers, an overall survival rate of 88% was observed, with a mean follow-up time ranging from 24 to 97 months. The main problems found were surface roughness, colour mismatch, and marginal discoloration (Lim et al., 2023). Resin composites were the material of choice used in the present study due to their lower cost and the possibility of performing a major rehabilitation in a few clinical sessions.

The success of restorative dental treatment is intrinsically linked to the clinician's technical expertise, the quality and appropriateness of the materials employed, and the patient's active cooperation throughout the process. The patient was thoroughly instructed on the expected longevity of the treatment and the behavioural habits essential to enhance long-term clinical success. Special emphasis was placed on maintaining rigorous oral hygiene, particularly in areas around the adhesive fixed dental prosthesis where flossing is limited or not feasible. Additional guidance included avoiding the intake of hard foods and refraining from using the teeth to manipulate objects, both of which could compromise the integrity of the restorations.

Conclusion

The therapeutic approach adopted, combining fiberglass posts, adhesive fixed dental prosthesis, and resin composite veneers, proved effective in re-establishing both the aesthetic and functional aspects of the smile. The success of the treatment highlights the importance of a multidisciplinary strategy, ensuring accurate diagnosis, comprehensive planning, and precise execution. This case demonstrates that it is possible to achieve predictable, satisfactory, and cost-effective outcomes, making advanced dental rehabilitation accessible to a broader range of patients and professionals.

References

Ahmed, K. E., Li, K. Y., Murray, C. A. (2017) Longevity of fiber-reinforced composite fixed partial dentures (FRC FPD) – Systematic review. *J. Dent.* **61**, 1–11.

Araújo, A. O., Manta, D. F., Lopes, M. J. P., da Silva Pedrosa, M., da Silva, C. H. V., de Almeida Durão, M. (2018) Prefabricated composite resin veneers: A clinical case report. *Braz. Dent. Sci.* **21(1)**, 119–125.

Badami, V., Ketineni, H., Sabiha, P. B., Akarapu, S., Mittapalli, S. P., Khan, A. (2022) Comparative evaluation of different post materials on stress distribution in endodontically treated teeth using the finite element analysis method: A systematic review. *Cureus* **14(9)**, e29753.

Cadore-Rodrigues, A. C., Guilardi, L. F., Wandscher, V. F., Pereira, G. K., Valandro, L. F., Rippe, M. P. (2020) Surface treatments of a glass-fiber reinforced composite: Effect on the adhesion to a composite resin. *J. Prosthodont. Res.* **64(3)**, 301–306.

Cardoso, G. C. D., Nakanishi, L., Isolan, C. P., Jardim, P. D. S., Moraes, R. R. D. (2019) Bond stability of universal adhesives applied to dentin using etch-and-rinse or self-etch strategies. *Braz. Dent. J.* **30(5)**, 467–475.

Collares, K., Opdam, N. J. M., Laske, M., Bronkhorst, E. M., Demarco, F. F., Correa, M. B., Huysmans, M. C. D. N. J. M. (2017) Longevity of anterior composite restorations in a general dental practice-based network. *J. Dent. Res.* **96(10)**, 1092–1099.

Dias, M. F., Espíndola-Castro, L. F., Lins-Filho, P. C., Teixeira, H. M., Guimarães, R. P. (2020) Influence of different thermopolymerization

methods on composite resin microhardness. *J. Clin. Exp. Dent.* **12(4)**, e335.

El-Safty, M. M. M., Nour, K. A., Mustafa, D. S. (2024) Effect of saliva contamination and different decontamination protocols on microshear bond strength of a universal adhesive to dentin. *Braz. Dent. Sci.* **27(2)**, e4159.

Espíndola-Castro, L. F., Monteiro, G. Q. M., Ortigoza, L. S., da Silva, C. H. V., Souto-Maior, J. R. (2019) Multidisciplinary approach to smile restoration: Gingivoplasty, tooth bleaching, and dental re-anatomization. *Compend. Contin. Educ. Dent.* **40(9)**, 590–599.

Fan, J., Xu, Y., Si, L., Li, X., Fu, B., Hannig, M. (2021) Long-term clinical performance of composite resin or ceramic inlays, onlays, and overlays: A systematic review and meta-analysis. *Oper. Dent.* **46(1)**, 25–44.

Gallo, J. R., Miller, T., Xu, X., Burgess, J. O. (2002) *In vitro* evaluation of the retention of composite fiber and stainless steel posts. *J. Prosthodont.* **11(1)**, 25–29.

Goracci, C., Ferrari, M. (2011) Current perspectives on post systems: A literature review. *Aust. Dent. J.* **56**, 77–83.

Khurshid, Z., Zafar, M., Qasim, S., Shahab, S., Naseem, M., AbuReqaiba, A. (2015) Advances in nanotechnology for restorative dentistry. *Materials (Basel)* **8(2)**, 717–731.

Korkut, B., Özcan, M. (2022) Longevity of direct resin composite restorations in maxillary anterior crown fractures: A 4-year clinical evaluation. *Oper. Dent.* **47(2)**, 138–148.

Lim, T. W., Tan, S. K., Li, K. Y., Burrow, M. F. (2023) Survival and complication rates of resin composite laminate veneers: A systematic review and meta-analysis. *J. Evid. Based Dent. Pract.* **23(4)**, 101911.

Oliveira, M. L., França, F. M. G., Basting, R. T., Turssi, C. P., Amaral, F. L. B. (2021) Long-term bond strength of glass fiber post to composite resin does not depend on surface treatment with silane coupling agent or universal adhesive. *Int. J. Adhes. Adhes.* **110**, 102931.

Perdigão, J., Sezinando, A., Monteiro, P. C. (2013) Effect of substrate age and adhesive composition on dentin bonding. *Oper. Dent.* **38(3)**, 267–274.

Robles, G., Huertas-Mogollón, G., Mendoza-Martiarena, Y., Ayala, G., Watanabe, R., Alvitez-Temoche, D., Mayta-Tovalino, F. (2020) Comparison of the resistance of bond strength of cemented fiberglass posts in different root thirds with and without silanization: An *ex vivo* study. *J. Contemp. Dent. Pract.* **21(3)**, 262–266.

Ruschel, G. H., Gomes, É. A., Silva-Sousa, Y. T., Pinelli, R. G. P., Sousa-Neto, M. D., Pereira, G. K. R., Spazzin, A. O. (2018) Mechanical properties and superficial characterization of a milled CAD-CAM glass fiber post. *J. Mech. Behav. Biomed. Mater.* **82**, 187–192.

Santos, M. C., Azevedo, L., Fonseca, P., Viana, P. C., Araújo, F., Villarinho, E., Fernandes, G. V. O., Correia, A. (2023) The success rate of the adhesive partial fixed prosthesis after five years: A systematic review. *Prosthesis* **5(1)**, 282–294.

Skupien, J. A., Luz, M. S., Pereira-Cenci, T. (2016) Ferrule effect: A meta-analysis. *JDR Clin. Trans. Res.* **1(1)**, 31–39.

Soares, C. J., Valdivia, A. D. C. M., da Silva, G. R., Santana, F. R., Menezes, M. de S. (2012) Longitudinal clinical evaluation of post systems: A literature review. *Braz. Dent. J.* **23(2)**, 135–740.

Thoma, D. S., Sailer, I., Ioannidis, A., Zwahlen, M., Makarov, N., Pjetursson, B. E. (2017) A systematic review of the survival and complication rates of resin-bonded fixed dental prostheses after a mean observation period of at least 5 years. *Clin. Oral Implants Res.* **28(11)**, 1421–1432.

Wolff, D., Wohlrab, T., Saure, D., Krisam, J., Frese, C. (2018) Fiber-reinforced composite fixed dental prostheses: A 4-year prospective clinical trial evaluating survival, quality, and effects on surrounding periodontal tissues. *J. Prosthet. Dent.* **119(1)**, 47–52.

Freeman-Sheldon Syndrome: A Rare Case Report with Dental Perspective

Sahil Mustafa Kidwai[1], Suman Sen[1], Nikil Kumar Jain[2], Sudhir Ramesh Maheshkar[2]

[1] Department of Oral Medicine and Radiology, Shree Bankey Bihari Dental College and Research Center, Ghaziabad, India;
[2] Department of Oral and Maxillofacial Surgery, Awadh Dental College and Hospital, Jamshedpur, India

Received December 12, 2024; Accepted November 21, 2025.

Key words: Freeman-Sheldon syndrome – Distal arthrogryposis – Skeletal malformations – Oro facial features – Dental management

Abstract: Freeman-Sheldon syndrome is a rare form of multiple congenital contracture syndromes (arthrogryposes) and is the most severe form of distal arthrogryposis. The main skeletal malformations include camptodactyly with ulnar deviation and talipes equinovarus while facial characteristics include deep-sunken eyes with hypertelorism, increased philtrum length, small nose and nostrils, and a small mouth. Here we report a rare case of Freeman-Sheldon syndrome (FSS) in an 8-years-old patient giving emphasis on the dental management of FSS.

Mailing Address: Prof. (Dr.) Suman Sen, Professor and Head, H-22, Indraprastha Apartment, plot 114, I.P Extension, Patparganj, Delhi 110092, India; e-mail: sumansen20@yahoo.co.in

https://doi.org/10.14712/23362936.2025.37

Introduction

Freeman-Sheldon syndrome (FSS) formerly known as whistling face syndrome is often autosomal dominant is a genetic disorder. Distal arthrogryposis (DA) includes a consistent pattern of distal joint (i.e. hands and feet) involvement, limited proximal joint involvement, autosomal dominant inheritance, reduced penetrance, and variable expressivity. DA syndromes were classified into 10 hierarchically related disorders (i.e. DA1–DA10). The prototypic DA is called DA type 1 which is characterized by contractures of the distal joints of the hands and feet, usually camptodactyly and clubfoot, respectively, without involvement of the facial muscles or other organ systems (Freeman and Sheldon, 1938; Bijumon and Johns, 2013). Freeman-Sheldon syndrome, also termed as distal arthrogryposis type 2A (DA2A), craniocarpotarsal dysplasia, cranio-carpo-tarsal syndrome, windmill vane hand syndrome, or whistling face syndrome, was originally described by Freeman and Sheldon in 1938 (Millner, 1991).

FSS is phenotypically similar to DA1. In addition to contractures of the hands and feet, FSS is characterized by oropharyngeal abnormalities, scoliosis, and a distinctive face that includes a very small oral orifice (often only a few millimeters in diameter at birth), puckered lips, and an H-shaped dimple of the chin; hence, FSS has been called "whistling face syndrome". The limb phenotypes of DA1 and FSS may be so similar that they can only be distinguished by the differences in facial morphology (Sung et al., 2003).

Here we report a rare case of Freeman-Sheldon syndrome with all the characteristic features in an 8-years-old patient. Here, we have also given emphasis on the dental management of FSS. The presence of decreased mouth opening and crowding of dentition makes oral hygiene maintenance difficult.

Case report

An 8-years-old male patient reported to the Department of Oral Medicine and Radiology with a chief complaint of multiple decayed teeth and difficulty in mouth opening. During the course of history taking his family history was non-contributory with no abnormalities observed in parents and younger brother. His height was 147 cm and weight was 35 kg. His face was expressionless (Figure 1), and his mouth puckered as he was whistling. His neck movement was limited in flexion and extension. General physical examination revealed hand deformities including ulnar deviation of fingers, campylodactyly (Figure 2). The patient had scoliosis (Figure 3), skin over his wrists was smooth with stiff elbows and ankles.

Oral examination revealed high narrow palate, microsomia and microglossia (Figure 4). Due to small tongue and limited movement of soft palate had caused nasal speech. Hard tissue examination revealed multiple carious teeth and poor oral hygiene. Panoramic radiograph was taken which revealed mixed dentition and confirmed the clinical dental findings (Figure 5).

On the basis of clinical and radiological examination, patient was diagnosed as a case of Freeman-Sheldon syndrome. Patient parents were counselled regarding the features and complications of this disorder. Genetic studies were then performed which confirmed the genetic association. Genetic testing of the *MYH3* gene can confirm the diagnosis. Patient had no known

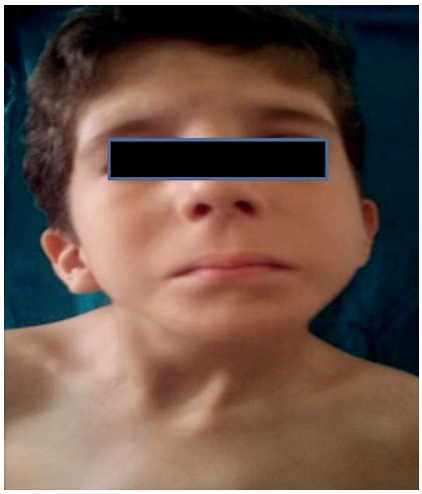

Figure 1: Expressionless face of the patient.

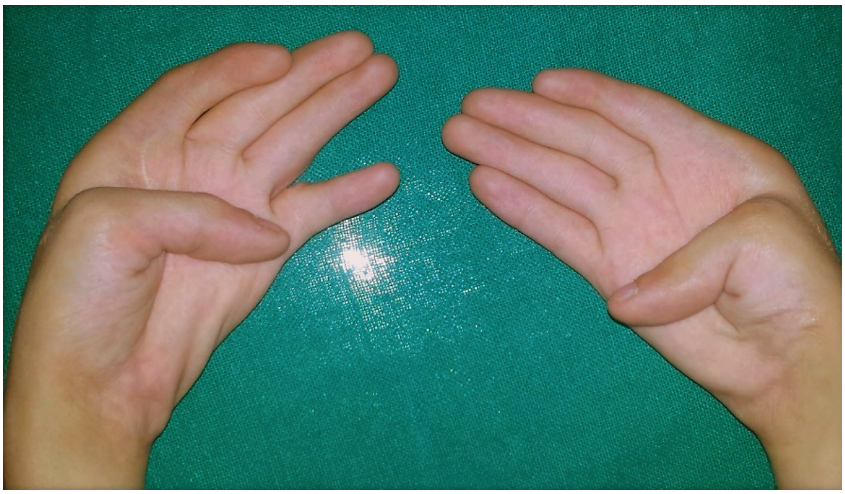

Figure 2: Revealing hand deformities including ulnar deviation of fingers, campylodactyly.

Prague Medical Report / Vol. 126 (2025) No. 4, p. 238–242

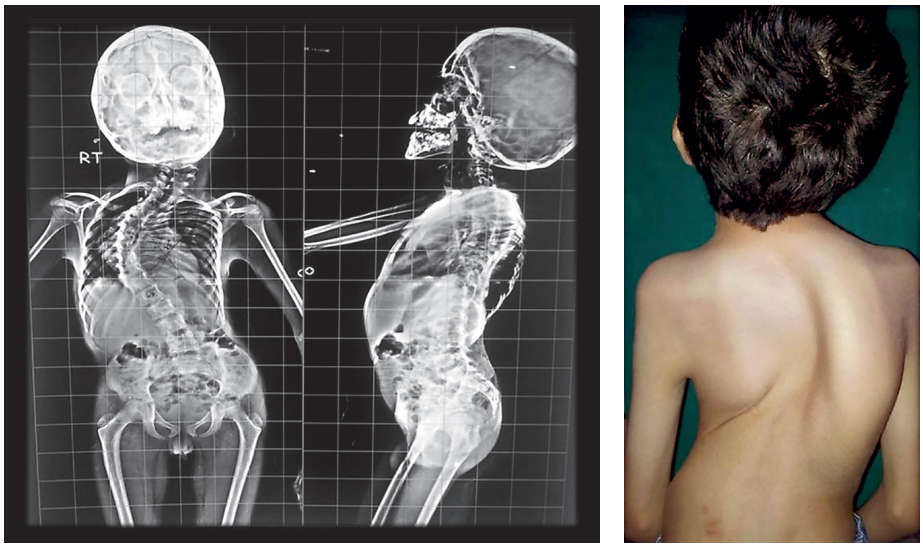

Figure 3: Presence of scoliosis.

Figure 4: Oral examination revealing high narrow palate, microsomia and macroglossia.

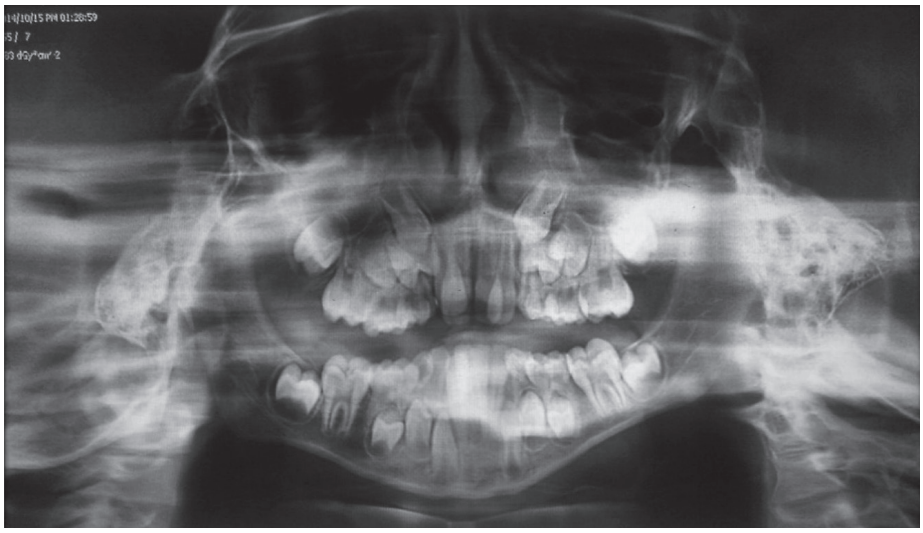

Figure 5: Panoramic radiograph showing crowding of teeth and multiple carious teeth.

family history of congenital abnormalities or consanguinity.

A thorough oral prophylaxis was performed, and rehabilitation of all carious lesions was done by composite tooth colour restorative material. Antimicrobial therapy and topical fluoride varnish was applied. Diet modifications and instructions were given to improve dental health. Emphasis was given for a recall visit of 3 months.

Discussion

The incidence of the disease is rare, and less than 100 cases have been reported in literature. In FSS, inheritance may be either autosomal dominant, most often demonstrated or autosomal recessive (MIM 277720). Males and females are affected in equal numbers. Some individuals present with minimal malformation; rarely patients have died during infancy as a result of severe central nervous systemic involvement or respiratory complications. Several syndromes are related to the Freeman-Sheldon syndrome spectrum, but more information is required before undertaking such nosological delineation (Buyukavci et al., 2005).

Diagnosis is made by clinical examination. Typical facial features, camptodactyly with ulnar deviation of fingers, and bilateral clubfeet are the fundamental findings in this syndrome. The other variable features could be scoliosis, articular stiffness, supra-orbital swelling, hypotrophic (myopathic) musculature, delayed milestones and short stature, hypertelorism, epicanthus, telecanthus, prominence of the supra-ciliary arches, hypoplasia of the nasal alae, low-set ears, contracture of the thumb in adduction, spina bifida occulta, and dysplasia or congenital dislocation of the hip (Mayhew, 1993). The orofacial findings include long philtrum, mouth puckering, microstomia, H-shaped chin dimple and microglossia (Laishley and Roy, 1986).

The diagnostic criteria for classical FSS comprise: the presence of >/2 of the major clinical manifestations of DA (ulnar deviation of the wrists and fingers, camptodactyly, hypoplastic and/or absent flexion creases, and/or overriding fingers at birth, talipes equinovarus and calcaneovalgus deformities, a vertical talus, and/or metatarsus varus) plus the presence of a small pinched mouth, prominent nasolabial folds, H-shaped dimpling of the chin (Poling and Dufresne, 2022). The presented patient fulfilled criteria for FSS.

For treatment, patients must have early consultation with craniofacial and orthopaedic surgeons, when craniofacial; clubfoot or hand correction is indicated to improve function or aesthetics. When operative measures are to be undertaken, they should be planned early in life to minimize developmental delays and negate the necessity of relearning basic functions. Due to the abnormal muscle physiology in Freeman-Sheldon syndrome, therapeutic measures may have unfavourable outcomes (Sehrawat et al., 2021). Difficult endotracheal intubations and vein access complicate operative decisions in many DA2A patients, and malignant hyperthermia (MH) may affect individuals with FSS, as well. Reports have been published about spina bifida occulta in anaesthesia management and cervical kyphoscoliosis in intubations (Poling and Dufresne, 2018).

Dental crowding is a universal finding in FSS patients. Several individuals required extraction of multiple teeth because of crowding and/or treatment for malocclusion. The presence of microstomia further exacerbated dental care, because access to the oral cavity for routine hygiene and treatment procedures becomes more difficult (Sen et al., 2021). Small oral openings necessitate the use of powered tooth brushes. The patient and the patient's parents should be made aware of the importance of home-based preventive measures such as diet control, oral hygiene maintenance, fluoride mouth rinse, and fluoride dentifrices. Professional care such as pit and fissure sealants, oral prophylaxis, and topical fluoride application must be provided (Biria et al., 2015).

Conclusion

FSS syndrome is a rare disorder which not only causes physical abnormalities but also social and psychological problems. Children with this syndrome may grow up to feel alone and "defective". Parental education is required early in the child's life. Treatment is supportive and in accordance with symptoms. Treatment of these patients requires a coordinated effort by a team of specialists, including a paediatrician, an anaesthesiologist, a plastic surgeon, a paediatric dentist, and an orthodontist. Much more research is warranted to evaluate this apparent relationship of idiopathic hyperpyrexia, MH, and stress. Further research is wanted to determine epidemiology of psychopathology in FSS and refine therapy protocols.

References

Bijumon, Johns, D. A. (2013) Freeman-Sheldon syndrome: A dental perspective. *J. Indian Soc. Pedod. Prev. Dent.* **31(3)**, 184–187.

Biria, M., Nazemi, B., Akbari, F., Rahmati, A. (2015) Freeman-Sheldon syndrome: A case report. *Eur. J. Paediatr. Dent.* **16(4)**, 311–314.

Buyukavci, M., Tan, H., Eren, S., Balci, S. (2005) A whistling face syndrome case with bilateral skin dimples. *Genet. Couns.* **16(1)**, 71–73.

Freeman, E. A., Sheldon, J. H. (1938) Cranio-carpo-tarsal dystrophy. *Arch. Dis. Child.* **13(75)**, 277–283.

Laishley, R. S., Roy, W. L. (1986) Freeman-Sheldon syndrome: Report of three cases and the anaesthetic implications. *Can. Anaesth. Soc. J.* **33(3 Pt 1)**, 388–393.

Mayhew, J. F. (1993) Anesthesia for children with Freeman-Sheldon syndrome. *Anesthesiology* **78(2)**, 408.

Millner, M. M., Mutz, I. D., Rosenkranz, W. (1991) Whistling face syndrome. A case report and literature review. *Acta Paediatr. Hung.* **31(3)**, 279–289.

Poling, M. I., Dufresne, C. R. (2018) Revisiting the many names of Freeman-Sheldon syndrome. *J. Craniofac. Surg*. **29(8)**, 2176–2178.

Poling, M. I., Dufresne, C. R. (2022) Re: "Periocular Anomalies in Freeman-Sheldon Syndrome". *Ophthalmic Plast. Reconstr. Surg*. **38(6)**, 609–610.

Sehrawat, S., Sural, S., Sugumar, P. A. A., Khan, S., Kar, S., Jeyaraman, M. (2021) Freeman-Sheldon syndrome with stiff knee gait – A case report. *J. Orthop. Case Rep*. **11(11)**, 64–68.

Sen, S., Sen, S., Kumari, M. G., Khan, S., Singh, S. (2021) Oral malignant melanoma: A case report. *Prague Med. Rep*. **122(3)**, 222–227.

Sung, S. S., Brassington, A. M., Grannatt, K., Rutherford, A., Whitby, F. G., Krakowiak, P. A., Jorde, L. B., Carey, J. C., Bamshad, M. (2003) Mutations in genes encoding fast-twitch contractile proteins cause distal arthrogryposis syndromes. *Am. J. Hum. Genet*. **72(3)**, 681–690.

Isolated Trapezium Fracture: A Rare and Challenging Diagnosis

Jheniffer Rodrigues Cação[1], Márcio Luís Duarte[1,2]

[1] Department of Radiology, Universidade de Ribeirão Preto – Campus Guarujá, Guarujá (SP), Brazil;
[2] Department of Radiology, Diagnósticos da América S. A., São Paulo (SP), Brazil

Received April 12, 2025; Accepted November 21, 2025.

Key words: Trapezium bone – Fracture – Magnetic resonance imaging – Conservative treatment

Abstract: Isolated trapezium fractures are a rare type of injury, accounting for approximately 4% of all carpal fractures. Due to their nonspecific symptoms and difficulty in detection with conventional radiography, these fractures are often underdiagnosed. This case report details a 22-year-old male who sustained a trapezium fracture after a motorcycle accident. The patient presented with wrist pain and mild edema, but radiographs were normal. However, computed tomography (CT) revealed a small fracture in the dorsal portion of the trapezium. Conservative treatment with wrist immobilization was administered, resulting in full recovery. The article discusses the rarity of trapezium fractures, their mechanisms of injury, diagnostic challenges, and treatment options. The use of imaging techniques such as CT and magnetic resonance imaging plays a crucial role in diagnosis, as they can detect fractures that may not be visible on plain X-rays. Early detection and treatment are essential to prevent complications such as arthritis, nonunion, and loss of thumb function. While there is no consensus on the optimal treatment approach, conservative management with immobilization or surgical interventions such as open reduction and internal fixation or closed reduction with pin placement are commonly used.

Mailing Address: Dr. Márcio Luís Duarte, Universidade de Ribeirão Preto (UNAERP) – Campus Guarujá, Av. D. Pedro I, 3.300, Enseada, Guarujá (SP), 11440-003, Brazil; e-mail: marcioluisduarte@gmail.com

https://doi.org/10.14712/23362936.2025.38

Prague Medical Report / Vol. 126 (2025) No. 4, p. 243–245

Introduction

Isolated trapezium fracture is a rare condition, occurring in only approximately 4% of carpal injuries. Its diagnosis requires high suspicion, since the symptoms are non-specific and identification on plain X-rays is more difficult, requiring computed tomography (CT) or magnetic resonance imaging (MRI) (Nammour et al., 2019). Early detection and treatment are extremely valuable, given the important function of the trapezium in promoting pinching and grasping actions in the carpometacarpal joint. Therefore, trapezium injuries should not be ignored (Ramoutar et al., 2009). The ideal method of treatment is still a matter of debate in the literature, and it is up to scientific discussion and clinical assessment to define the best approach for each case (Roy et al., 2022).

This article will report a case diagnosed as a trapezium fracture, in order to explore the condition, its causes, consequences and resolution.

Case report

A 22-year-old male presented with right-hand pain for seven days following a motorcycle accident. He reports worsening pain when riding a motorcycle or performing hand movements since the incident.

On physical examination, mild wrist edema and tenderness were observed, particularly in the radial region, with pain during thumb movement. There were no visible hematomas or signs of joint instability.

The hand radiograph did not reveal any bone or joint abnormalities. However, CT showed a small fracture line in the dorsal portion of the trapezium bone, confirming the diagnosis of a trapezium fracture (Figure 1).

The treatment was conservative, with wrist immobilization using a splint for four weeks. Physical therapy was not required. After the immobilization period, the patient reported complete resolution of symptoms.

Discussion

The carpus is a complex structure composed of eight bones that interact to facilitate movements such as flexion and extension. The trapezium is part of the distal row of the carpus, along with the trapezoid, capitate, and hamate. Among them, the trapezium is considered the most mobile and, by forming the carpometacarpal joint, it plays a crucial role in pinching and grasping actions (Kaewlai et al., 2008; Ramoutar et al., 2009).

Fractures isolated to the trapezium are rare due to its position and anatomical shape, accounting for approximately 4% of carpal bone injuries. Its diagnosis is extremely challenging, and management may also be complex. The longer the time without detection, the lower the chance of recovering normal thumb movement (Nammour et al., 2019; Roy et al., 2022).

Isolated trapezium fractures typically result from high-energy trauma to the hand, which causes displacement of the bone. This injury can occur, for example, from an impact on the hand with the wrist hyperextended and radially deviated in a vertical longitudinal pattern, or from direct trauma (Roy et al., 2022; Aldeeb et al., 2023).

The signs and symptoms are usually nonspecific, as most patients only report pain and edema in the area, which can often be confused with scaphoid injuries. Furthermore, on physical examination, the presentation is typically minimal, with mild edema, no deformities, or joint effusion (Nammour et al., 2019; Aldeeb et al., 2023).

Imaging exams that aid in the diagnosis include CT and MRI, as it is rarely possible to detect the injury through plain radiography (Aldeeb et al., 2023).

The diagnosis relies on a high clinical suspicion to properly request imaging exams, which in turn leads

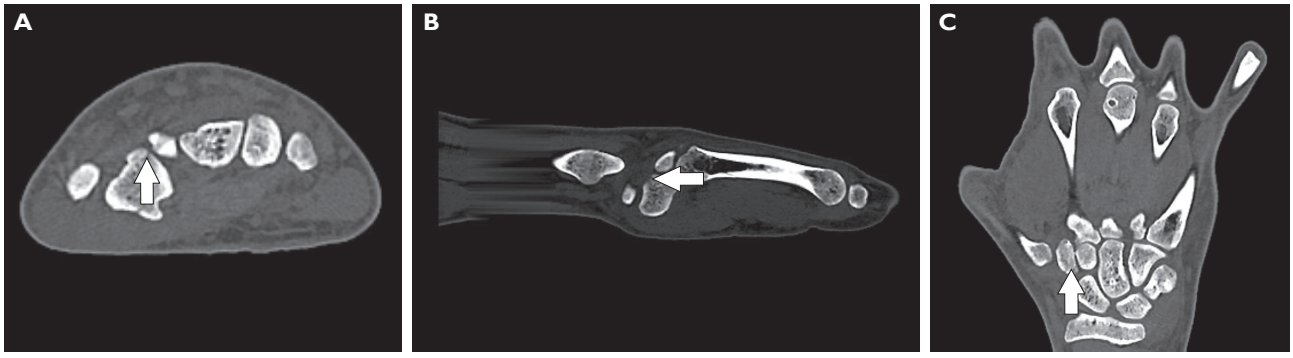

Figure 1: Wrist computed tomography scan in axial (A), sagittal (B) and coronal (C) sections demonstrating the trapezium fracture (white arrow).

to the detection of the trapezium fracture and the initiation of early treatment (Ramoutar et al., 2009; Nammour et al., 2019; Roy et al., 2022).

Complications of a delayed diagnosis and treatment of a trapezium fracture include a range of conditions such as nonunion, arthritis, malunion, decreased grip and pinch strength, pain, and osteonecrosis (Nammour et al., 2019; Aldeeb et al., 2023).

There is still no consensus in the literature on the best treatment for trapezium fractures. However, many professionals recommend open reduction and internal fixation for intra-articular trapezium fractures, a technique initially described by Cordrey and Ferrer-Torrels. Alternatively, closed reduction and pin placement, as recommended by Foster and Hastings, is also commonly used (Aldeeb et al., 2023).

Conclusion

In conclusion, isolated trapezium fractures, being rare and nonspecific, present a significant diagnostic and therapeutic challenge. Early identification through advanced imaging techniques, such as computed tomography and magnetic resonance imaging, is essential to avoid treatment delays and minimize impacts on thumb functionality. Although there is no definitive consensus on the best therapeutic approach, techniques such as open reduction with internal fixation or closed reduction with pin placement have been widely used to preserve mobility and restore function of the affected limb.

References

Aldeeb, M., Aminake, G. N., Khalil, I. A., Hayton, M., Ksantini, O. E. K., Hagert, E. (2023) Isolated trapezoid fracture in adolescent goalkeepers: A scoping review of the literature and a report of two cases. *J. Hand Surg. Glob. Online* **6(1)**, 46–52.

Kaewlai, R., Avery, L. L., Asrani, A. V., Abujudeh, H. H., Sacknoff, R., Novelline, R. A. (2008) Multidetector CT of carpal injuries: Anatomy, fractures, and fracture-dislocations. *Radiographics* **28(6)**, 1771–1784.

Nammour, M., Desai, B., Warren, M., Godshaw, B., Suri, M. (2019) Approach to isolated trapezoid fractures. *Ochsner J.* **19(3)**, 271–275.

Ramoutar, D. N., Katevu, C., Titchener, A. G., Patel, A. (2009) Trapezium fracture – A common technique to fix a rare injury: A case report. *Cases J.* **2**, 8304.

Roy, A., Dutta, S., Kar, G. G. (2022) Late isolated comminuted trapezium fracture with carpometacarpal subluxation: A case report. *Int. J. Orthop. Surg.* **30(2)**, 67–69.

Bilateral Accessory Clavicular Heads of Sternocleidomastoid Stenosing Supraclavicular Fossa in Human: Case Report

Dibakar Borthakur, Harisha Kusuma, Mohammed Ahmed Ansari

Department of Anatomy, All India Institute of Medical Sciences, New Delhi, India

Received January 31, 2025; Accepted November 21, 2025.

Key words: Anatomical variation – Cleidooccipital muscle – Sternocleidomastoid muscle

Abstract: The sternocleidomastoid muscle (SCM) is an important landmark for many clinical procedures performed in the neck. Typically, the SCM consists of two heads of origin, sternal and clavicular. We came across bilateral accessory clavicular fibers of the SCM having extended attachment up to the middle third of the clavicle in an elderly cadaver. On the right side, the accessory fibers formed a distinct, separate belly in the form of cleidooccipital muscle. On the left side, four clavicular heads of SCM were observed, which were partially separated from each other. The presence of accessory clavicular fibers may stenose supraclavicular fossa. Additionally, the SCM with accessory clavicular fibers is not a reliable surface landmark and hence may pose difficulties in important procedures in the region such as central venous catheterization.

Mailing Address: Harisha Kusuma, MBBS., MD., Department of Anatomy, Teaching Block, Room No. 1027 (B), All India Institute of Medical Sciences, Ansari Nagar, New Delhi 110029, India; e-mail: kusumaharisha@gmail.com

https://doi.org/10.14712/23362936.2025.39

Introduction

The sternocleidomastoid muscle (SCM) is a key muscle of the neck bordering the anterior triangle from the posterior triangle. The SCM is also an important surface landmark in the neck. As the name implies, it has three distinct attachments, namely the sternal, clavicular and mastoid. The inferior attachments are from the sternum and the clavicle, and superior attachment extends onto the mastoid process of the temporal bone as well as the lateral part of the superior nuchal line of the occipital bone (Standring, 2016; Silawal et al., 2022). The rounded, tendinous sternal head arises from the ventral surface of the manubrium and adjoining capsule of sternoclavicular joint which then merges with the flat clavicular head arising from the superior aspect of the medial third of the clavicle. A rounded muscle belly thus forms and ascends laterally upwards (Standring, 2016; Byrd et al., 2022). The muscle is thick and narrow centrally, and broader and thinner at superior and inferior ends. The clavicular head spirals and blends with the sternal head in the middle of the neck and forms a thick round muscle belly. The usual pattern of arrangement is superficial obliquely directed sternal fibers attached to the occiput and the deep clavicular fibers attached on to the mastoid process. The muscle fibers thus have cruciate and spiralized fiber arrangement and therefore the pull of the two heads are different (Standring, 2016). Anteriorly the muscle is related to the carotid arteries, the internal jugular, facial and lingual veins, the deep cervical group of lymph nodes, the vagus nerve and the branches of the ansa cervicalis (Nayak et al., 2006; Standring, 2016). The important posterior relation of the muscle is the accessory nerve appearing just below the middle of the posterior border. The spinal root of the accessory nerve provides motor innervation to the SCM and trapezius muscles, and branches of the cervical plexus provide proprioceptive afferents. Clinical evidence also suggests that some of the branches of the cervical nerves may be motor to the muscle (Standring, 2016).

Based on the fiber arrangement, the SCM has been subdivided into several distinct parts, viz. the sternomastoid, cleidomastoid, sternooccipital and cleidooccipital (Natsis et al., 2009). The sternomastoid portion of the muscle is clearly distinguishable from the cleidomastoid portion in lower mammals only (Mehta et al., 2012). The SCM plays an important role in execution of various head movements and is crucial for maintaining the steadiness of the cervical spine (Byrd et al., 2022). SCM also acts as a short-range and long-range rotator of the neck through its clavicular and sternal fibers respectively (Kim et al., 2015). In addition to this, it also flexes the cervical as well as the thoracic vertebrae and acts as an accessory muscle in deep inspiration (Nayak et al., 2006). Morphological variations of the sternal and clavicular heads of the SCM, including several patterns of accessory clavicular head, have been described in erstwhile reports (Nayak et al., 2006). We report here a rare anatomical variation of SCM wherein bilateral broad and extensive attachment of the clavicular head of SCM has been observed.

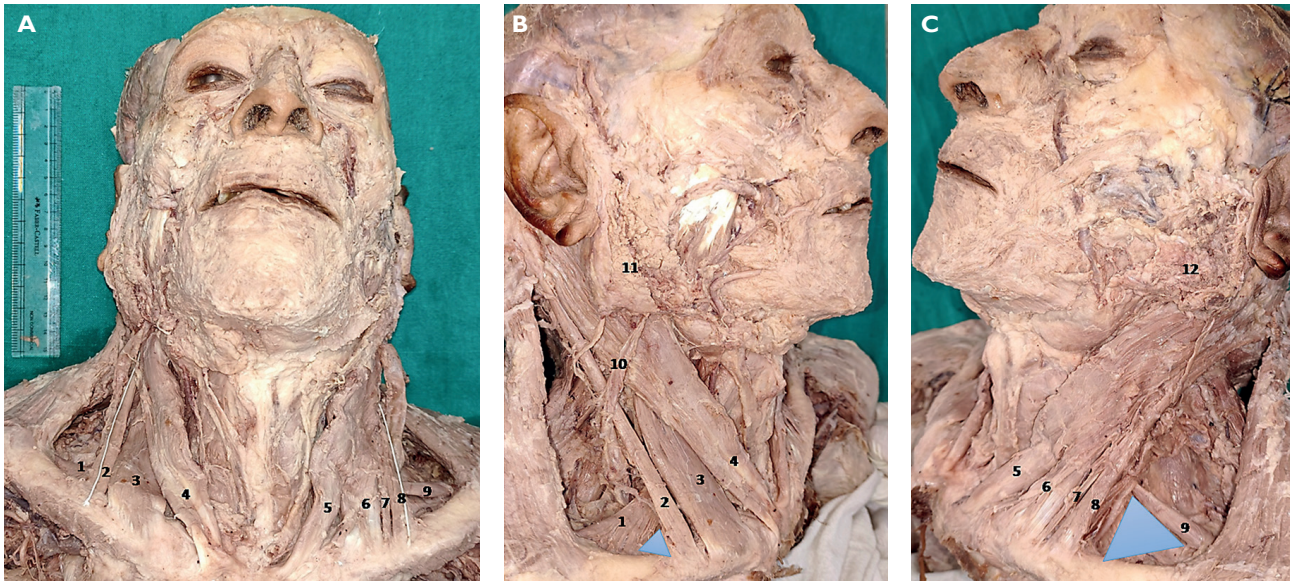

Figure 1(A–C): Dissected triangles of the neck; 1 – right omohyoid muscle (inferior belly); 2 – cleidooccipital fibers of the right sternocleidomastoid muscle (SCM); 3 – main clavicular head of the right SCM; 4 – sternal head of the right SCM; 5 – sternal head of the left SCM; 6 – main clavicular head of the left SCM; 7, 8 – cleidooccipital fibers of the left SCM; 9 – left omohyoid (inferior belly); 10 – right external jugular vein; 11 – right parotid gland; 12 – left parotid gland; blue shaded areas on either side depict the dimension of the supraclavicular fossae. The white cotton thread placed over the lateral edges of the cleidooccipital fibers for taking the measurements.

Prague Medical Report / Vol. 126 (2025) No. 4, p. 246–250

Case report

The neck region of a male cadaver aged 70 years was dissected following standard steps, and the findings were recorded and photographed. There were bilateral variations of the clavicular fibers of the SCM. The SCM on the right side had an extra clavicular head originating from the superior surface of the middle third of the clavicle located lateral to the main clavicular head. The dimensions of the extra clavicular head on the right side were 8.5×1.2 cm. The clavicular head ascended obliquely and laterally upwards to gain attachment on the superior nuchal line as a separate cleidooccipital muscle lateral to the attachment of the main belly of the SCM (Figure 1A and B). The nerve point corresponding to the emergence of superficial cutaneous branches of the cervical plexus and spinal accessory nerve was observed along the posterior border of the cleidooccipital muscle (Figure 1A and B). On the left side, four separate bundles of the clavicular fibers were observed, which did not appear as distinct individual heads, but were organized in different fascicles at the root of the neck. The widths of the four heads at its clavicular origin were 2.6 cm, 3.2 cm, 0.4 cm and 2.1 cm respectively from medial to lateral aspect respectively (Figure 1A and C). These four fascicles of the SCM merged into a single belly at the level of the upper border of the cricoid cartilage, and then ascended laterally upwards and attached on the lateral part of the superior nuchal line. In addition to that, the right external jugular vein was observed to be lying deep to the investing layer of the deep cervical fascia and passed deep to the investing layer at the level of midpoint of the posterior border of the SCM (Figure 1A).

Discussion

There is considerable variation in the extent and manner in which the heads of the SCM originate, fuse and arrange (Saha et al., 2014). Prevalence of supernumerary clavicular heads of SCM is up to 33% (Kim et al., 2015; Tubbs et al., 2016). The cleidooccipital muscle is a distinct entity from the main clavicular heads as observed on the right side of the cadaver. Such a case is extremely rare in occurrence and therefore clinically relevant because it can stenose the supraclavicular fossa (Raikos et al., 2012; Tubbs et al., 2016). The width of the any variant of the clavicular head of SCM is variable, and it can have attachment anywhere from sternal end to the acromial end (Tubbs et al., 2016). Slips from the SCM can get attached to a variety of neighbouring structures such as the cervical vertebrae, parotid gland, thyroid gland etc. Reports of accessory sternal heads (Nayak et al., 2006; Natsis et al., 2009; Kim et al., 2015) and accessory clavicular heads (Mehta et al., 2012; Saha et al., 2014; Kim et al., 2015; Oh et al., 2019; Fulmali et al., 2020; Heo et al., 2020) of the SCM have been described in previous literature. 13 headed SCM has also been reported in erstwhile literature (Nayak et al., 2016). Some notable and clinically relevant variants of SCM reported during the last decade with their significant findings are tabulated in Table 1. Even though cases of accessory clavicular fibers of the SCM are not infrequent, bilateral extensive attachment that encroaches the posterior triangle which has the potential to stenose the supraclavicular fossa is however very rare.

The early development of the trapezius and SCM share a "common embryonic anlage" innervated by the spinal accessory in the mammalian neck. The "common embryonic anlage" is referred to as the trapezius-SCM system and is derived from the lateral plate mesoderm. It has been observed that the caudal part of the "common embryonic anlage" splits at Carnegie stage (CS) 16 corresponding to the 6 weeks of development in human embryo. At CS 18 (corresponding to 7th week of development) and CS 20 (which corresponds to 8 weeks of development), the SCM and trapezius muscles get separated further and extend posteriorly. However, at this stage the two muscles can be identified as two muscles only inferiorly and are connected to each other at their cranial ends. The developing clavicle and the trapezius of the pectoral girdle further augment the separation of the two muscles and are believed to be important drivers of the process along with the pull of the developing digastric muscle (Cho et al., 2020). The completely separated two muscles are observed distinctly during 21st week of intrauterine life. The reason for development of an unusual accessory head is believed to be extensive splitting of the mesoderm of the sixth pharyngeal arch (Mehta et al., 2012; Sirasanagandla et al., 2012). It has been also suggested to be due to failure of fusion of the individual mesodermal units within the mesoderm of the sixth pharyngeal arch before they unite and form a single muscle (Kim et al., 2015). The proper development of the neural crest derived muscles of the posterior cervical region is under the molecular control of *HOX* genes. Aberration of expression of *HOX* genes may be involved in the molecular pathway to lead to the occurrence of the variation (Dupont et al., 2018).

The clinical relevance of the extra heads of the SCM can be understood from the myriads of important relations of SCM that can readily get compressed in the presence of an accessory head. The presence of anatomical variations of the SCM

Table 1: Reports of anatomical variations of the sternocleidomastoid muscle (SCM) across different population groups with their notable findings

Authors, population, study type	Notable findings	
	Sternal head	**Clavicular head**
Nayak et al. (2006), Indian, single case	Bilateral accessory sternal heads	–
Natsis et al. (2009), Greek, single case	Bilateral accessory sternal heads	Bilateral three accessory clavicular heads
Mehta et al. (2012), Indian, single case	–	Bipartite clavicular head of SCM on the left side
Sirasanagandla et al. (2012), Indian, single case	Third head of SCM arising from investing layer of deep cervical fascia	
Saha et al. (2014), Indian, 18 cases	–	5 out of 18 cadavers revealed accessory clavicular heads, 16.7% unilateral and 11.1% bilateral occurrence
Kim et al. (2015), French, single case	Two sternal heads on the left side	Bilateral two accessory clavicular heads, one cleidooccipital muscle on either side
Nayak et al. (2016), Indian, single case	–	Four clavicular heads on the right side, none qualified to be cleidooccipital muscle
Oh et al. (2019), Korean, single case	–	Bilateral supernumerary clavicular heads
Heo et al. (2020), Korean, single case	Atypical muscular slip from the sternal head joined clavicular fibers	Accessory clavicular head on the left side
Fulmali et al. (2020), Indian single case	–	Single accessory clavicular head on the left side
Silawal et al. (2022), German, single case	Muscular slip of the sternal head had attachment to the superior pharyngeal constrictor muscle on the right side	–
Dupont et al. (2018), American, single case	–	Bilateral six clavicular heads, all heads were attached along the entire extent of the superior nuchal line and thus termed cleidooccipital muscle

renders the muscle less utilizable as anatomical landmark for locating desired structures. Branchial cysts are usually located at the junction of the upper and the middle third of the SCM muscle and branchial fistula typically present as a small pit adjacent to the anterior border of the lower third of SCM (Stranding, 2016). Accessory clavicular heads of the SCM may pose difficulty in precise identification of sites for needle insertion during central venous catheterization procedures. Identification of important structures, such as the accessory nerve may be difficult (Nayak et al., 2006; Natsis et al., 2009). Extra SCM heads could serve as excellent vascularized free muscle flaps for reconstruction surgeries involving the face (Mehta et al., 2012). Accessory clavicular heads of SCM are frequently implicated in the causation of torticollis in adults (Mehta et al., 2012; Mansoor and Rathore, 2018). The accessory clavicular head, especially the more laterally placed cleidooccipital muscle is believed to generate more force from the distal clavicle (Byrd et al., 2022). In our case, the cleidooccipital fibers on the right side encroached and thus stenosed the right supraclavicular fossa. It can be a situation that causes hindrance accessing the subclavian or internal jugular vein during central venous catheterization. Clinicians planning an intervention in the region should have knowledge about such accessory clavicular heads of the SCM (Mehta et al., 2012). The deep course of the external jugular vein on the right posterior triangle may additionally pose more difficulty in the central venous access.

Conclusion

The present case highlights that the cleidooccipital portion of the sternocleidomastoid muscle on the right side has the potential to stenose the supraclavicular fossa. The utility of the muscle as a landmark may become non reliable. Furthermore, extensive and broad attachment of clavicular fibers can compress the external jugular vein. Prior awareness about the possibility of encountering such a variation and prompt intervention may ameliorate the complications.

References

Byrd, J. J., McCumber, T. L., Snow, E. L. (2022) Cadaveric case report and biomechanical analysis of an accessory clavicular head to the sternocleidomastoid. *Transl. Res. Anat.* **28**, 100215.

Cho, K. H., Morimoto, I., Yamamoto, M., Hanada, S., Murakami, G., Rodríguez-Vázquez, J. F., Abe, S. (2020) Fetal development of the human trapezius and sternocleidomastoid muscles. *Anat. Cell Biol.* **53(4)**, 405–410.

Dupont, G., Iwanaga, J., Altafulla, J. J., Lachkar, S., Oskouian, R. J., Tubbs, R. S. (2018) Bilateral sternocleidomastoid variant with six distinct insertions along the superior nuchal line. *Anat. Cell Biol*. **51(4)**, 305–308.

Fulmali, D. G., Thute, P. P., Keche, H. A., Chimurkar, V. K. (2020) Variant sternocleidomastoid with extra clavicular head – A case report. *J. Evol. Med. Dent. Sci.* **9(43)**, 3258–3260.

Heo, Y. R., Kim, J. W., Lee, J. H. (2020) Variation of the sternocleidomastoid muscle: A case report of three heads and an accessory head. *Surg. Radiol. Anat.* **42(6)**, 711–713.

Kim, S. Y., Jang, H. B., Kim, J., Yoon, S. P. (2015) Bilateral four heads of the sternocleidomastoid muscle. *Surg. Radiol. Anat.* **37(7)**, 871–873.

Mansoor, S. N., Rathore, F. A. (2018) Accessory clavicular sternocleidomastoid causing torticollis in an adult. *Prog. Rehabil. Med.* **3**, 20180006.

Mehta, V., Arora, J., Kumar, A., Nayar, A. K., Ioh, H. K., Gupta, V., Suri, R. K., Rath, G. (2012) Bipartite clavicular attachment of the sternocleidomastoid muscle: A case report. *Anat. Cell Biol*. **45(1)**, 66–69.

Natsis, K., Asouchidou, I., Vasileiou, M., Papathanasiou, E., Noussios, G., Paraskevas, G. (2009) A rare case of bilateral supernumerary heads of sternocleidomastoid muscle and its clinical impact. *Folia Morphol. (Warsz.)* **68(1)**, 52–54.

Nayak, S. B., Surendran, S., Reghunathan, D., Nelluri, M. V. M. (2016) Sternocleiodomastoid muscle with five fleshy bellies and thirteen heads of origin. *Online J. Health Allied Sci.* **15(3)**, 4–6.

Nayak, S. R., Krishnamurthy, A., Sj, M. K., Pai, M. M., Prabhu, L. V., Jetti, R. (2006) A rare case of bilateral sternocleidomastoid muscle variation. *Morphologie* **90(291)**, 203–204.

Oh, J. S., Kim, C. E., Kim, J., Yoon, S. P. (2019) Bilateral supernumerary clavicular heads of sternocleidomastoid muscle in a Korean female cadaver. *Surg. Radiol. Anat.* **41(1)**, 699–702.

Raikos, A., Paraskevas, G. K., Triaridis, S., Kordali, P., Psillas, G., Brand-Saberi, B. (2012) Bilateral supernumerary sternocleidomastoid heads with critical narrowing of the minor and major supraclavicular fossae: Clinical and surgical implications. *Int. J. Morphol*. **30(3)**, 927–933.

Saha, A., Mandal, S., Chakraborty, S., Bandyopadhyay, M. (2014) Morphological study of the attachment of the sternocleidomastoid muscle. *Singapore Med. J.* **55(1)**, 45–47.

Silawal, S., Morgan, S., Ruecker, L., Schulze-Tanzil, G. (2022) A unilateral sternopharyngeal branch of the sternocleidomastoid muscle in an aged Caucasian male: A unique cadaveric report. *Folia Morphol. (Warsz.)* **82(2)**, 434–438.

Sirasanagandla, S. R., Bhat, K. M. R., Pamidi, N., Somayaji, S. N. (2012) Unusual third head of the sternocleidomastoid muscle from the investing layer of cervical fascia. *Int. J. Morphol.* **30(3)**, 783–785.

Standring, S. (2016) *Gray's Anatomy E-Book*. Elsevier Health Sciences.

Tubbs, R. S., Shoja, M. M., Loukas, M. (2016) *Bergman's Comprehensive Encyclopedia of Human Anatomic Variation*. John Wiley and Sons, New York.

Instructions to Authors

Prague Medical Report is an English multidisciplinary biomedical journal published quarterly by the First Faculty of Medicine of the Charles University. Prague Medical Report (Prague Med Rep) is indexed and abstracted by Index-medicus, MEDLINE, PubMed, EuroPub, CNKI, DOAJ, EBSCO, and Scopus.

Articles issued in the journal

a) Primary scientific studies on the medical topics (not exceeding 30 pages in standardized A4 format – i.e. 30 lines and 60–65 characters per line – including tables, graphs or illustrations)
b) Short communications
c) Case reports
d) Reviews
e) Lectures or discourses of great interest
f) Information about activities of the First Faculty of Medicine and other associated medical or biological organizations

Layout of the manuscript

a) Title of the study (brief and concise, without abbreviations)
b) Information about the author(s) in the following form:
   - first name and surname of the author(s) (without scientific titles)
   - institution(s) represented by the author(s)
   - full corresponding (mailing) author's reference address (including first name, surname and scientific titles, postal code, phone/fax number and e-mail)
c) Abstract (maximum 250 words)
d) Key words (4–6 terms)
e) Running title (reduced title of the article that will appear at the footer (page break), not more than 50 typewritten characters including spaces)
f) Introduction
   - The use of abbreviations should be restricted to SI symbols and those recommended by the IUPAC-IUB. Abbreviations should be defined in brackets on first appearance in the text. Standard units of measurements and chemical symbols of elements may be used without definition.
g) Material and Methods
h) Results
i) Discussion
j) Conclusion
k) References
   - All the sources of relevant information for the study should be cited in the text (citations such as "personal communication" or "confidential data" are not accepted).
   - It is not permitted to cite any abstract in the References list.
   - References should be listed alphabetically at the end of the paper and typed double-spaced on separate pages. First and last page numbers must be given. Journal names should be abbreviated according to the Chemical Abstract Service Source Index. All co-authors should be listed in each reference (et al. cannot be used).
   - Examples of the style to be used are:
     Yokoyama, K., Gachelin, G. (1991) An Abnormal signal transduction pathway in CD4–CD8– double-negative lymph node cells of MRL *lpr/lpr* mice. *Eur. J. Immunol.* **21**, 2987–2992.
     Loyd, D., Poole, R. K., Edwards, S. W. (1992) *The Cell Division Cycle. Temporal Organization and Control of Cellular Growth and Reproduction.* Academic Press, London.
     Teich, N. (1984) Taxonomy of retroviruses. In: *RNA Tumor Viruses,* eds. Weiss, R., Teich, N., Varmus, H., Coffin, J., pp. 25–207, Cold Spring Harbor Laboratory, Cold Spring Harbor, New York.
     References in the text should be cited as follows: two authors, Smith and Brown (1984) or (Smith and Brown, 1984); three or more authors, Smith et al. (1984) or (Smith et al., 1984). Reference to papers by the same author(s) in the same year should be distinguished in the text and in the reference list by lower-case letters, e.g. 1980a, or 1980a, b.
l) tables, figures, illustrations, graphs, diagrams, photographs, etc. (incl. legends)

Technical instructions

a) Manuscripts (in UK English only) must be delivered in the electronic form via Online Manuscript Submission and Tracking system (http://www.praguemedicalreport.org/). In case of problems, contact the Prague Medical Report Office (medical.report@lf1.cuni.cz). The online submission has to

Prague Medical Report / Vol. 126 (2025) No. 4, p. 251–252

include the complete version of the article in PDF format, separately the manuscript as a MS Word file and a cover letter. The detailed version of the Instructions to Authors can be found at: http://www.praguemedicalreport.org/download/instructions_to_authors.pdf.

b) Text should be written in MS WORD only. We accept only documents that have been spell-checked with UK English as a default language.
c) Please, write your text in Times New Roman script, size 12, and line spacing 1.5.
d) Text should be justified to the left, with no paragraph indent (use Enter key only); do not centre any headings or subheadings.
e) Document must be paginated-numbered beginning with the title page.
f) Tables and graphs should represent extra files, and must be paginated too.
g) Edit tables in the following way: Make a plain text, indent by Tab (arrow key) all the data belonging to a line and finish the line by Enter key. For all the notes in table, use letter x, not *.
h) Make your graphs only in black-and-white. Deliver them in electronic form in TIFF or JPG format only.
i) Deliver illustrations and pictures (in black-and-white) in TIFF or JPG format only. The coloured print is possible and paid after agreement with the Prague Medical Report Office.
j) Mark all the pictures with numbers; corresponding legend(s) should be delivered in an extra file. Mark the position of every picture (photo) in the manuscript by the corresponding number, keep the order 1, 2, 3…

Authors' Declaration

The corresponding (or first author) of the manuscript must print, fill and sign by his/her own hand the Authors Declaration and fax it (or send by post) to the Prague Medical Report Office. Manuscript without this Declaration cannot be published. The Authors' Declaration can be found by visiting our web pages: http://pmr.lf1.cuni.cz or web pages of Prague Medical Report Online Manuscript Submission and Tracking system: http://www.praguemedicalreport.org/.

Editorial procedure

Each manuscript is evaluated by the editorial board and by a standard referee (at least two expert reviews are required). After the assessment the author is informed about the result. In the case the referee requires major revision of the manuscript, it will be sent back to the author to make the changes. The final version of the manuscript undergoes language revision and together with other manuscripts, it is processed for printing.

Concurrently, proofs are electronically sent (in PDF format) to the corresponding (mailing) author. Author is to make the proofs in PDF paper copy and deliver it back to the editorial office by fax or as a scanned file by e-mail. Everything should be done in the required time. Only corrections of serious errors, grammatical mistakes and misprints can be accepted. More extensive changes of the manuscript, inscriptions or overwriting cannot be accepted and will be disregarded. Proofs that are not delivered back in time cannot be accepted.

Article processing charge

Authors do not pay any article processing charge.

Open Access Statement

Copyright Statement

Editorial Office
Prague Medical Report
Kateřinská 32, 121 08 Prague 2
Czech Republic
e-mail: medical.report@lf1.cuni.cz
Phone: +420 224 964 570
Fax: +420 224 964 574

Annual Contents

No. 1

No. 2

Prague Medical Report / Vol. 126 (2025) No. 4, p. 253–255

Case Reports

No. 3

Primary Scientific Studies

Case Reports

No. 4

Prague Medical Report / Vol. 126 (2025) No. 4, p. 256–257

Annual Nominal Index

ISSN 1214–6994